Volume 5 ▪ Issue 2 ▪ May 2011



INTERNATIONAL JOURNAL OF

# BIOMETRICS AND BIOINFORMATICS (IJBB)

ISSN : 1985-2347
Publication Frequency: 6 Issues / Year

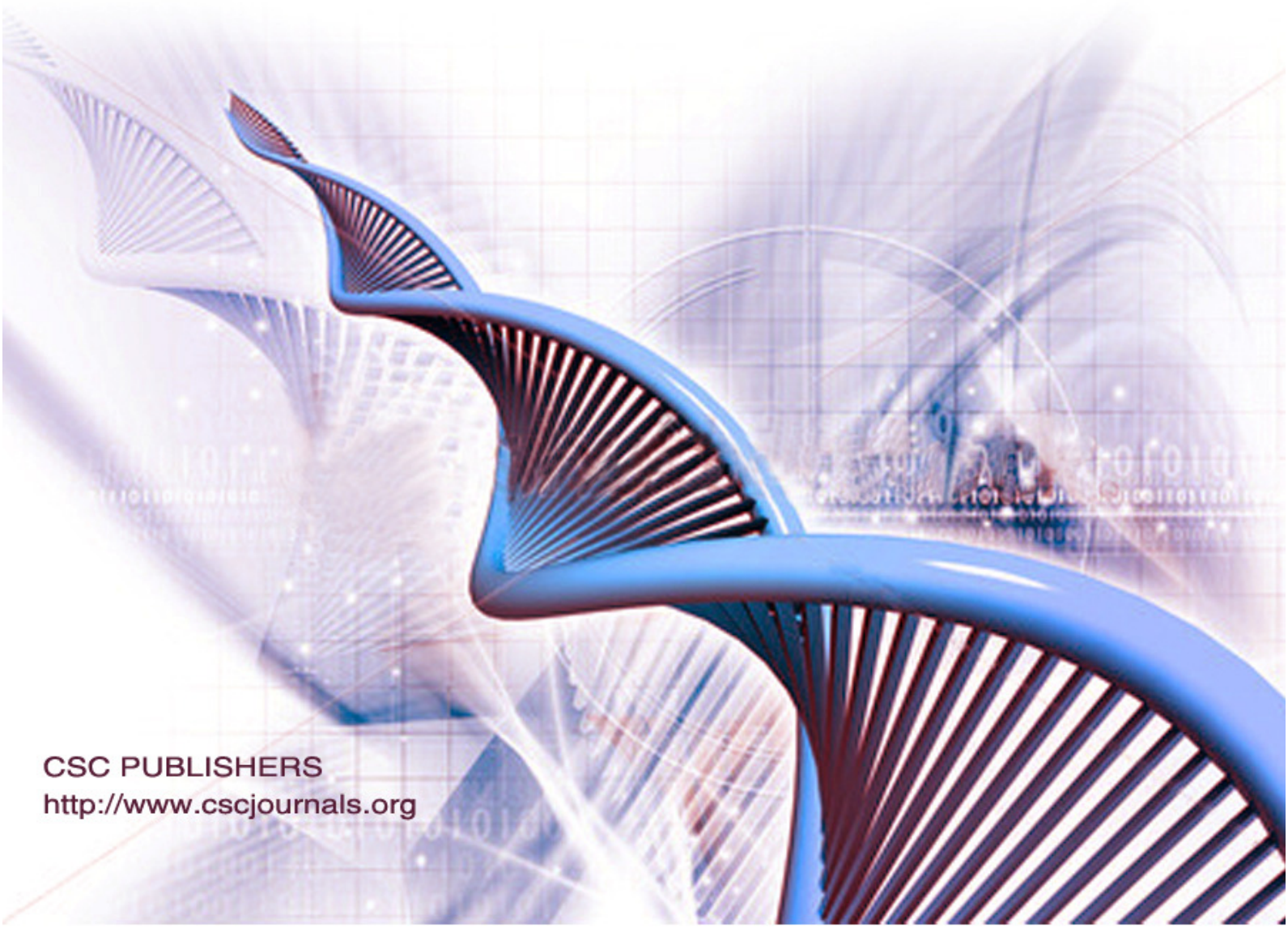

CSC PUBLISHERS
http://www.cscjournals.org

# INTERNATIONAL JOURNAL OF BIOMETRICS AND BIOINFORMATICS (IJBB)

**VOLUME 5, ISSUE 2, 2011**

**EDITED BY**
**DR. NABEEL TAHIR**

ISSN (Online): 1985-2347

International Journal of Biometrics and Bioinformatics (IJBB) is published both in traditional paper form and in Internet. This journal is published at the website http://www.cscjournals.org, maintained by Computer Science Journals (CSC Journals), Malaysia.

IJBB Journal is a part of CSC Publishers

Computer Science Journals

http://www.cscjournals.org

# INTERNATIONAL JOURNAL OF BIOMETRICS AND BIOINFORMATICS (IJBB)

Book: Volume 5, Issue 2, May 2011
Publishing Date: 31-05-2011
ISSN (Online): 1985-2347



IJBB Journal is a part of CSC Publishers
http://www.cscjournals.org


Published in Malaysia

Typesetting: Camera-ready by author, data conversation by CSC Publishing Services – CSC Journals, Malaysia

**CSC Publishers, 2011**

# EDITORIAL PREFACE

This is the second issue of volume five of International Journal of Biometric and Bioinformatics (IJBB). The Journal is published bi-monthly, with papers being peer reviewed to high international standards. The International Journal of Biometric and Bioinformatics is not limited to a specific aspect of Biology but it is devoted to the publication of high quality papers on all division of Bio in general. IJBB intends to disseminate knowledge in the various disciplines of the Biometric field from theoretical, practical and analytical research to physical implications and theoretical or quantitative discussion intended for academic and industrial progress. In order to position IJBB as one of the good journal on Bio-sciences, a group of highly valuable scholars are serving on the editorial board. The International Editorial Board ensures that significant developments in Biometrics from around the world are reflected in the Journal. Some important topics covers by journal are Bio-grid, biomedical image processing (fusion), Computational structural biology, Molecular sequence analysis, Genetic algorithms etc.

The initial efforts helped to shape the editorial policy and to sharpen the focus of the journal. Starting with volume 5, 2011, IJBB appears in more focused issues. Besides normal publications, IJBB intend to organized special issues on more focused topics. Each special issue will have a designated editor (editors) – either member of the editorial board or another recognized specialist in the respective field.

The coverage of the journal includes all new theoretical and experimental findings in the fields of Biometrics which enhance the knowledge of scientist, industrials, researchers and all those persons who are coupled with Bioscience field. IJBB objective is to publish articles that are not only technically proficient but also contains information and ideas of fresh interest for International readership. IJBB aims to handle submissions courteously and promptly. IJBB objectives are to promote and extend the use of all methods in the principal disciplines of Bioscience.

IJBB editors understand that how much it is important for authors and researchers to have their work published with a minimum delay after submission of their papers. They also strongly believe that the direct communication between the editors and authors are important for the welfare, quality and wellbeing of the Journal and its readers. Therefore, all activities from paper submission to paper publication are controlled through electronic systems that include electronic submission, editorial panel and review system that ensures rapid decision with least delays in the publication processes.

To build its international reputation, we are disseminating the publication information through Google Books, Google Scholar, Directory of Open Access Journals (DOAJ), Open J Gate, ScientificCommons, Docstoc and many more. Our International Editors are working on establishing ISI listing and a good impact factor for IJBB. We would like to remind you that the success of our journal depends directly on the number of quality articles submitted for review. Accordingly, we would like to request your participation by submitting quality manuscripts for review and encouraging your colleagues to submit quality manuscripts for review. One of the great benefits we can provide to our prospective authors is the mentoring nature of our review process. IJBB provides authors with high quality, helpful reviews that are shaped to assist authors in improving their manuscripts.

**Editorial Board Members**
International Journal of Biometric and Bioinformatics (IJBB)

# EDITORIAL BOARD

# TABLE OF CONTENTS

Volume 5, Issue 2, May 2011

## Pages

# Biometric Template Protection With Robust Semi – Blind Watermarking Using Image Intrinsic Local Property

**Mita C. Paunwala** *mpaunwala@yahoo.co.in*
*Assistant Professor, ECC dept.*
*C.K.Pithawala college of Engg. & Tech.*
*Surat, 395007, India*

**Suparva Patnaik** *ssp@eced.svnit.ac.in*
*Professor, ECED*
*S V National Institute of Technology*
*Surat, 395007, India*

**Abstract**

This paper addresses a biometric watermarking technology sturdy towards image manipulations, like JPEG compression, image filtering, and additive noise. Application scenarios include information transmission between client and server, maintaining e-database and management of signatures through insecure distribution channels. Steps involved in this work are, a) generation of binary signature code for biometric, b) embedding of the binary signature to the host image using intrinsic local property, that ensures signature protection, c) host image is then made exposed to various attacks and d) signature is extracted and matched based on an empirical threshold to verify the robustness of proposed embedding method. Embedding relies on binary signature manipulating the lower order AC coefficients of Discrete Cosine Transformed sub-blocks of host image. In the prediction phase, DC values of the nearest neighbor DCT blocks is utilized to predict the AC coefficients of centre block. Surrounding DC values of a DCT blocks are adaptively weighed for AC coefficients prediction. Linear programming is used to calculate the weights with respect to the image content. Multiple times embedding of watermark ensures robustness against common signal processing operations (filtering, enhancement, rescaling etc.) and various attacks. The proposed algorithm is tested for 50 different types of host images and public data collection, DB3, FVC2002. FAR and FRR are compared with other methods to show the improvement.

**Keywords:** Biometric Watermarking, Image Manipulation, Edge Block Analysis, Fingerprint Matching, Security System.

## 1. INTRODUCTION

Biometric technologies are defined as automated methods of identifying or authenticating the identity of a person based on unique physiological or behavioral characteristics. Biometric technologies used in well-designed ID systems ensure that the individual presenting a secure ID credential has the absolute right to use that credential. Biometric watermarking applications are broadly classified into two categories. In one scenario one biometric is embedded in another, which merely acts as a carrier to secure the former genuine biometric. In the second scenario, two biometrics first one embedded in the second biometric is further encoded in smart cards to enhance the security. Smart ID cards often provide the secure, convenient and cost-effective ID technology that stores the enrolled biometric template and compares it to the "live" biometric template. Smart cards are finding their applications in identification areas such as driving licenses, national identity cards, electronic passports, new generation credit cards, driving licenses etc. A secure ID system using smart card and biometric technology provides:

- Enhanced privacy, securing information on the card, allowing the individual to control access to that information and removing the need for central database access during identity verification.
- Improved system return on investment through the flexibility and upgradability that smart cards provide, allowing support of different authentication methods and multiple, evolving applications.

Ratha et al. [1] produce a generic biometric system with eight possible sources of attacks. The hierarchical positions of attacks are shown in the figure 1. These attacks can be any one or more from the followings, fake biometric (fake finger, a face mask etc), an old recorded signal (old copy of fingerprint, recorded audio signal of a speaker etc.), a feature extractor could be forced to produce feature value chosen by attacker than that of the actual one, synthetic feature set, artificially match score, manipulated template and a channel between stored template and matcher change the content of the stored template. All of these attacks decrement the overall efficiency of the system.

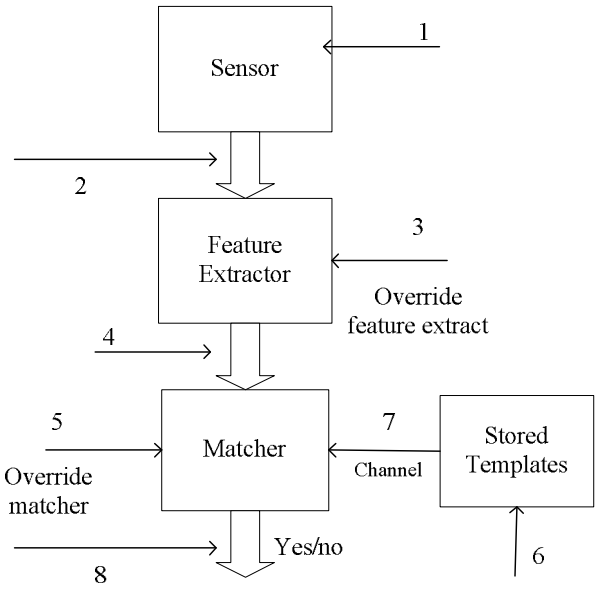


**FIGURE 1:** Generic biometric based system with possible attacks [2].

In [2] author points out that a biometrics based verification system works properly only if the verifier system gives guarantee that the biometric data came from the genuine person at the time of enrollment and also at the access time of the system. Though biometric data gives uniqueness to the person, it is not secure. However the user will not learn that his/her biometric is revealed as he/she leaves fingerprint on surface he/she touches and the face of the person can be easily captured by camera. As a solution to attacks at level 6, 7 and above mentioned problem we proposed an idea to hide biometric data into an visually uncorrelated host image to reduce the manipulation rate.

Many of the biometric security system have been proposed and reviewed in [3] [4] [5] [6] etc. Compared with other biometrics features, the fingerprint technique is the most solicited and has the largest market shares as well as it can be easily used and their features are highly reliable. There are several watermarking techniques which have been proposed and experimented with promising methods for copyright protection, authentication and other applications. Most of the recent work in watermarking can be grouped into two categories: spatial domain methods [7], [8], [9] and frequency domain methods [10], [11] and [12]. There is a current trend towards approaches that make use of information about the human visual system (HVS) to produce a more robust watermark. Such techniques use explicit information about the HVS to exploit the limited dynamic range of the human eye and are presented in [13] [14] and [15].

There have been only a few published papers on biometric watermarking of fingerprint images. In [16] author proposed Bio-hashing and cancelable fingerprint template transformation techniques based on six metrics to protect biometric trait, facilitates the security evaluation and vulnerable to linkage attacks. In [17] author proposed multiple watermarking algorithm in texture regions of fingerprint image using discrete wavelet transform. They used Face and text information as watermark. Their approach is resilient to common attacks such as compression, filtering and noise. In [18] spatial domain fragile watermarking method for fingerprint image verification was proposed. The method can localize any region of image that has been tampered. Authors conclude that their watermarking technique does not lead to a significant performance loss in fingerprint verification. The fragile watermarking method discussed is used to detect the tampering effect but fail for retrieving original biometric. In [19] author proposed scheme for template protection with steganography in which the secret key (which is in the form of pixel intensities) will be merged in the picture itself while encoding, and at decoding end only the authentic user will be allowed to decode. But author has not discussed sturdiness of algorithm for various channel attacks. In [20], a semi unique key based on local block averages was used to detect tampering of host images, which includes fingerprints and faces. The technique is robust enough to detect even the most minor changes and determine where such changes took place in the image. In [21] two spatial domain watermarking methods for fingerprint images are used, in which the first method utilizes gradient orientation analysis in watermark embedding and second method preserves the singular points in the fingerprint image. Multiple times embedding of watermark results in almost accurate retrieval of watermark but it fails against compression and rotation attacks since watermarking approach is in special domain.

Our proposed algorithm is intended for applications like electronic passport (Fig.2). The e-passport represents a major shift in passport technology, with the introduction of semiconductor chips and biometrics. The major security issues that need to be addressed while using a contact less chip to store secure information are skimming, eavesdrop ping, cloning etc. The problem can be solved by providing ID card along with user fingerprint data hidden inside, instead of having chip. The verification requires simultaneous submission of the live biometric and ID card. At an access control site, the same biometric, for example the fingerprint of the person possessing the card, will be sensed and at the same time the fingerprint feature hidden inside the card ( Fig.2) is extracted for matching. Person identified as genuine or pretender based on match score obtained by proposed matching algorithm. Our approach can be used for other application in which user gives pin code/password and based on that, biometric data of particular user is accessed from data base and match with biometric of user present at the place (dash-dot line representation in Fig.2). However the idea can be extended for other trait or multimodality. An application scenario with various components is shown in Fig.2. It also presents interconnection of various sections.

Section 2 describes the detailed approach of minutiae extraction algorithm. Section 3 and 4 explains the proposed watermarking and matching algorithm respectively. The results obtained and concluding remarks are illustrated in section 5.

## 2. FINGERPRINT MINUTIAE EXTRACTION

In this work our main inclination is towards hiding of biometric template. This section briefly explains fingerprint minutiae (biometric template) extraction technique. To employ fingerprint minutiae extraction step sensed print undergoes few necessary steps. In this work we have routed the raw finger print through steps like a) pre-processing: to extract level fingerprint area and remove the boundary, morphological OPEN operation to removes peaks introduced by background noise and CLOSE to eliminates small cavities generated by improper pressure of fingerprint b) thinning: required to remove erroneous pixels; destroy the integrity of spurious bridges and spurs, exchange the type of minutiae points and miss detect true bifurcations. c) False minutiae removal: required to remove false ridge breaks due to insufficient amount of ink and ridge cross-connections due to over inking. Furthermore, all the earlier stages themselves occasionally introduce some artifacts which later lead to spurious minutia. Finally, we get the feature vector comprising of minutiae position and orientation, later used for matching purpose.

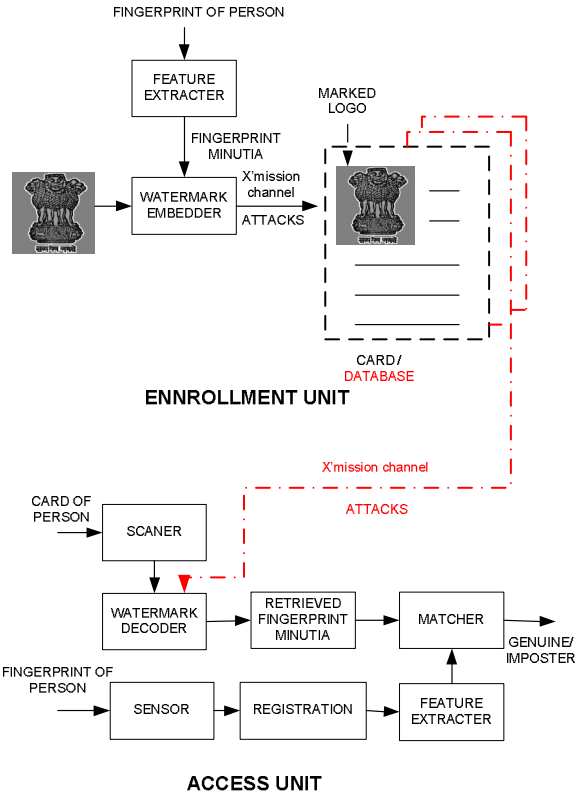


**FIGURE 2:** Application Scenario.

## 3. PROPOSED WATERMARKING APPROACH

We have proposed a DCT based semi-blind watermarking technique. In which watermark (fingerprint minutiae template) is embedded by modulating low frequency band AC coefficients of 8 x 8 block by its estimated values. Estimation is done using the DC coefficients of 8 neighboring blocks**.** In [22] authors provide the relation between estimated AC coefficient and neighborhood DC coefficients but not considered the variations in the image for AC coefficient estimation. The proposed method considers the local block variations in the image and accordingly AC coefficients are estimated with different equations. Linear Programming based optimization technique [23] is then considered to calculate weights based on image content. Furthermore each watermark bit is embedded multiple times to ensure robustness against various attacks and signal processing operations.

### 3.1 Optimization procedure

Any linear program (LP) consists of four parts: a set of decision variables, parameters, objective function, and a set of constraints. The objective function is to fulfill the decision-maker's desire (objective), whereas the constraints which shape the feasible region usually come from the decision-maker's environment putting some restrictions/conditions on achieving the objective.

#### *3.1.1 Block wise DCT Computation*

In the proposed approach linear programming based optimization is used to estimate the coefficients using the neighborhood knowledge. Original image X of some arbitrary size M x N is divided into 8 x 8 blocks. Let $x_{ij}$ be a pixel value from the block, then 1≤ i ≤8 and 1≤ j ≤8. Each block is transformed into $y_{ij}$ by applying two dimensional DCT (Discrete Cosine Transform).

Each $x_{ij}$ block is then categorized into smoother block or edge blocks by measuring block variance.

$$v = \frac{\sum_{i=1}^{8}\sum_{j=1}^{8}\left(x_{ij} - \mu\right)^2}{63} \quad (1)$$

Where $\mu$ is mean of block. Variance being very sensitive to uncertainties is used as a decisive parameter to decide the block sensitivity with further uncertainties. The blocks with variance ($v$) greater than threshold (th) are classified as edge blocks and block variance equal or less than threshold (th) are marked as smoother blocks. Optimization procedure is applied only to smoother blocks. Variance being very sensitive to uncertainties is used as a decisive parameter to decide the block sensitivity towards uncertainties. Watermark embedding causes intensity alteration leading to rise in uncertainties. Blocks with lesser sensitivity are suitable for embedding.

*3.1.2 Weight Computation*

To calculate the weight, first known AC coefficients values of benchmark images are used. AC prediction method uses unquantized DC values of a 3x3 neighborhood blocks to estimate the AC coefficients for the center block. As shown in Fig. 3 estimation of various AC coefficients of block-5 is done using DC1~DC9.

| | | |
|---|---|---|
| DC1 | DC2 | DC3 |
| DC4 | DC5 | DC6 |
| DC7 | DC8 | DC9 |

**FIGURE 3:** Neighborhood of DCT blocks.

AC components AC(1,2) and AC(1,3) represents the horizontal variations. Hence, DC4, DC5 and DC6 are considered in the objective function. AC components AC(2,1) and AC(3,1) represents the vertical variations. Hence, DC2, DC5 and DC8 are considered in the objective function. AC(2,2) represents the diagonal variations. Hence, DC1, DC3, DC7 and DC9 are considered. Decision variables are K1 to K14. Objective functions to be optimized are given below:

$$\begin{aligned} AC(1,2) &= k_1 * DC4 + k_2 * DC6 \\ AC(2,1) &= k_3 * DC2 + k_4 * DC8 \\ AC(2,2) &= k_5 * DC1 + k_6 * DC3 + k_7 * DC7 + k_8 * DC9 \\ AC(1,3) &= k_9 * DC4 + k_{10} * DC5 + k_{11} * DC6 \\ AC(3,1) &= k_{12} * DC2 + k_{13} * DC5 + k_{14} * DC8 \end{aligned} \quad (2)$$

Constraints are $-1 \leq k_1, \ldots, k_{14} \leq 1$. The solution of the above equation gives optimal weights.

**3.1.3 Semi Blind Watermarking Approach**

Technique of watermarking proposed here avoids use of host image for watermark detection and hence is blind. Discrete Cosine Transform is not rotation invariant and hence is not robust against rotation attack. As a solution we will transmit principal direction of watermarked image along with it hence is semi blind. Principal direction is the direction along which there are more straight lines. The Radon transform along this direction usually has larger variations. The variance of the projection of Radon transform of the image at this direction is locally maximum. If the variance of the projection has more than one local maximum, we may calculate the second derivative of the variance to distinguish between all local maxima.

As we know, most of the signal energy of the block DCT is compressed in the DC component and the remaining energy is distributed diminishingly in the AC components in zigzag scan order. For watermarking, robustness and imperceptions are the challenges. Hiding of watermark bit in DC co-efficient gives more robustness but perception of watermark is then a major issue and vice versa is true for high frequency AC coefficients.

In our approach we have selected AC co-efficient nearest to DC coefficient for each smoother blocks as in Fig.3, unlike the DC coefficient used in choi's method [24] for hiding watermark (fingerprint minutia). Furthermore we embed each watermark bit multiple times to get robustness. Embedding steps are as given below.

Step 1: Apply radon transform to the host image and calculate the variance for all angles between 0 - 179 degree.
Step 2: Find out local maxima by applying second order derivative. Find out corresponding direction where maximum is projected. The resultant direction is known as principal direction of host image ($\phi_o$).
Step 3: Convert minutia points into binary pattern 'w'.
Step 4: Apply 8 x 8 DCT to the host image and categorized edge block and smoother block.
Step 5: Select the $AC_i$ ,1≤ i ≤5 coefficient nearest to its DC coefficient of smoother block and estimates its value ($\overset{\Lambda}{AC_i}$ ) from its neighborhood blocks $DC_j$, 1≤ j ≤ 9 co-efficient as in Eq.(2).
Step 6: Modulate each selected AC coefficient with following translation rule

$$
\begin{aligned}
&For\ \ w(k)=1\\
&\quad if\ \ AC_i > \overset{\Lambda}{AC}_i\\
&\qquad then\ \ AC_i = AC_i + TH_i\\
&\quad else\\
&\qquad AC_i = \overset{\Lambda}{AC}_i + TH_i\\
&for\ \ w(k)=0\\
&\quad if\ \ AC_i < \overset{\Lambda}{AC}_i\\
&\qquad then\ \ AC_i = AC_i - TH_i\\
&\quad else\\
&\qquad AC_i = \overset{\Lambda}{AC}_i - TH_i
\end{aligned}
$$

where, $TH_i$ is threshold value which gives robustness against various attacks. Higher the value of $TH_i$, robustness is better but at the same time perceptibility (artifacts) is high. So selection of $TH_i$ is a tradeoff between robustness and imperceptions. Its value is decided locally, as 10-20% of corresponding coefficient.
Step 7: Embed each watermark bit at multiple location.
Step 8: Apply inverse 8x8 DCT with modified AC coefficients values to get watermarked image.

At the decoding side, before extracting watermark bit first find principal direction of watermarked image ($\phi_r$). If watermarked image is rotated then principal direction of the watermarked image is different than that of transmitted direction. Take a difference of both direction and de-rotate watermarked image by difference angle ($\phi_d$). Decoding of watermark bit requires estimated value $\overset{\Lambda}{AC_i}$ of coefficient and original $AC_i$ to extract watermark bit. If $AC_i$ > $\overset{\Lambda}{AC_i}$ then extracted bit is '1', otherwise if $AC_i$ < $\overset{\Lambda}{AC_i}$ then extracted bit is '0'. Each watermark bit gathered from multiple locations and maximum of that is considered as retrieved bit. The technique proposed here is semi blind watermarking as it requires knowledge of principal direction ($\phi_o$).

## 4. MATCHING APPROACH

Matching stage used here is similar to that proposed in [25], establish the number of consequent minutia pairs to compute the final matching score after alignment. The difference of our approach is only that, we calculates minutiae matching score based on similarity between matching minutiae pair by avoiding triangular matching method and fix feature vector length to avoid

complexity. Furthermore, we limit the ridge orientation between 0° and 180°. Matching task can be easily completed, if two minutia patterns are exactly aligned. However, in practice, such a situation is rarely encountered.
Non-linear deformation of fingerprint makes impossible to have exact location of minutia point than that in the template. Also location and direction error makes matching task complex. Therefore, the matching algorithm needs to be elastic which means that it should be capable of tolerating, the deformations due to the location and direction errors and non-linear deformations to some extent. Keeping the above idea as the target, we have proposed a relaxed idea as the part of matching algorithm in this paper.
In alignment stage, the global structure of a minutia describes a rotation and translation invariant feature of the minutia in its neighborhood. The novel structure of each minutia we construct in this paper is not sensitive to noise because it only depends on the global finger print orientation field which is relatively robust to noise. Our structure capturing the affluent information on fingerprint ridge-orientation pattern which is more discriminative than the local minutia structure described in [26].

### 4.1 Feature Vector Structure

A minutia point $M_k$ detected from a fingerprint can be described by a feature vector given by

$$F_k = (x_k\, y_k \phi_k), \tag{3}$$

Where, ($x_k$, $y_k$) describes the location and $\varnothing_k$ is the ridge orientation. Note that in a fingerprint image, there is no difference between a local ridge orientation of 0° and 180°, since the ridges oriented at 0° and the ridges oriented at 180° in a local neighborhood cannot be differentiated from each other. So, the value of $\varnothing_k$ is commonly set in the range from 0 to π according to the Eq. (4). Given a minutia point $M_k$ with orientation $\varnothing_k$, we define a grid structure with N directional metric. Principal axis oriented along the orientation of $M_k$.

$$\phi_k = \begin{cases} \phi_k & if \;\; 0 \le \phi_k < \pi, \\ \phi_k - \pi & if \;\; \pi \le \phi_k < 2\pi \end{cases} \tag{4}$$

Let $\theta_1 = \varnothing_k$, $\theta_2 = \theta_1 + 360/N$ and $\theta_N = \theta_{N-1} + 360/N$. We plot N metric along the angles [$\theta_1$, $\theta_2$, $\theta_3$,…$\theta_N$] with respect to X axis through the minutia point $M_k$ as shown in Fig. 4(a). Grid nodes as shown in Fig. 4(b) are marked along each metric at an interval of τ starting with the minutia point $M_k$. Larger the value of N and smaller the value of τ will increase the size of feature vector. This will give better accuracy at the cost of increased computational complexity. By defining the orientation of grid nodes as, (1 ≤ dm ≤ N), we calculate the relative direction between minutia $M_k$ and grid nodes as

$$\psi^{k}_{i,d_m} = d\psi(\phi_k, \phi^{k}_{i,d_m}) \tag{5}$$

is free from the rotation and translation of the fingerprint. Where, $\phi^{k}_{i,d_m}$, represents the orientation of grid nodes. The orientation of grid node falls in furrows is considered as 0 degree. We have considered five grid nodes for each directional metric, specified feature vector of size 1 x 15 for each minutiae point as shown in Eq. (6). The final feature vector $F_k$ of a minutia $M_k$ that describes its structure characteristic with global fingerprint orientation field is given by Eq. (7).

$$[0.12,\ 0.78,\ 0,\ 0,\ -0.15,\ -0.15,\ -0.15,\ 0.58,\ 0.78,\ 0,\ 0,\ 0,\ 0.78,\ 0.78,\ 0] \tag{6}$$

$$F_k = \left\{ \left\{ \psi^{k}_{i,d_m} \right\}_{i=1}^{n^{k}_{d_m}} \right\}_{m=1}^{N} \tag{7}$$

Where, $n^{k}_{d_m}$ gives number of grid nodes along the direction metric $d_m$ corresponding to $k^{th}$ minutiae. The structure feature vector $F_k$ is invariant to rotation and translation of the fingerprint.

Suppose $F_i$ and $F_j$ are the structure feature vectors of minutia $i$ from input fingerprint and minutia $j$ from template fingerprint, respectively. A similarity level is defined as

$$S(i,j)=\begin{cases}\dfrac{T-\left|F_i-F_j\right|}{T} & if\ \left|F_i-F_j\right|<T,\\ 0 & otherwise\end{cases} \tag{8}$$

Where, $|F_i - F_j|$ is the Euclidean distance between feature vectors $F_i$ and $F_j$ and $T$ is the predefined threshold between 0 and 1. Here the selection of the value of $T$ is tradoff between FAR and FRR, high value of T increases FAR and opposite is true for FRR. Here, the similarity level describes a matching assurance level of a structure pair and define as $S(i, j)$, $0 \le S(i, j) \le 1$, instead of simply matched or not matched. $S(i, j)$=1 implies a perfect match, while $S(i, j)$=0 implies a total mismatch.

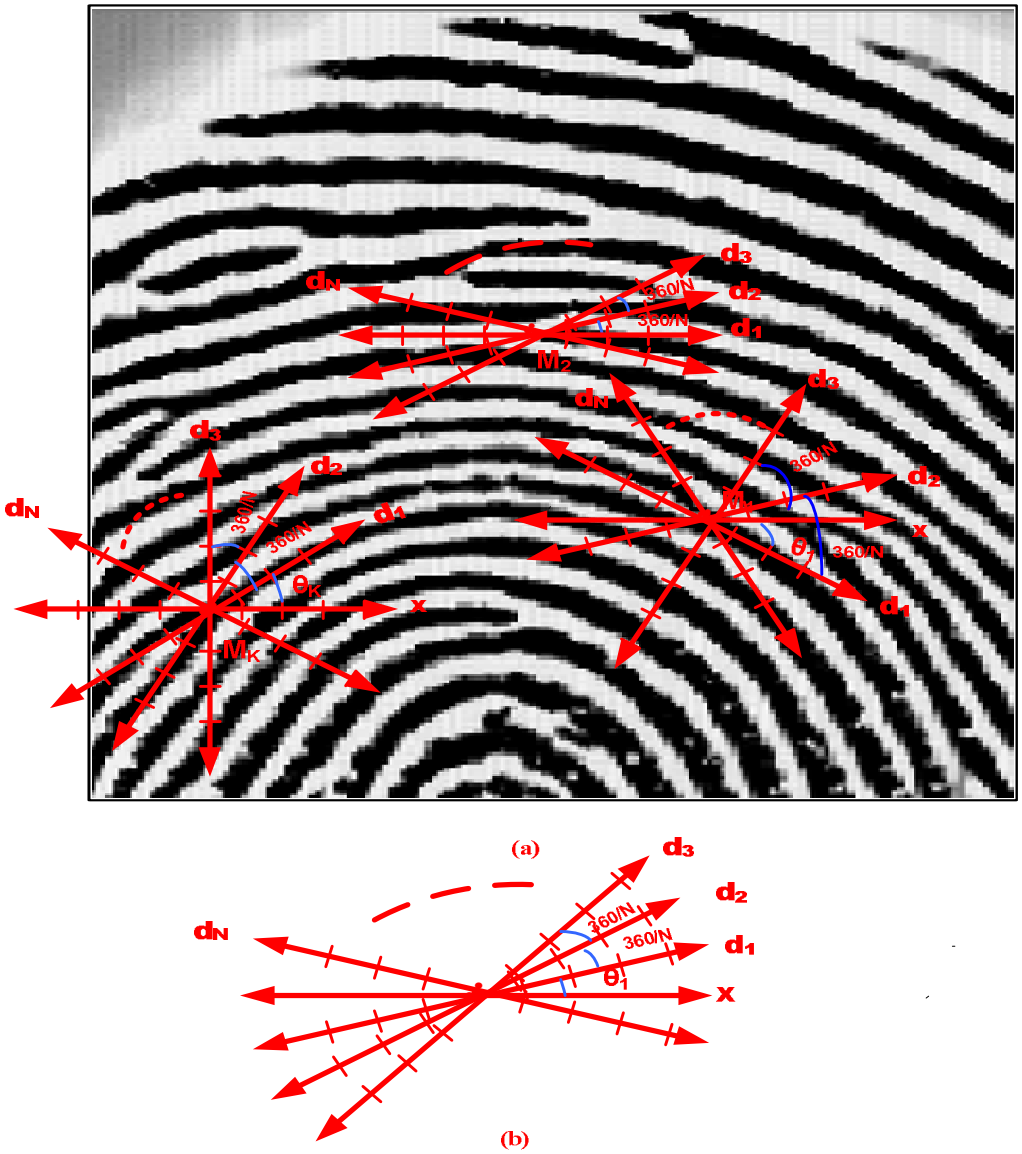


**FIGURE 4:** (a) N lines around a minutia detail (b) Grid nodes organized on directional metric.

### 4.2 Matching of Global Minutiae Structure

With the defined feature vectors, we compute matching score based on consequent minutia pairs. Degree of similarity between two fingerprint decides genuine/imposter attempt. In order to compute matching score, we need to identify a set of consequent minutia pairs from template and input fingerprint.

System identifies a user truly if the match score is computed with reliable consequent point pairs. In order to have reliable consequent point pair input finger must be properly aligned with template fingerprint. The alignment stage is intended to recover the geometric transformation between the two fingerprint impressions. In our work, the rigid transformation, i.e., translation vector ($t = [tx, ty]^T$) and rotation angle ($\emptyset$), is recovered by the best-matched structure pair that exhibits the largest similarity value in Eq. (8). The best-matched minutia structure pair (s1, s2), minutia s1 from the input fingerprint and another s2 from the template fingerprint is obtained by maximizing the similarity level as

$$S(s_1, s_2) = \max_{i,j}(S(i, j))$$

$$\phi = D(s_2) - D(s_1) \text{ and } t = P(s_2) - R_{\phi}(s_1) \tag{9}$$

Where, $R_{\emptyset}$ denotes the 2 × 2 operator of counter clockwise rotation used to find the position of rotated minutia (s1) and the position of a minutia s2 are denoted by $P(s2) = [x(s2), y(s2)]^T$. Direction of minutia is denoted by $D(s)$. Applying the estimated geometric transformation onto the minutiae from the test fingerprint we obtain the list comprising the aligned minutiae. Also, the orientation field from the test fingerprint will be aligned using the estimated transformation simultaneously.

The non-linear deformations and deformations due to the location and direction errors can be tolerate to some extent by having elastic matching algorithm, achieved by selecting bounding box Bg in the feature space instead of an exact matching. A small size bounding box *Bg* is chosen to get two consequent minutiae lists L1 and L2 which are from the template fingerprint and the test fingerprint, respectively. The pairs with the largest similarity level values in Eq. (8), which, also fall in the bounding box *Bg* are considered as consequent minutiae pairs. Here the size of bounding box is tradeoff between the false acceptance rate (FAR) and the false rejection rate (FRR).

### 4.3 Matching Score Computation

With the introduction of our minutia structures and similarity of consequent minutia pairs, matching score can be determined by Mm. Let N1 and N2 denote the number of minutiae located inside the intersection of the two fingerprint images for test and template fingerprints, respectively. The minutia matching score Mm can be calculated according to the following equation.

$$M_m = \frac{\sum_{i,j} S(i, j)}{\max\{N_1, N_2\}}, \tag{10}$$

where i, j is the consequent minutiae pair, one from test fingerprint and another from template fingerprint, respectively, and S(i, j) is computed according to Eq. (8).

## 5. EXPERIMENTAL EVALUATION

Experiments are performed on four bench mark images as given in Fig. 5 to calculate the optimal weights. All objective functions are simplified by using above four images based on image content. Variance threshold of 1000 is selected to distinguish smoother blocks from edge blocks. Weights derived from experiments are given in Table 1.

The algorithm proposed above is tested on the public domain collection of fingerprint images, DB3 in FVC2004. It comprises 800 fingerprint images of size 300×480 pixels captured at a resolution of 512dpi, from 100 fingers (eight impressions per finger). Individual minutiae data sets contained between 25 to 35 minutiae points, with an average of 30 minutiae points. Experiment is performed for 50 different types (low freq, medium freq., high freq., highly textured etc.) of host images of size 512 x 512. Out of them results for four images shown in Fig. 6 are presented here.

Before hiding, first watermark (fingerprint minutia) is converted into bit stream. Each minutia is represented by 27 bit.


(a) Lena

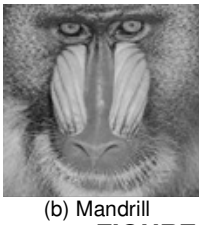
(b) Mandrill

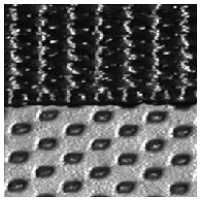
(c) Texture

(d) Bank logo

**FIGURE 5:** Benchmark Images

| $K_1$ | $K_2$ | $K_3$ | $K_4$ | $K_5$ | $K_6$ | $K_7$ | $K_8$ | $K_9$ | $K_{10}$ | $K_{11}$ | $K_{12}$ | $K_{13}$ | $K_{14}$ |
|---|---|---|---|---|---|---|---|---|---|---|---|---|---|
| 0.20 | -0.20 | 0.19 | -0.19 | 0.03 | 0.03 | -0.03 | -0.03 | 0.06 | -0.12 | 0.06 | 0.09 | -0.18 | 0.09 |

**TABLE 1:** Weights of Objective functions

We watermark each host image with our method as well as with Choi's method. Let I (i, j) the original host image and I'(i, j) is the watermarked image. We measure the imperceptibility of watermark by calculating PSNR value as per Eq. (11).

$$PSNR = 20\log_{10}(255/RMSE)$$
$$where, RMSE = \left\{\sum[I(i,j) - I'(i,j)]^2 / N^2\right\}^{1/2} \quad (11)$$

Here N is total no. of pixels in Image I.

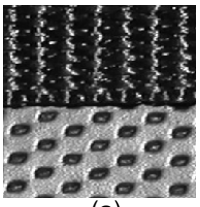
(a)


(b)


(c)

(d)

**FIGURE 6:** Host images (a) Texture (high frequency) (b) cameraman (medium frequency) (c) India logo (low frequency) (d) Bank logo (low frequency)

PSNR values for four types of images are listed in Table 2. It shows that the PSNR value of our method is higher than Choi's method. This is because in Choi's method watermark is embedded into DC Coefficient, which decides the block average. So, even a small variation in DC coefficients only effects intensity of all the pixels within the block and hence results in low PSNR.

| Image | Imperceptibility Measurement PSNR | | Quality Factor (Q) | Compre - ssion (BPP) | Watermark Extraction BER(%) | | FAR (%) | | FRR (%) | |
|---|---|---|---|---|---|---|---|---|---|---|
| | Our Method | Choi's | | | Our Method | Choi's | Our Method | Choi's | Our Method | Choi's |
| Texture | 37.2025 | 35.7245 | 90 | 2.8527 | 0 | 0.93 | 0.17 | 0.20 | 0.18 | 0.21 |
| | | | 80 | 2.1015 | 0 | 0.93 | 0.17 | 0.20 | 0.18 | 0.21 |
| | | | 75 | 1.8981 | 0 | 0.93 | 0.17 | 0.20 | 0.18 | 0.21 |
| Cameraman | 38.2340 | 34.8972 | 90 | 2.1323 | 0 | 2.47 | 0.17 | 0.24 | 0.18 | 0.22 |
| | | | 80 | 1.4608 | 0 | 2.47 | 0.17 | 0.24 | 0.18 | 0.22 |
| | | | 75 | 1.2816 | 0.1 | 2.47 | 0.17 | 0.24 | 0.18 | o.22 |
| India logo | 48.7235 | 36.8863 | 90 | 2.5463 | 0 | 0.93 | 0.17 | 0.20 | 0.18 | 0.21 |
| | | | 80 | 1.8955 | 0 | 0.93 | 0.17 | 0.20 | 0.18 | 0.21 |
| | | | 75 | 1.7143 | 0 | 0.93 | 0.17 | 0.20 | 0.18 | 0.21 |
| Bank logo | 42.0910 | 39.6230 | 90 | 1.9196 | 0 | 1.35 | 0.17 | 0.20 | 0.18 | 0.21 |
| | | | 80 | 1.4365 | 0 | 1.35 | 0.17 | 0.20 | 0.18 | 0.21 |
| | | | 75 | 1.3010 | 0.5 | 1.35 | 0.17 | 0.20 | 0.18 | 0.21 |

**TABLE 2:** Watermark Extraction Error Rate due to JPEG Compression and Matching Accuracy of fingerprint

We have compared the robustness of our method with existing Choi's method under different channel attacks like compression, salt & pepper noise and rotation. Comparison is done based on watermark extraction error rate, False Acceptance rate (FAR) and False Rejection Rate (FRR).
The results in Table 2 illustrate the extraction error rate for JPEG compressed watermarked image. With the same measuring parameter, Table 3 shows the extraction error rate for salt & pepper noise attacked watermarked image. Table 4 shows results for measuring parameter after combine above two attacks. In all cases our method appears better than Choi's method. Our matching algorithm results FAR and FRR as 0.17% and 0.18% respectively, without watermarking, which remains exactly same with our watermarking technique without any attack. In presence of different attacks FAR and FRR undergoes minor change, unlike to Choi's method. These are highlighted in Table 2, 3 and 4. Proposed technique is also robust against various signal processing operations like enhancement (gamma=), rescaling (512-256-512) and filtering (average). For all mentioned operation FAR and FRR of the system remains same as without watermarking approach.

| Image | Watermark Extraction BER(%) | | FAR (%) | | FRR (%) | |
|---|---|---|---|---|---|---|
| | Our Method | Choi's | Our Method | Choi's | Our Method | Choi's |
| Texture | 0 | 1.33 | 0.17 | 0.19 | 0.18 | 0.21 |
| cameraman | 0.02 | 2.25 | 0.17 | 0.24 | 0.18 | 0.24 |
| India logo | 0.08 | 1.45 | 0.17 | 0.19 | 0.18 | 0.21 |
| Bank logo | 0.01 | 3.97 | 0.17 | 0.26 | 0.18 | 0.25 |

**TABLE 3:** Watermark Extraction Error Rate due to salt & pepper noise (Density = 0.02) and Matching Accuracy of fingerprint

| Image | Quality Factor (Q) | Watermark Extraction BER(%) | | FAR (%) | | FRR (%) | |
|---|---|---|---|---|---|---|---|
| | | Our Method | Choi's | Our Method | Choi's | Our Method | Choi's |
| Texture | 90 | 0.32 | 1.36 | 0.17 | 0.20 | 0.18 | 0.21 |
| | 80 | 0.32 | 1.36 | 0.17 | 0.20 | 0.18 | 0.21 |
| | 75 | 0.32 | 1.36 | 0.17 | 0.20 | 0.18 | 0.21 |
| cameraman | 90 | 0.74 | 3.39 | 0.17 | 0.24 | 0.18 | 0.22 |
| | 80 | 0.74 | 3.35 | 0.17 | 0.24 | 0.18 | 0.22 |
| | 75 | 0.44 | 3.35 | 0.17 | 0.24 | 0.18 | 0.22 |
| India logo | 90 | 0.2 | 4.23 | 0.17 | 0.26 | 0.18 | 0.26 |
| | 80 | 0.2 | 1.59 | 0.17 | 0.20 | 0.18 | 0.22 |
| | 75 | 3.2 | 4.26 | 0.23 | 0.24 | 0.21 | 0.22 |
| Bank logo | 90 | 0.39 | 4.45 | 0.17 | 0.26 | 0.18 | 0.26 |
| | 80 | 0.39 | 4.43 | 0.17 | 0.26 | 0.18 | 0.26 |
| | 75 | 2.9 | 4.39 | 0.20 | 0.26 | 0.20 | 0.26 |

**TABLE 4:** Watermark Extraction Error Rate due to above combined attacks and matching accuracy of fingerprint

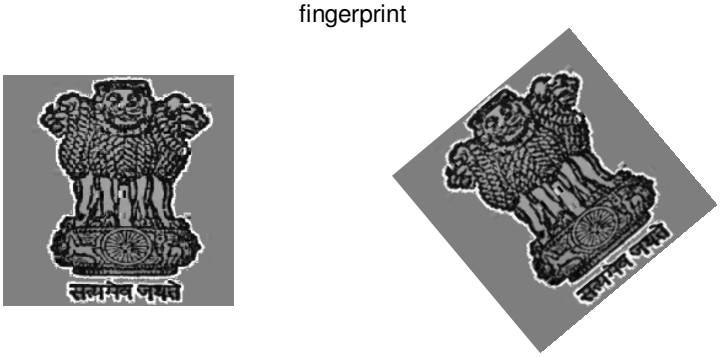

**FIGURE 7:** (a) Watermarked Image (b) Watermarked Image Rotated at 40°

We have also tested robustness of our algorithm for rotation attack. Fig.7 (a) and (b) shows watermarked and watermarked image rotated at 40° angle respectively. Plot of variance of the projections of Radon transformed coefficients for both images are shown in Fig.8 (a) and (b). For rotated image two local maxima was observed. To distinguish between these two maxima, we have calculated 2nd order derivative of the variance as shown in Fig.9.

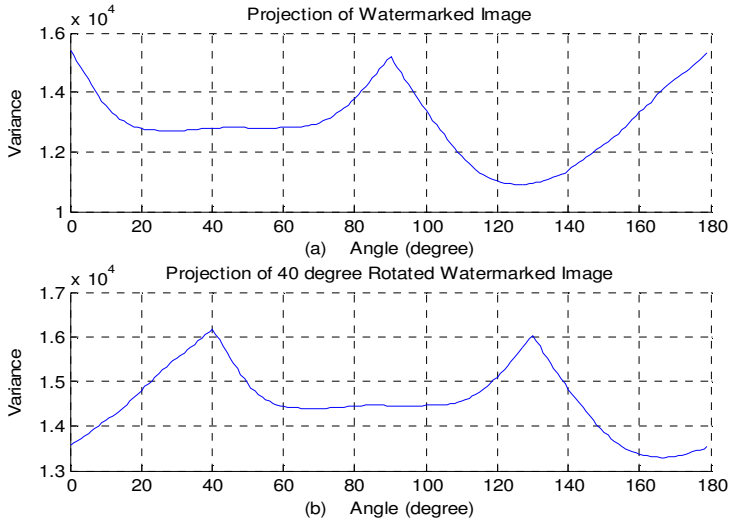


**FIGURE 8:** Variance of projection at different angles for (a) Watermarked Image (b) Rotated watermarked image

In Fig.9 maxima of rotated image is noted at 130°($\phi_r$). The transmitted watermarked image maxima is at 90°($\phi_o$) (Fig.8(a)). The difference between these angles is the required de-rotation angle $\phi_d$.

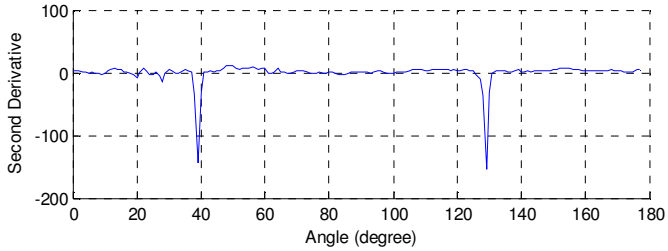


**FIGURE 9:** Second Order Derivative of 8(b)

| Image | Rotation Angle ($Ø_d$) | Watermark Extraction BER(%) | FAR (%) | FRR (%) |
|---|---|---|---|---|
| Texture | 15 | 6.5 | 0.27 | 0.27 |
| | 35 | 7.5 | 0.28 | 0.28 |
| | 75 | 6.5 | 0.27 | 0.28 |
| cameraman | 15 | 8.5 | 0.3 | 0.31 |
| | 35 | 8.5 | 0.3 | 0.31 |
| | 75 | 8.5 | 0.3 | 0.31 |
| India logo | 15 | 10 | 0.35 | 0.33 |
| | 35 | 8 | 0.29 | 0.29 |
| | 75 | 9 | 0.29 | 0.29 |
| Bank logo | 15 | Destroyed | Destroyed | Destroyed |
| | 35 | Destroyed | Destroyed | Destroyed |
| | 75 | Destroyed | Destroyed | Destroyed |

**TABLE 5:** Watermark Extraction Error Rate due to Rotation attack and Matching Accuracy of fingerprint

Table 5 illustrates the performance of security system in terms of FAR and FRR for rotated watermarked image. Here, high watermark extraction error rate is observed due to interpolation bit during de-rotation.

## 6. CONSLUSION & FUTURE WORK

In this paper we present application scenario of security system. In order to overcome the problem of security of fingerprint data we introduced strong semi-blind watermarking algorithm which hides fingerprint data into host image. Thus fingerprint data is protected while transmitted through channel/client to server.

Feature points (minutia points) of fingerprint with explained minutia extraction algorithm are extracted. Our minutia extraction algorithm gives strong feature points by removing false minutia and finally we have 25 to 30 minutia points per finger. These minutia points are embedded into host image by proposed semi-blind watermarking algorithm which is decided by neighborhood based estimation criteria. Our estimator uses AC coefficients as container unlike DC coefficient in Choi's method. It is difficult to set strength of watermark bit in DC coefficient because human eyes are very sensitive to the variation in DC component. In our approach modification in AC coefficients reduces the chances of perceptibility of watermark even with large strength of watermark bit. The payload capacity we obtained is far better than Choi's method. Furthermore, the global channel attack which affects original value as well as estimated value and our watermark extraction algorithm extract watermark bit based on relative value between both, gives good robustness against attack like JPEG compression and salt & noise. Even though we are not able to get 100 percent watermark bit pepper under attacks, our strong distortion-tolerant matching algorithm gives FAR and FRR that are almost same as FAR and FRR without watermarking approach. Our proposed idea can also be used for multimodal system provided, watermarking approach should have high capacity.

## 7. REFERENCES

[1] N.K. Ratha, J.H. Connell, and R.M. Bolle, "*An Analysis of Minutiae Matching Strength*," Proc. Third Int'l.Conf. Audio- and Video-Based Biometric Person Authentication, pp. 223-228, June 2001.

[2] B. Schneier, "*The Uses and Abuses of Biometrics*," Comm. ACM, vol. 42, no. 8, p. 136, Aug. 1999.

[3] Yi Chen, "*Extended Feature Set and Touchless Imaging for Fingerprint Matching*", Ph.D Theses, University of Michigan State, 2009.

[4] Salil Prabhakar, "*Fingerprint Classification and Matching Using a Filterbank",* Ph.D Theses, University of Michigan State, 2001.

[5] Panyayot Chaikan, Montri Karnjanadecha, "*The Use of Top-View Finger Image for Personal Identification"* Proceedings of the 5th International *IEEE* Symposium on image and Signal Processing and Analysis, 343-346, Nov. 2007.

[6] A. K. Jain D. Maltoni, D. Maio and S. Prabhakar. *Handbook of Fingerprint Recognition*. Springer, New York, 2003.

[7] Ashourian, M.; Enteshary, R., "IEEE Conference on Convergent Technologies for Asia-Pacific Region", TENCON, Vol. 1, pp 428-431, 2003.

[8] B. Verma, S. Jain, D. P. Agarwal, and A. Phadikar, "A New color image watermarking scheme," *Infocomp, Journal of computer science*, vol. 5,N.2, pp. 37-42, 2006.

[9] X. Wu and Z.-H. Guan, "A novel digital watermark algorithm based on chaotic maps," *Physics Letters A*, vol. 365, pp. 403-406, 2007.

[10] Feng Yang, Lei Li, "An adaptive, SVM -based watermarking in frequency domain", International Conference on Wavelet Analysis and Pattern Recognition, pp. 465 – 469, Hongkong, 30 sep., 2008.

[11] L. Chun-Shien, H. Shih-Kun, S. Chwen-Jye, and L. Hong-Yuan Mark, "Cocktail watermarking
for digital image protection," *Multimedia, IEEE Transactions on*, vol. 2, pp.209-224, 2000.

[12] W. Lu, H. Lu, and F.L. Chung, "Robust digital image watermarking based on subsampling," *Applied Mathematics and Computation*, vol.181, pp. 886-893, 2006.

[13] Wang-sheng Fang, Kang Chen, "A Wavelet Watermarking Based on HVS and Watermarking Capacity Analysis", IEEE International Conference on Multimedia Information Networking and Security, pp. 141-144, Hubei, Dec., 2009.

[14] Hongping Xu, Xiaoxia Wan, "International Conference on Computer Science and Software Engineering", pp. 245- 248,Hubei, Dec., 2008.

[15] Yanhong Zhang, "Blind watermark algorithm based on HVS and RBF neural network in DWT domain", WSEAS Transactions on Computers, Volume 8, Issue 1, January 2009.

[16] Nagar Abhishk, Nandkumar Karthik, Jain Anil k., "*Biometric Template Transformation: a security analysis*," Proc. SPIE, the International Society for Optical Engineering, vol.7541, 2010.

[17] Noore A., Singh R., Vatsa M. and Houck M.M., " *Enhancing Security of Fingerprints Through Contextual Biometric Watermarking*", Journal of Forensic Science International, Vol. 169, Issue 2, Pp. 188-194 ,July 2007.

[18] S. Pankanti and M.M. Yeung, "*Verification Watermarks on Fingerprint Recognition and Retrieval*," Proc. SPIE, vol. 3657, pp. 66-78, 1999.

[19] Chander Kant, Ranjender Nath & Sheetal Chaudhary, "Biometrics Security using steganography", International Journal of Security, Vol. 2 : Issue (1).

[20] S. Jain, "*Digital Watermarking Techniques: A Case Study in Fingerprints & Faces*," Indian Conf. Computer Vision, Graphics, and Image Processing, pp. 139-144, Dec. 2000.

[21] B. Gunsel, U. Uludag, and A.M. Tekalp, "*Robust Watermarking of Fingerprint Images*," Pattern Recognition, vol. 35, no. 12, pp. 2739-2747, Dec. 2002.

[22] Yulin Wang , Alan Pearmain, "*Blind image data hiding based on self reference"* Pattern Recognition Letters 25, 1681–1689, 2004.

[23] Hiller and Lieberman, *" Introduction to Operations Research*," Seventh edition, Tata McGraw-Hill, 2001.

[24] Choi, Y., Aizawa, I., "*Digital watermarking using interblock correlation*", In: Proc. Internat. Conf. on Image Processing, vol. 2, pp. 16–220, 24–28 October 1999.

[25] J. Qi. and Y. Wang, "*A robust fingerprint matching method*", Pattern Recognition, vol. 35, pp.1655-1671, 2005.

[26] X. Jiang, W.Y. Yau," *Fingerprint minutiae matching based on the local and global structures*", Proc. of the 15th International Conference on Pattern Recognition, vol. 2, pp. 1038–1041, 2000.

# dFuse: An Optimized Compression Algorithm for DICOM-format Image Archive

**Suresh Jaganathan** *whosuresh@gmail.com*
*Assistant Professor*
*Department of Computer Science and Engineering*
*Sri Sivasubramania Nadar College of Engineering,*
*Chennai, Tamilnadu, India*

**Geetha Manjusha M B** *geethamtech0911@gmail.com*
*PG Scholar*
*Department of Computer Science and Engineering*
*Sri Sivasubramania Nadar College of Engineering,*
*Chennai, Tamilnadu, India*

**Abstract**

Medical images are useful for knowing the details of the human body for health science or remedial reasons. DICOM is structured as a multi-part document in order to facilitate extension of these images. Additionally, DICOM defined information objects are not only for images but also for patients, studies, reports, and other data groupings. More information details in DICOM, resulted in large size, and transferring or communicating these files took lots of time. To solve this, files can be compressed and transferred. Efficient compression solutions are available and they are becoming more critical with the recent intensive growth of data and medical imaging. In order to receive the original and less sized image, we need effective compression algorithm. There are different algorithms for compression such as DCT, Haar, Daubechies which has its roots in cosine and wavelet transforms. In this paper, we propose a new compression algorithm called "dFuse". It uses cosine based three dimensional transform to compress the DICOM files. We use the following parameters to check the efficiency of the proposed algorithm, they are i) file size, ii) PSNR, iii) compression percentage and iv) compression ratio. From the experimental results obtained, the proposed algorithm works well for compressing medical images.

**Keywords:** Medical Image, Image Compression, DICOM, Wavelets, Cosine Transforms

## 1. INTRODUCTION

Medical imaging is a regulation within the medical arena which makes use of technology to acquire images of inside the human body. These images are utilized in analytics, as training tools, and in regular healthcare. This sometimes specified as diagnostic imaging, because it is often helps doctors to diagnose easily. One kind of medical images is DICOM. DICOM not only stores the image, but also some details such as patient name, patient-id and date scanned etc. DICOM varies from other data formats, as it contain groups of information together into a data set. A DICOM data object comprises of a number of attributes, comprising items such as ID, DOB, date, name etc. Also one single attribute comprising the image pixel data. In order to maintain more details, file size increases, because of this transferring the file takes a lot of time. To avoid this difficulty, efficient compression techniques [1] are needed.

Image compression focuses [2] on the difficulty of decreasing the quantity of information that are needed to signify an image. This is used to decrease the image storage and transmission requirements. The inverse process of the image compression is called decompression and it is applied to the compressed data to get back the reconstructed image. The goal of compression is to decrease the number of bits as much as possible, while maintaining the resolution and the visual excellence of the reconstructed image as close to the original image. Image compression

has many benefits. Image compression [3] provides a potential cost savings coupled with sending a smaller amount of data over switched telephone. It not only reduces storage requirements but also overall execution time. It reduces the probability of transmission errors since fewer bits are transferred. It offers a level of security against illicit monitoring. There are different compression methods available in medical imaging such as cosine [4], wavelet transforms [5].

The rest of the paper is organized as follows. Section 2 brief introduction to medical images, Section 3 describes the definitions of various compression algorithms. Section 4 narrates the proposed architecture and explains the algorithm proposed. Section 5 discusses the experimental results obtained and finally Section 6 concludes the paper.

## 2. MEDICAL IMAGES

Medical images [6, 7] are used to provide a photograph of the inner side of the body as clear as it is. These images are helpful to recognize unusual things in inner parts of the body, such as tumors, blood vessels, broken bones, and so on. The most famous types of diagnostic images are the x-ray images that use radiation to take a stationary image of a specific area of the body. Doctors can know the medical outcomes of a calculated tomography scan that can be retrieved via a commercial computer. Behind the scenes, gigantic amount of data is compressed, so that doctor observes it on a computer screen. Computed tomography scans, along with magnetic resonance imaging and positron emission tomography scans form substantial amounts of data. Data is not stockpiled on a typical hard drive and the gap required to accumulate these images in a clinical background would engage in a complete wing of the hospital and also with current electronic medical records custody laws.

The DICOM Standards Committee survives to produce and sustain international standards for communication of biomedical diagnostics and curative information in restraints that utilize digital images and allied data. The objectives of DICOM are to accomplish companionability and to increase workflow effectiveness. DICOM is used by every medical profession that exploits images within the healthcare industry. These include dentistry, mammography, ophthalmology, endoscopy, orthopedics, radiology, cardiology, surgery, pediatrics, radiation therapy, pathology etc. DICOM also tackles the assimilation of information created by these various areas of expertise applications in the patient's e-Medical Record. This defines the network and media swapping services permitting storage and retrieval to these DICOM objects for these record systems. The compression of DICOM files has an enormous value. Compression of an image can be a solitary image or set of images. The DICOM standard has been very disinclined to accept demise algorithms in medical practice. However, the diagnostic information created by hospitals has statistically enhanced and a compression technique is desired that outcomes with larger data diminutions and so transmission speed.

## 3. DEFINITIONS

### 3.1. Cosine transforms

Cosine transform helps to detach an image into parts of differing significance based on frequency, such as higher frequency part and lower frequency part. It renovates a signal or image from the spatial domain to the frequency domain. There are different types of cosine transforms [8] such as DCT, 2DDCT and 3DDCT [9].

DCT is mainly used for changing a signal into elementary frequency components and extensively used in image compression. DCT is described as the product of a vector. It consists of $n \times n$ orthogonal matrix whose rows are the basis vectors. The matrix must be orthogonal and each basis vector relates to a sinusoid of a definite frequency. The general equation for DCT is represented as:

$$F(u) = (2/N)^{\frac{1}{2}} \sum_{0}^{N-1} A(i).\cos\left[\frac{\pi u}{2N}(2i+1)\right] f(i) \text{ where } A(i)=\begin{cases} \frac{1}{\sqrt{2}} & if \ \epsilon = 0 \\ 1 & Otherwise \end{cases}$$

$F$ is represented as a linear combination of the basis vector. These coefficients which we get are the elements of the inverse transform, it might be observed as mirroring the amount of each frequency, there in the input $F$. The one-dimensional DCT is useful for processing only one-dimensional signals such as speech waveforms. For analysis of two-dimensional (2D) signals such as images, 2D version of the DCT is used.

2DDCT is two dimensional version of DCT. DCT is applied vertically and then horizontally. 2DDCT uses a domain data which is calculated using the below formula $\alpha = \sqrt{256/N_c N_r}$ where $Nc, Nr$ is the number of columns and rows respectively. The general equation for 2D-DCT is represented as

$$X(V,W) = \sum_{n=0}^{N_c-1} \sum_{y=0}^{N_r-1} \alpha * C_V^{2n+1} C_W^{2p+1},$$

where $\alpha$ is the time domain data and $C_W^{2p+1}$ are all Cosine coefficients and defined as

$$C_W^{2p+1} = \cos[((2p + 1) * w * 3.14)/2Nr.$$

The same definition is applied on $C_V^{2n+1}$. There are some demerits in 2DDCT.Spatial correlation of the pixels within the single 2-D block is measured and the adjacent block values are neglected. It fails to perform proficiently for binary images characterized by huge periods of invariable amplitude followed by brief periods of sharp transitions.

### 3.2. Wavelet Transforms

Different algorithms depending on wavelets have been exposed to image compression [10, 11]. Separating the smooth variations and details of the image can be done by decomposition of the image using wavelet transform. The similar extension details were being absolute for bi-orthogonal wavelets particularly for low frequency images. There are different types of wavelet transforms such as Haar and Daubechies, DWT, DTCWT.

The Haar wavelet is a certain sequence of rescaled "square-shaped" functions which together form a wavelet family or basis. Wavelet analysis is similar to Fourier analysis in that it allows a target function over an interval to be represented in terms of an orthonormal function basis.
The Haar wavelet's mother wavelet function ψ (*t*) can be described as

$$\varphi(t) = \begin{cases} 1 & 0 \le t < 1/2 \\ -1 & 1/2 \le t < 1 \\ 0 & \text{Otherwise} \end{cases}$$

Its scaling function φ(*t*) can be described as

$$\phi(t) = \begin{cases} 1 & 0 \le t < 1 \\ 0 & \text{Otherwise} \end{cases}$$

Haar transform is discontinuous and does not approximate continuous signals very well. Also Haar eliminates the noise to some extent, but also it disturbs the rest of the signal. Daubechies overcomes these problems by adopting more scaling functions. Hence Daubechies produces accurate averages and differences. This makes a tremendous improvement in the capabilities of transforms. Daubechies transform consists of four scaling function coefficients and wavelets represented as shown below:

$$p_0 = \frac{1+\sqrt{3}}{4\sqrt{2}}, p_1 = \frac{3+\sqrt{3}}{4\sqrt{2}}, p_2 = \frac{3-\sqrt{3}}{4\sqrt{2}}, p_3 = \frac{1-\sqrt{3}}{4\sqrt{2}}$$

In each step, the wavelet transform pertain the scaling function to the input data. If the original data has $N$ values, then the scaling function applied in the wavelet transform is $N/2$ values. These values are stored in lower half of the $N$ element data input vector. The wavelet transform function coefficient values are calculated using the functions shown below:

$$q_0 = p_3, \; q_1 = -p_2, q_2 = p_1, \; q_3 = -p_0$$

The scaling function values are stored in upper half of the $N$ element data input vector. The wavelet and scaling functions are computed by considering the inner product of the coefficients and four data values. The scaling function is represented as shown below:

$$\alpha_i = p_0 s_{2i} + p_1 s_{2i+1} + p_2 s_{2i+2} + p_0 s_{2i+3}$$

$$a[i] = p_0 s[2i] + p_1 s[2i+1] + p_2 s[2i+2] + p_3 s[2i+3]$$

The wavelet function is represented as shown below:

$$c_i = q_0 s_{2i} + q_1 s_{2i+1} + q_2 s_{2i+2} + q_0 s_{2i+3}$$

$$c[i] = q_0 s[2i] + q_1 s[2i+1] + q_2 s[2i+2] + q_3 s[2i+3]$$

## 4. ARCHITECTURE OF dFUSE

Figure 1 shows the architecture of the proposed algorithm "dFuse". This technique is entitled as "dFuse" because "Fuse" means combination. Proposed algorithm combines the power of both spatial and temporal representations to compress the DICOM files. For the sake of compressing DICOM files, this fuse is used. Hence the technique is called "dFuse". DICOM standard is the most required images in the field of medical imaging. DICOM files not only contain the images but also the details of the patients and other details. Hence there is a need of large amount of storage for the maintaining of these records. The intricacy in storing these images is they require additional space and memory. To avoid this difficulty there is a need of tumbling the space without damaging the quality of images. Many compression techniques are worked out to solve this problem [12, 13]. dFuse technique works well by avoiding the complexities in other algorithms. dFuse reduces the i) computational complexity and ii) storage space. Proposed algorithm has two parts encoder and decoder. Encoder part compresses the DICOM files and Decoder does the inverse operation.

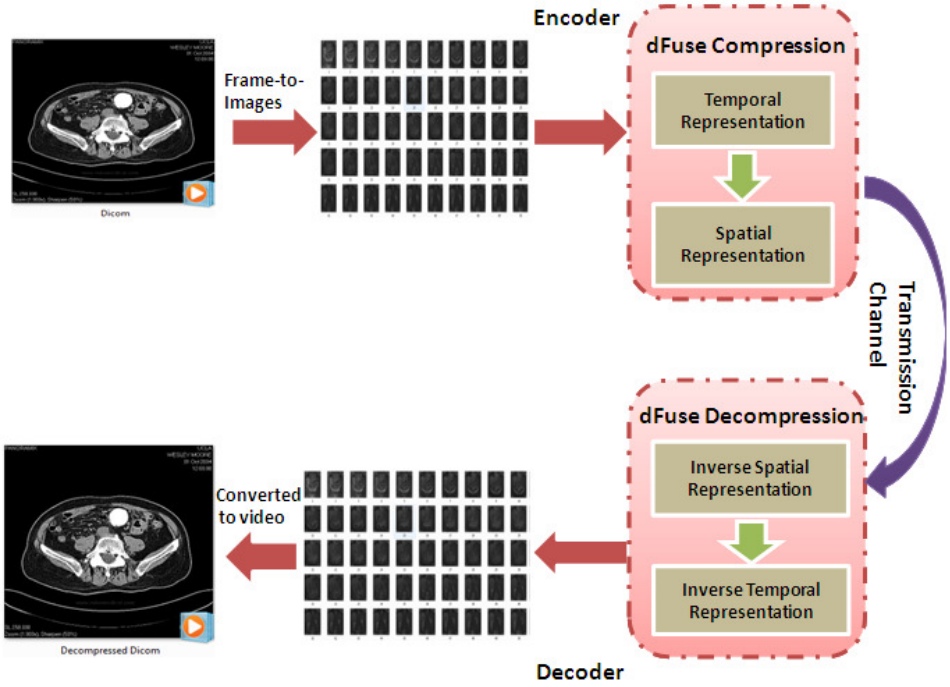


**FIGURE 1:** dFuse Architecture

### 4.1 Spatial and Temporal Representations

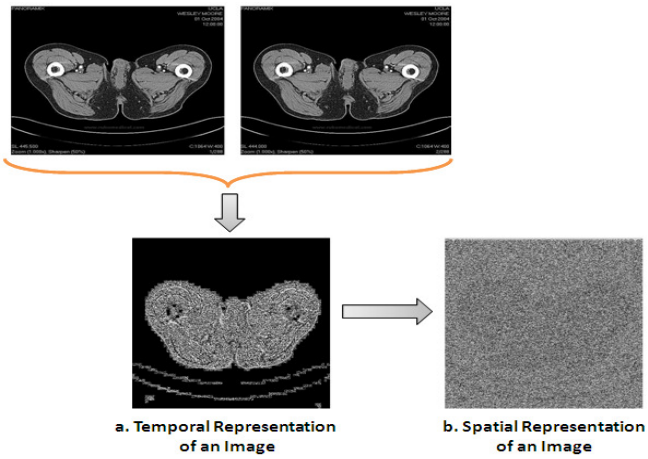


**FIGURE 2:** Spatial & Temporal Representations

dFuse uses two representations for images known as spatial and temporal representation [14]. In spatial representation (Figure 2b), an image is compressed based on width and height. In this type of representation, redundancies within frames are removed. In the case of temporal representation (Figure 2a), redundancies between frames are removed. Here, when a set of frames are passed to this module, a single base frame is fixed and from which redundancies in the following frames are computed. A simple example of this is to consider every second frame as a base frame and calculate difference values between temporally related pixels between frames. This data would be much lesser in size as compared to the original data and can be exploited to achieve higher compression ratios. This would result in a large number of zero values are being computed for every second frame. This algorithm exploits redundancies that occur due to recurrent patterns in data and offers good compression for data comprising large numbers of frequently occurring patterns. There by saving memory and bandwidth.

### 4.2 dFUSE Algorithm

**Encoder Part**

Step: 1 Convert video to images

Step: 2 Extract rgb values from each image

Step: 3 Apply temporal compression

a. Consider the first two images which are more similar and consider the first image as reference image

b. Let RGB1 is the rgb values taken from the reference image and RGB2 is the rgb values taken from the another image

c. Apply the formula $RGB = RGB_1 - RGB_2$

Step: 4 Apply spatial compression [Forward dFuse]

a. Calculate time domain data $\alpha = \sqrt{256/N_f N_c N_r}$ where $N_f, N_c, N_r$ is the number of frames, columns, rows of an image.

b. X (P,Q,R) = $\sum_{m=0}^{N_f-1}\sum_{n=0}^{N_c-1}\sum_{p=0}^{N_r-1} \alpha * C_P^{2m+1} C_Q^{2n+1} C_R^{2p+1}$, where α is the time domain data and $C_R^{2p+1}$ all cosine coefficients and defined as $C_R^{2p+1} = \cos[((2p+1) * w * 3.14)/2N_r]$

c. Apply the same definition to $C_P^{2m+1}$ and $C_Q^{2n+1}$

Step: 5 Archive and send it through transmission channel

**Decoder Part**

Step: 1 Apply spatial decompression [Inverse dFuse]

a. Extract the rgb values from the spatially compressed image.

b. Calculate time domain data $\alpha = \sqrt{256/N_f N_c N_r}$ where $N_f, N_c, N_r$ is the number of frames, columns, rows of an image.

c. $Y(P`,Q`,R`) = \sum_{m=0}^{N_f-1} \sum_{n=0}^{N_c-1} \sum_{p=0}^{N_r-1} X(P,Q,R)/(\alpha * K_P^{2m+1} K_Q^{2n+1} K_R^{2p+1})$ , where α is the time domain data and $K_R^{2p+1}$ is cosine coefficients and defined as

$K_R^{2p+1} = \cos[((2p + 1) * w * 3.14)/2Nr]$

d. Apply the same definition to $K_P^{2m+1}$ and $K_Q^{2n+1}$ .

Step: 2 Apply temporal decompression

a. Group the images.

b. Calculate $RGB_1 = RGB_{ref} + RGB_2$

c. Calculate $RGB_2 = RGB_1 - RGB_{ref}$

d. Reconstruct the images from rgb values.

Step: 3 Reconstruct the video from the reconstructed images.

## 5. EXPERIMENTAL RESULTS

Proposed algorithm is implemented and then checked its efficiency using these parameters, i)file size, ii) compressed ratio, iii) PSNR ratio and iv) compression percentage.

### 5.1. File Size

DICOM files of different sizes have been taken for compression. Table 1 tabulate and compare the results obtained from different sized files and various other compression algorithms. There is a large size difference between the original video and the compressed video. The video size has been reduced drastically. When compared to other compression algorithms, the proposed algorithm is most efficient. Figure 3 shows the plotted graph for the Table 1 values and from graph, we can notice the drastic reduction in video size, for e.g. 444 MB sized file is compressed to 16.8MB, which is efficient when comparing other algorithms.

| Video Size[MB] | Wavelet Transforms | | Cosine Transforms | |
|---|---|---|---|---|
| | Haar [MB] | Daubechies [MB] | 2D-DCT [MB] | dFuse [MB] |
| 0.5 | 0.11 | 0.09 | 0.08 | 0.036 |
| 12 | 0.871 | 0.6 | 0.53 | 0.44 |
| 35 | 2.38 | 1.62 | 1.51 | 0.96 |
| 41 | 3.07 | 2.56 | 2.04 | 1.15 |
| 83 | 3.81 | 2.70 | 2.58 | 1.47 |
| 216 | 14.7 | 15.6 | 13.3 | 8.11 |
| 444 | 28.12 | 24.58 | 23.46 | 16.8 |

**TABLE 1:** Comparing compression video file size for different compression algorithms

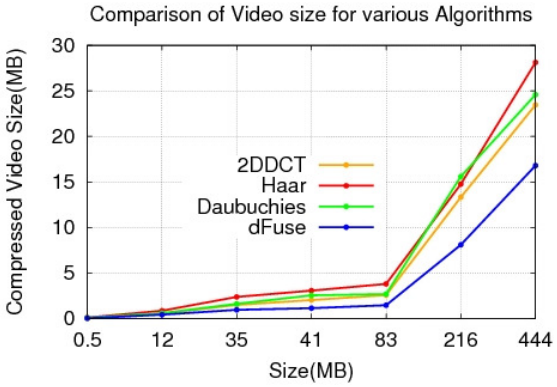


**FIGURE 3:** Comparing compression video file size for different compression algorithms

### 5.2. PSNR Calculation

Peak-signal-to-noise-ratio is used as a quality parameter for reconstruction of compression images or videos. Here signal is in the original data and the noise is in the compressed data. Calculating PSNR values is used as an estimation to human awareness for reconstructing quality of compressed data i.e. higher PSNR, high quality of video.

*PSNR Calculation:*

Step 1: Calculate Mean Square Error [MSE]

$$d(f(x,y), f^{'}(x,y)) = \|(f(x,y) - f^{'}(x,y)\|^{2}$$

$$= \frac{1}{mn}\sum_{i=0}^{m-1}\sum_{j}^{n-1}\left((f(x,y) - f^{'}(x,y)^{2}\right)$$, where $f(x,y)$ and $f^{'}(x,y)$ are original and reconstructed images respectively, m and n are image size.

Step 2: PSNR=$10\log_{10} {}^{1}/_{MSE}$

Videos of different sizes are considered and PSNR values are calculated. Table 2 shows PSNR values obtained for different comparison techniques. Figure 4 displays the graph plotted with various video sizes vs. obtained PSNR values. We can notice that the desperate increase in PSNR values which are in acceptable range and efficient when compared to other algorithms, e.g. 444 MB sized file has PSNR value of 49.998.

| Video Size[MB] | Wavelet Transforms | | Cosine Transforms | |
|---|---|---|---|---|
| | Haar [dB] | Daubechies [dB] | 2DDCT [dB] | dFuse [dB] |
| 0.5 | 20.141 | 28.785 | 43.359 | 48.136 |
| 12 | 19.542 | 27.127 | 40.349 | 49.214 |
| 35 | 19.128 | 28.992 | 41.484 | 46.412 |
| 41 | 18.194 | 27.947 | 40.441 | 49.128 |
| 83 | 15.426 | 17.389 | 34.151 | 40.361 |
| 216 | 18.114 | 20.666 | 40.888 | 49.365 |
| 444 | 21.147 | 30.845 | 44.541 | 49.998 |

**TABLE 2:** Comparing PSNR values different compression algorithms

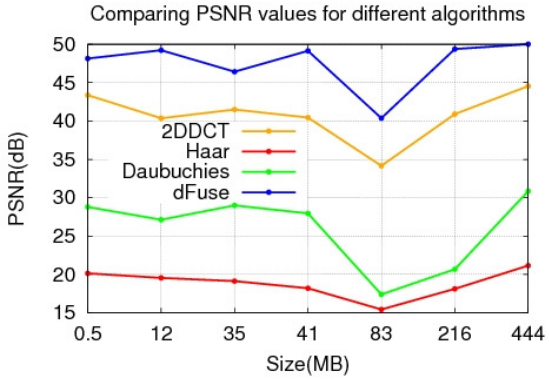


**FIGURE 4:** Comparing PSNR values different compression algorithms

### 5.3. Compression Percentage

Compression percentage is the ratio of difference between the original image and compressed image. This percentage gives how much quantity the original image is compressed. Compression percentage is calculated by using the following formula, $CP = \frac{(O_{size} - C_{size})}{O_{size}} * 100$, where $O_{size}$ is the size of original video and $C_{size}$ is the size of compressed video. Table 3 shows the obtained compression percentage for different video sizes and for various compression algorithms including the proposed one. Figure 5 illustrates the graph of obtained compression percentage for various video sizes vs. different compression algorithms. Proposed algorithm reaches maximum of 96.2 compression percentage for 444 MB sized DICOM file, denoting that the algorithm compresses well than the other algorithms which has maximum of 93 to 94 compression percentage.

| Video Size[MB] | Wavelet Transforms | | Cosine Transforms | |
|---|---|---|---|---|
| | Haar [%] | Daubechies [%] | 2DDCT [%] | dFuse [%] |
| 0.5 | 78 | 82 | 84 | 94 |
| 12 | 92.7 | 95 | 95.5 | 96.3 |
| 35 | 93.2 | 95.3 | 95.6 | 97.2 |
| 41 | 92.5 | 93.7 | 95 | 97.1 |
| 83 | 95.4 | 96.7 | 96.8 | 98.2 |
| 216 | 93.1 | 92.7 | 93.8 | 98.5 |
| 444 | 93.6 | 94.4 | 94.7 | 96.2 |

**TABLE 3:** Comparison of compression percentage for different compression algorithms

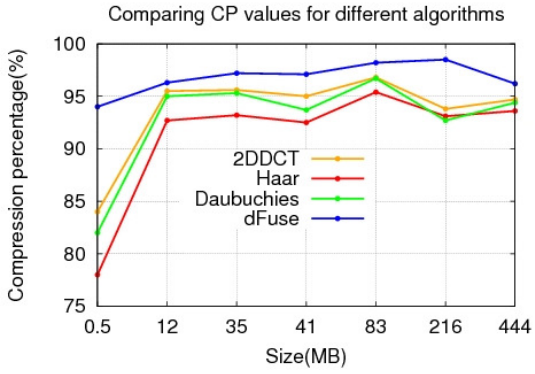


**FIGURE 5:** Comparison of compression percentage of different compression algorithms

### 5.4. Compression Ratio

Compression ratio is the ratio of original image to compressed image. This ratio gives how much quantity the image is compressed when compared to original image. Compression ratio is calculated by using the following formula, $CR = \frac{O_{size}}{C_{size}}$ , where $O_{size}$ is the size of original video and $C_{size}$ is the size of the compressed video. Table 4 illustrates the compression ratio obtained for proposed and for various other algorithms.

| Video Size[MB] | Wavelet Transforms | | Cosine Transforms | |
|---|---|---|---|---|
| | Haar | Daubechies | 2DDCT | dFuse |
| 0.5 | 4.5:1 | 5.5:1 | 6:1 | 13.8:1 |
| 12 | 13.7:1 | 20:1 | 22.6:1 | 27.2:1 |
| 35 | 14.7:1 | 21.6:1 | 23.1:1 | 36.5:1 |
| 41 | 13.3:1 | 16:1 | 20:1 | 35.6:1 |
| 83 | 21.7:1 | 30.7:1 | 32.1:1 | 56.4:1 |
| 216 | 14.6:1 | 13.84:1 | 16.24:1 | 26.6:1 |
| 444 | 15.7:1 | 18:1 | 18.9:1 | 26.4:1 |

**TABLE 4:** Comparison of compression ratio of different compression algorithms

## 6. CONCLUSION

In this paper, we proposed a modified three dimensional discrete cosine algorithm called dFuse. Experimental results obtained from various check point, the proposed algorithm reveals good results in compression and maintains high video quality for reconstructed video. dFuse has high compression ratio and compression percentage, which saves bandwidth and solves the low bandwidth problems. Also Peak-to-Signal Noise (PSNR) ratio is high and in acceptable range when compared to other compression algorithms. Another interesting and useful feature in dFuse is it saves storage space as it reduces the video size drastically. It compresses up to 97% of a video with high quality. The proposed algorithm is created, keeping in mind, to reduce the size of DICOM-format image archives only and have not applied to other medical images such as X-Ray, Ultrasound, CRT scan and MRI scan, which will be our future work.

## 7. REFERENCES

[1] M. Nelson and J. L. Gailly, “The Data Compression Book”, 2nd ed. Newyork, M & T Books, 1996.

[2] A. C. Bovik, “The Essential Guide to Image Processing”, Academic Press, 2009.

[3] A. K. Jain, “Image data compression: A review”, In proceedings of IEEE, vol. 69, pp. 349–389, 1981.

[4] K. Rao, P. Yip, "Discrete Cosine Transform: Algorithms, Advantages, and Applications", NY Academic, 1990.

[5] Graps, A. "An introduction to wavelets", IEEE Computational Science & Engineering, vol.2, no.2, pp.50-61, Summer 1995, doi: 10.1109/99.388960, 1995.

[6] P.C. Cosman, R.M. Gray, and R.A. Olshen, “Evaluation Quality of Compressed Medical Images: SNR, Subjective Rating, and Diagnostic Accuracy”, In proceedings of the IEEE, vol. 82, No. 6 , pp. 919-932,June, 1994.

[7] D. Feng, D. Ho, H. Iida, and K. Chen, “Techniques for functional imaging,” in Medical Imaging Systems Techniques and Applications: General Anatomy, C. T. Leondes, Ed. Amsterdam, The Netherlands: Gordon and Breach, invited chapter, pp. 85–145,1997.

[8] Lodge, N.K, “Video compression techniques”, Applications of Video Compression in Broadcasting, IEE Colloquium on, 2/1 214, 2002.

[9] Ouni T, Ayedi W, Abid M, ”New low complexity DCT based video compression method ”, In Proceedings of Tele Communication ICT09, doi:10.1109/ICTEL2009.5158644, pp:202-207,2009.

[10] Gargour, C., Gabrea, M., Ramachandran, V., Lina, J.M., "A short introduction to wavelets and their applications," IEEE Circuits and Systems Magazine, vol.9, no.2, pp.57-68, doi: 10.1109/MCAS.2009.932556, 2009.

[11] S. Mallat., “A Wavelet Tour of Signal Processing”, Third Edition: The Sparse Way. Academic Press, 2008.

[12] Nadia Benamor and Najoua Essaokri Ben amara, "DICOM Image Compression By Wavelet Transform," In proceedings of IEEE Systems Man and Cybernetics (SMC), Harnmamet, Tunisia, 2002.

[13] Suapang, P., Dejhan K., Yimmun S., "Medical image compression and DICOM-format image archive”, ICCAS-SICE, pp.1945-1949, 2009.

[14] D. Ho, D. Feng, and K. Chen, “Dynamic image data compression in spatial and temporal domains: Theory and algorithm,” IEEE Trans. Inform. Technol. Biomed., vol. 1, pp. 219–228, Dec. 1997.

# A Novel and Efficient Lifting Scheme based Super Resolution Reconstruction for Early Detection of Cancer in Low Resolution Mammogram Images

**Liyakathunisa** *liyakath@indiatimes.com*
*Ph.D Research Scholar*
*Dept of Computer Science & Engg*
*S. J. College of Engineering*
*Mysore, India.*

**C.N .Ravi Kumar** *kumarcnr@yahoo.com*
*Professor & Head of Department*
*Dept of Computer Science & Engg*
*S. J. College of Engineering*
*Mysore, India.*

**Abstract**

Mammography is the most effective method for early detection of breast diseases. However, the typical diagnostic signs, such as masses and microcalcifications, are difficult to be detected because mammograms are low contrast and noisy images. We concentrate on a special case of super resolution reconstruction for early detection of cancer from low resolution mammogram images. Super resolution reconstruction is the process of combining several low resolution images into a single higher resolution image. This paper describes a novel approach for enhancing the resolution of mammographic images. We are proposing an efficient lifting wavelet based denoising with adaptive interpolation for super resolution reconstruction. Under this frame work, the digitized low resolution mammographic images are decomposed into many levels to obtain different frequency bands. We use Daubechies (D4) lifting schemes to decompose low resolution mammogram images into multilevel scale and wavelet coefficients. Then our proposed novel soft thresholding technique is used to remove the noisy coefficients, by fixing optimum threshold value. In order to obtain an image of higher resolution adaptive interpolation is applied. Our proposed lifting wavelet transform based restoration and adaptive interpolation preserves the edges as well as smoothens the image without introducing artifacts. The proposed algorithm avoids the application of iterative method, reduces the complexity of calculation and applies to large dimension low-resolution images. Experimental results show that the proposed approach has succeeded in obtaining a high-resolution mammogram image with a high PSNR, ISNR ratio and a good visual quality.

**Keywords:** Adaptive Interpolation, Lifting Wavelet Transform, Mammogram, Super Resolution, Soft Thresholding.

## 1. INTRODUCTION

Breast cancer is the most common cause of cancer death in women between age of 40 and 45 years. It is one of the leading causes of mortality in women. The World Health Organization's International Agency for Research on Cancer in Lyon, France, estimates that more than 1,50,000 women worldwide die of breast cancer each year [4]. It is expected that 89,000 new cases of breast cancer will be found each year. One out of every 15 newly born girls is expected to develop breast cancer. Mammography, Xeroradiography and Thermography are used for the detection of cancer.

A cancerous tumor in the breast is a mass of breast tissue that is growing in an abnormal, uncontrolled way. The primary signatures of this disease are masses and micro calcifications. Masses are space occupying lesions, described by their shapes, margins and dense properties. Micro calcification is tiny deposits of calcium that appear as small bright spots in the mammogram. Small clusters of micro calcification appearing as collection of white spots on mammograms show an early warning of breast cancer. Primary prevention seems impossible, since the cause of this disease is still remains unknown. An improvement of early diagnostic technique is critical for women's quality of life.

There is a clear evidence which shows that early diagnosis and treatment of breast cancer can significantly increase the chance of survival for patients [5] [6]. The early detection of cancer may lead to proper treatment. Mammography is the main test used for screening and early diagnosis. Mammograms are good at catching infiltrating breast cancer. The current clinical procedure is difficult, time consuming and demands great concentration during reading. Due to large number of normal patients in the screening programs, there is a risk that radiologists may miss some subtle abnormalities.

When a cancer is non-invasive, it is harder to catch with a mammography in women under 50 because of their breast density. Some of the drawbacks of film mammography are, it gives a lot of false negatives. Lumps have an easier time hiding from mammograms in dense breast tissues. The quality of diagnoses depends on the resolution of the mammograms, higher resolutions provides a higher level of detail that normally leads to improved accuracy.

However, to obtain higher resolutions, larger doses of radiation are necessary, which may have harmful effects for patients. Another draw back is that mammograms can be painful and uncomfortable. In order to get a good picture, the technician must apply moderate pressure to the breast. The patient may feel uncomfortable while her breast is being flattened (compressed). To alleviate the above problems we have proposed Super Resolution reconstruction of low resolution mammogram images, in our proposed approach a set of low resolution inputs are used to detect the cancerous tissues, from which a high resolution image is obtained. High Resolution (HR) images give better and accurate results for early detection of cancer in most of the cases. Our proposed approach also lessen the pain and the humiliation that most of the women's faces during mammography. Digital mammography provides the opportunity to apply sophisticated digital processing techniques to aid in screening.

Digital mammography systems have the ability to reprocess the images with mathematical settings that enhance the images. Dense tissues can be seen more clearly through digital enhancements. In recent years several research groups have started to address the goal of resolution augmentation in medical imaging as software post processing challenge. The motivation for this initiative emerged following major advances in the domains of image and video processing that indicated the possibility of enhancing the resolution using Super Resolution algorithms. Super Resolution deals with the task of using several low resolution images from a particular imaging system to estimate, or reconstruct, the high resolution image.

The flow of the topics is as follows; in section II we provide a brief review of the SR algorithm for medical imaging. In section III Mathematical Formulation for Super Resolution Model is created and described in the context of mammographic images, section IV presents the Lifting schemes, in section V the Proposed method for super resolution reconstruction of LR mammogram images is discussed, section VI provide the proposed Super Resolution Reconstruction algorithm, Experimental results are presented and discussed in section VII and finally section VIII consists of conclusion.

## 2. RELATED WORK

Super Resolution problem was extensively addresses in the literature during the last two decades. A variety of reconstruction algorithm have been proposed in literature, where the common goal is to estimate the HR image as accurately as possible, while minimizing the noise, and preserving the image smoothness. In 2001 and 2003 initial attempts were made to adapt super resolution algorithms from the computer vision community to medical imaging applications, initial research dealt with Magnetic Resonance Imaging (MRI) and Position Emission Tomography (PET) modality. Results were encouraged and were reproduced around the world. In this paper we will discuss the main reconstruction algorithms that are in use, such as Iterative Back Projection (IBP)[7] , Projection on to Convex Sets(POCS)[10], Frequency Domain Techniques[8][9] . Green Span and Peled [11] and Kennedy et. al [12] suggested Super Resolution Reconstruction for MRI images where they used IBP. In the IBP approach, an estimate of the high resolution image is compared with low resolution image estimates. The differences between the estimated low resolution images and the actual low resolution images are then used to refine the high resolution image in an iterative manner. Hsu et al. [13] proposed to create high resolution cardiovascular images using a super resolution method based on Projection on Convex Sets (POCS). In the POCS approach, a convex constraint set is set up to maintain consistency with the low resolution images. The estimated high resolution image is projected onto each constraint within the convex constraint set until the desired condition is satisfied. Frequency domain technique was suggested by Tsai and Huang [8] and Kim et al [9]; most frequency domain methods are based on transforming the input images to the frequency domain (using 2-D discrete Fourier transform (DFT)), combining the spectral data and returning the output image. (After applying 2-D IDFT) Phase adaptive Super resolution was proposed by Alexander et al [14] in 2009. In this approach the SR problem is formulated as a constrained optimization problem using a third order Markov prior model, and adapts the priors based on the phase variations of the LR mammographic images. In 2010 super resolution for mammograms was proposed by Jun et al. [15]. In their approach, the algorithm combines machine learning methods and stochastic search to learn the mapping from LR to HR mapping using a data set of training images. In this paper we have proposed a novel and efficient wavelet based super resolution reconstruction of low resolution mammogram images.

## 3. MATHEMATICAL FORMULATION FOR THE SUPER RESOLUTION MODEL

In this section we give the mathematical model for super resolution image reconstruction from a set of Low Resolution (LR) mammographic images. During acquisition image is often corrupted by noise and because of the slight difference in X-ray attenuation between masses, the images may appear with low contrast and often very blurred. They are also down sampled and wrapped, resulting in a set of aliased, blurred, noisy and shifted (mis -registered) images. In practice the image shifts can be obtained by the x-ray tube rotations or by moving the imaged object with respect to the x-ray source.

Let us consider the low resolution sensor plane by $M_1 \; by \; M_2$ . The low resolution intensity values are denoted as $\{y(i,j)\} where \; i = 0.....M_1 - 1 \; and \; j = 0.....M_2 - 1$ ; if the down sampling parameters are $q_1 \; and \; q_2$ in horizontal and vertical directions, then the high resolution image will be of size $q_1 M_1 \times q_2 M_2$ . We assume that $q_1 = q_2 = q$ and therefore the desired high resolution image Z will have intensity values $\{Z(k,l)\}$ where $k = 0 \; ... \; qM_1 - 1 \; and \; l = 0 \; ... \; qM_2 - 1$.

Given $\{z(k,l)\}$ the process of obtaining down sampled LR aliased image $\{y(i,j)\}$is

$$y(i,j) = \frac{1}{q^2} \sum_{k=qi}^{(q+1)i-1} \sum_{l=qj}^{(q+1)j-1} z(k,l) \qquad (1)$$

i.e. the low resolution intensity is the average of high resolution intensities over a neighborhood of $q^2$ pixels. We formally state the problem by casting it in a Low Resolution restoration frame work.

There are P observed images $\{Y_m\}_{m=1}^{p}$ each of size $M_1 \times M_2$ which are decimated, blurred and noisy versions of a single high resolution image Z of size $N_1 \times N_2$ where $N_1 = qM_1$ and $N_2 = qM_2$.

After incorporating the blur matrix, and noise vector, the image formation model is written as

$$Y_m = H_m DZ + \eta_m \qquad \text{Where m=1…P} \qquad (2)$$

here D is the decimation matrix of size $M_1M_2 \times q^2 M_1M_2$, H is PSF of size $M_1M_2 \times M_1M_2$, $\eta_m$ is $M_1M_2 \times 1$ noise vector and P is the number of low resolution observations Stacking P vector equations from different low resolution images into a single matrix vector

$$\begin{bmatrix} y_1 \\ . \\ . \\ y_p \end{bmatrix} = \begin{bmatrix} DH_1 \\ . \\ . \\ DH_p \end{bmatrix} Z + \begin{bmatrix} \eta_1 \\ . \\ . \\ \eta_p \end{bmatrix} \qquad (3)$$

the matrix D represents filtering and down sampling process of dimensions $q^2M_1M_2 \times 1$ where q is the resolution enhancement factor in both directions. Under separability assumptions, the matrix D which transforms the $qM_1 \times qM_2$ high resolution image to $N_1 \times N_2$ low resolution images where $N_1 = qM_1$, $N_2 = qM_2$ is given by

$$D = D_1 \otimes D_1 \qquad (4)$$

where $\otimes$ represents the kronecker product, and the matrix $D_1$ represents the one dimensional low pass filtering and down sampling. When q=2 the matrix $D_1$ will be given by

$$D_1 = \frac{1}{2}\begin{bmatrix} 11\,00\,00\,.....00 \\ 00\,11\,00.....00 \\ :\ :\ :\ \ \ :\ \ \ : \\ :\ :\ :\ \ \ :\ \ \ : \\ 00\ \ 00\ \ \ \ \ \ 11 \end{bmatrix} \qquad (5)$$

and

$$D = \frac{1}{2^2}\begin{bmatrix} 11\,00\,00\,.....00 \\ 00\,11\,00.....00 \\ :\ :\ :\ \ \ :\ \ \ : \\ :\ :\ :\ \ \ :\ \ \ : \\ 00\ \ 00\ \ \ \ \ \ 11 \end{bmatrix} \qquad (6)$$

the square matrix H of dimensions $PN_1 \times PN_2$ represents intra channel and inter channel blur operators. i.e. 2D convolution of channel with shift-invariant blurs. The blur matrix is of the from

$$H_I = \begin{bmatrix} H_{(0)} & H_{(1)} \ldots\ldots\ldots & H_{(M-1)} \\ H_{(M-1)} & H_{(0)} \ldots\ldots\ldots & H_{(M-2)} \\ : & : \ldots\ldots\ldots & : \\ : & : \ldots\ldots\ldots & : \\ H_{(1)} & H_{(2)} \ldots\ldots\ldots & H_{(0)} \end{bmatrix} \tag{7}$$

and it is circulant at the block level. In general each $H_{(i)}$ is an arbitrary $PM_1 \times PM_2$, but if shift invariant circular convolution is assumed $H_{(i)}$ becomes

$$H_{(i)} = \begin{bmatrix} H_{(i,0)} & H_{(i,1)} \ldots\ldots\ldots & H_{(i,M-1)} \\ H_{(i,M-1)} & H_{(i,0)} \ldots\ldots\ldots & H_{(i,M-2)} \\ : & : \ldots\ldots\ldots & : \\ : & : \ldots\ldots\ldots & : \\ H_{(i,1)} & H_{(i,2)} \ldots\ldots\ldots & H_{(i,0)} \end{bmatrix} \tag{8}$$

which is also circulant at the block level $H_{(i,j)}$. Each $P \times P$ sub matrix (sub blocks) has the form

$$H_{(i,j)} = \begin{bmatrix} H_{11(i,j)} & H_{12(i,j)} \ldots\ldots & H_{ip(i,j)} \\ H_{21(i,j)} & H_{22(i,j)} \ldots\ldots\ldots & H_{2p(i,j)} \\ : & : \ldots\ldots & : \\ : & : \ldots\ldots & : \\ H_{p1(i,j)} & H_{p2(i,j)} \ldots\ldots\ldots & H_{pp(i,j)} \end{bmatrix} \tag{9}$$

where $H_{ii(m)}$ is intra channel blurring operator, $H_{ij(m)} i \neq j$ is an inter channel blur i.e. P x P non circulant blocks are arranged in a circulant fashion, it's called Block Semi-Block Circulant (BSBC); which can be easily solved using blind deconvolution or regularization.

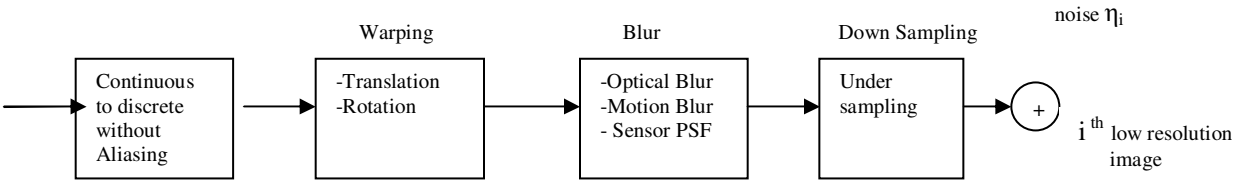


**FIGURE 1:** Low Resolution Observation Model

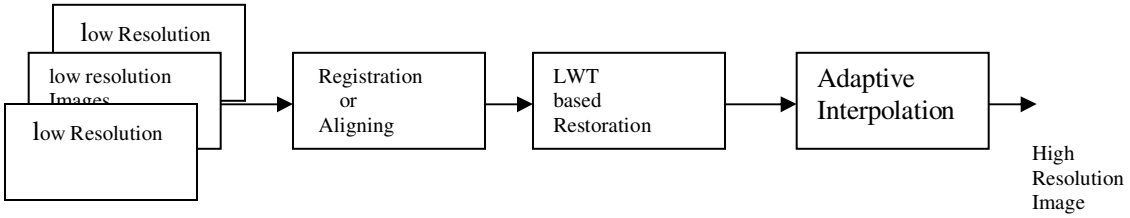


**FIGURE 2:** Super Resolution Reconstruction Model

## 4. LIFTING SCHEMES

Wavelet algorithms are recursive. The output of one step of the algorithm becomes the input for the next step. The initial input data set consists of 2n elements. Each successive step operates on 2n-i elements, where i = 1 ... n-1. For example, if the initial data set contains 128 elements, the wavelet transform will consist of seven steps on 128, 64, 32, 16, 8, 4, and 2 elements. In this case $step_{j+1}$ follow $step_j$. If element i in step j is being updated, the notation is $step_{j,i}$. The forward lifting scheme wavelet transform divides the data set being processed into an even half and an odd half. In the notation below $even_i$ is the index of the $i^{th}$ element in the even half and $odd_i$ is the $i^{th}$ element in the odd half (even and odd halves are both indexed from 0). Viewed as a continuous array (which is what is done in the software) the even element would be a[i] and the odd element would be a [i+ (n/2)]. The wavelet Lifting Scheme is a method for decomposing wavelet transforms into a set of stages. Lifting scheme algorithms have the advantage that they do not require temporary arrays in the calculation steps, as is necessary for some versions of the Daubechies D4 wavelet algorithm[ 16]. The simplest version of a forward wavelet transform expressed in the Lifting Scheme is shown in Figure 3. The predict step calculates the wavelet function in the wavelet transform. This is a high pass filter. The update step calculates the scaling function, which results in a smoother version of the data (low pass filter) [16].

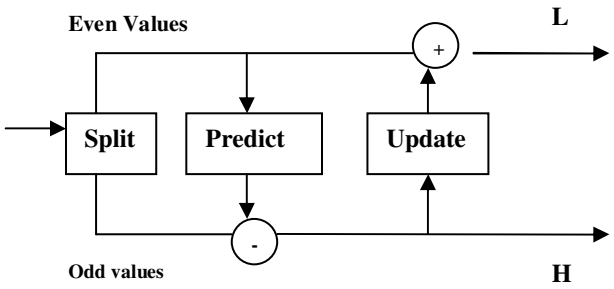


**FIGURE 3:** Lifting Scheme Forward Wavelet Transform

**Predict** The predict step uses a function that approximates the data set. The difference between the approximation and the actual data replaces the odd elements of the data set. The even elements are left unchanged and become the input for the next step in the transform. The predict step, where the odd value is "predicted" from the even value is described by the equation.

$$odd_{j+1,i} = odd_{j,1} - P(even_{j,i}) \quad (10)$$

The inverse predicts transform adds the prediction value to the odd element (reversing the prediction step of the forward transform). In the inverse transform the predict step is followed by a merge step which interleaves the odd and even elements back into a single data stream.

**Update:** The update phase follows the predict phase. The original value of the odd elements has been overwritten by the difference between the odd element and its even "predictor". So in calculating an average the update phase must operate on the differences that are stored in the odd elements. The update step replaces the even elements with an average. These results in a smoother input for the next step of the next step of the wavelet transform. The odd elements also represent an approximation of the original data set, which allows filters to be constructed.

$$even_{j+1,i} = even_{j,i} + U(odd_{j+1,i}) \tag{11}$$

### 4.1 A Lifting Scheme Version of the Daubechies (D4) Transform

Lifting scheme wavelet transforms are composed of update and predict steps. In this case a normalization step has been added as well.

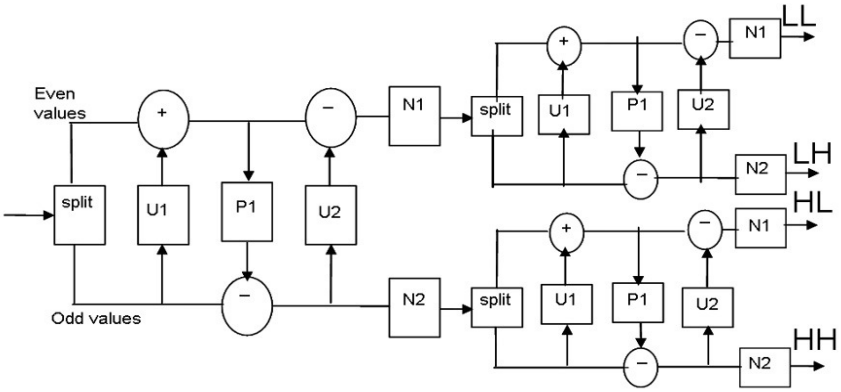


**FIGURE 4:** Two stage Daubechies D4 Forward lifting Wavelet Transform

The split step divides the input data into even elements which are stored in the first half of an N element array section ( $S_0$ to $S_{half-1}$) and odd elements which are stored in the second half of an N element array section ($S_{half}$ to $S_{N-1}$). In the forward transform equations below the expression S [half+n] references an odd element and S[n] references an even element. The LL represents the low frequency components and LH, HL, HH are the high frequency components in the horizontal, vertical and diagonal directions.

The forward step equations are

Update1 (U1):
For n= 0 to half -1

$$S[n] = S[n] + \sqrt{3}S[half + n] \tag{12}$$

Predict (P1):

$$S[half] = S[half] - \frac{\sqrt{3}}{4}S[0] - \frac{\sqrt{3}-2}{4}S[half - 1] \tag{13}$$

for n=1 to half -1

$$S[half + n] = S[half + n] - \frac{\sqrt{3}}{4}S[n] - \frac{\sqrt{3}-2}{4}S[n-1] \tag{14}$$

Update2 (U2):

for n=0 to half -2

$$S[n] = S[n] - S[half + n + 1]$$
$$S[half - 1] = S[half - 1] - S[half] \tag{15}$$

Normalize (N):
for n=0 to half-1

$$S[n] = \frac{\sqrt{3}-1}{\sqrt{2}} S[n]$$
$$S[n+half] = \frac{\sqrt{3}+1}{\sqrt{2}} S[n+half] \quad (16)$$

the inverse transform is a mirror of the forward transform, in which addition and subtraction operations interchanged.

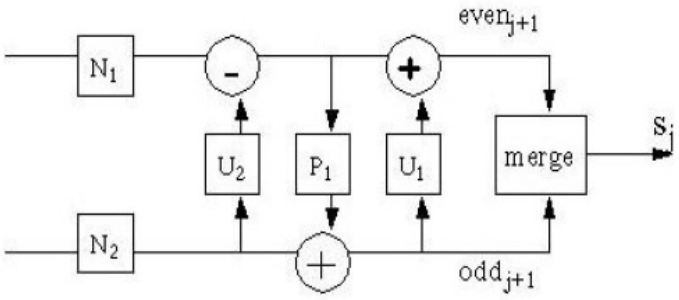


**FIGURE 5:** Daubechies D4 Inverse Lifting Wavelet Transform

## 5. PROPOSED SUPER RESOLUTION RECONSTRUCTION OF LOW RESOLUTION MAMMOGRAM IMAGES

Our Low Resolution mammogram images consist of the degradations such as geometric registration wrap, sub sampling, blurring and additive noise. Based on these phenomena our implementation consists of the following consecutive steps.

Step 1: Image registration, which means estimating the geometrical registration wrap between different images.
Step 2: Fusion and Restoration of the registered low resolution images using our proposed efficient Lifting scheme based denoising.
Step 3: Adaptive interpolation of the resulting image from step 2 to obtain a super resolution Mammogram image.

### 5.1 Image Registration

For super resolution reconstruction, image registration is performed first in order to align the LR images as accurately as possible. It is a process of overlaying two or more images of the same scene taken at different times, from different view points and or by different sensors. Typically one image called the base image is considered the reference to which the other images called input images are compared. The objective is to bring the input image into alignment with the base image by applying a spatial transformation to the input image. Spatial transformation maps locations in one image into a new location in another image. Image registration is an inverse problem as it tries to estimate from sampled images $Y_m$, the transformation that occurred between the views $Z_m$ considering the observation model of Eq(2). It is also dependent on the properties of the camera used for image acquisition like sampling rate (or resolution) of sensor, the imperfection of the lens that adds blur, and the noise of the device. As the resolution decreases, the local two dimensional structure of an image degrades and an exact registration of two low resolution images becomes increasingly difficult. Super resolution reconstruction requires a registration of high quality. Different methods exists for estimating the motion or sub pixel shift between the two images[17].The registration technique considered in our research is a modified

phase correlation based on Fast Fourier Transform proposed by Fourier Mellin and DeCastro [18].

The transformation considered in our research is rotation, translation and shift estimation. Let's consider the translation estimation, the Fourier transform of the function is denoted by $F\{f(x,y)\}$ or $\hat{f}(w_x, w_y)$. The shift property of the Fourier transform is given by

$$F\{f(x+\Delta x, y+\Delta y)\} = \hat{f}(w_x, w_y) e^{i(w_x \Delta x + w_y \Delta y)} \tag{17}$$

Eq (17) is the basis of the Fourier based translation estimation algorithms. Let $I_1(x,y)$ be the reference image and $I_2(x,y)$ is the translated version of the base image, i.e

$$I_1(x,y) = I_2(x+\Delta x, y+\Delta y) \tag{18}$$

by applying the Fourier transform on both the sides of Eq (18). We get

$$\hat{I}_1(w_x, w_y) = \hat{I}_2(w_x, w_y) e^{i(w_x \Delta x + w_y \Delta y)} \tag{19}$$

or equivalently,

$$\frac{\hat{I}_1(w_x, w_y)}{\hat{I}_2(w_x, w_y)} = e^{i(w_x \Delta x + w_y \Delta y)} \tag{20}$$

$$corr(x,y) \cong F^{-1}\left( \frac{\hat{I}_1(w_x, w_y)}{\hat{I}_2(w_x, w_y)} \right) = \delta(x+\Delta x, y+\Delta y) \tag{21}$$

for discrete images we replace the FT in the computation above with FFT, and $\delta(x+\Delta x, y+\Delta y)$ is replaced by a function that has dominant maximum at $(\Delta x, \Delta y)$ as

$$(\Delta x, \Delta y) = \arg\max\{corr(x,y)\} \tag{22}$$

calculate the cross power spectrum by taking the complex conjugate of the second result. Multiplying the FT together element wise, and normalizing this product element wise.

$$corr(w_x, w_y) \cong \frac{\hat{I}_1(w_x, w_y)}{\hat{I}_2(w_x, w_y)} \bullet \left| \frac{\hat{I}_1(w_x, w_y)}{\hat{I}_2(w_x, w_y)} \right| \tag{23}$$

$$corr(w_x, w_y) = R \cong \frac{\hat{I}_1(w_x, w_y) \hat{I}_2^*(w_x, w_y)}{\left| \hat{I}_2(w_x, w_y) \right| \left| \hat{I}_1^*(w_x, w_y) \right|} = e^{i(w_x \Delta x + w_y \Delta y)}$$

(24)

where * denotes the complex conjugate. Obtain the normalized cross correlation by applying the inverse FT. i.e. $r = F^{-1}\{R\}$, determine the location of the peak in r. This location of the peak is exactly the displacement needed to register the images

$$(\Delta x, \Delta y) = \arg\max\{r\} \tag{25}$$

The angle of rotation is estimated by converting the Cartesian coordinates to log polar form. We observe that the sum of a cosine wave and a sine wave of the same frequency is equal to phase shifted cosine wave of the same frequency. That is if a function is written in Cartesian form as

$$v(t) = A\cos(t) + B\sin(t) \tag{26}$$

then it may also be written in polar form as

$$v(t) = c\cos(t - \varphi) \tag{27}$$

we may write the Eq (27) in polar form as

$$Y = y(x) = \frac{a_0}{2} + \sum_{k=1}^{N} m_k \cos(2\pi f_k x - \varphi_k) \tag{28}$$

where

$$m_k = \sqrt{a_k{}^2 + b_k{}^2} \ldots.(magnitude)$$

$$\varphi_k = \tan^{-1}\left(\frac{b_k}{a_k}\right) \ldots.(Phase) \tag{29}$$

The Shift is estimated by finding cross power spectrum and computing Eq.(20). We obtain the normalized cross correlation by applying the inverse FT. i.e. $r = F^{-1}\{R_2\}$, determines the location of the peak in r. This location of the peak is exactly the shift $I(x_0, y_0)$ needed to register the images. Once we estimated the angle of rotation, translation and shift, a new image is constructed by reversing the angle of rotation translation and shift.

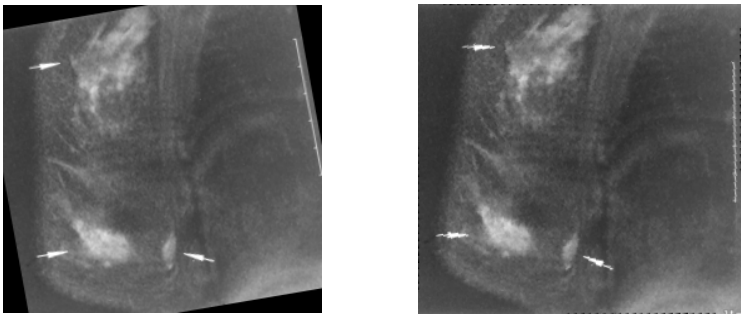

(a) (b)

**FIGURE 6**: (a) Rotated, shifted Mammogram Image (b) Registered Mammogram Image

In the second phase the low resolution registered images are fused using fusion rule, then restoration is performed using our proposed novel denoising technique. In the final phase proposed adaptive interpolation is performed to obtain an image with double, quadrupled the resolution of the original.

### 5.2 Lifting Wavelet based Restoration

Images are obtained in areas ranging from everyday photography to astronomy, remote sensing, medical imaging and microscopy. In each case there is an underlying object or scene we wish to observe, the original or the true image is the ideal representation of the observed scene. Yet the observation process is never perfect, there is uncertainty in the measurement occurring as blur, noise and other degradations in the recorded images. Image restoration aims to recover an estimate of the original image from the degraded observations. Classical image restoration seeks an estimate of the true image assuming the blur is known, whereas blind image restoration tackles the much more difficult but realistic problem where the degradations are unknown.
The low resolution observation model of Eq.(2) is considered. We formally state by casting the problem in multi channel restoration format, the blur is considered as between channels and within channel of the low resolution images. In order to remove the blur and noise from the LR images we have proposed an efficient wavelet based denoising using thresholding, our proposed approach performs much better when compared to other approaches.

#### 5.2.1. Proposed Efficient lifting Wavelet Transform Based Denoising for SRR Using Thresholding

Image denoising techniques are necessary to remove random additive noises while retaining as much as possible the important image features. The main objective of these types of random noise removal is to suppress the noise while preserving the original image details [19]. Statistical filter like average filter, wiener filter can be used for removing such noises but wavelet based denoising techniques proved better results than these filters. The wavelet transforms compresses the essential information in an image into a relatively few, large coefficients which represents image details at different resolution scales. In recent years there has been a fair amount of research on wavelet thresholding and threshold selection for image denoising [20][21][22] .
Let Z be an M x M image from Eq. (2), during transmission the image Z is corrupted by zero mean White Gaussian noise $\eta$ with standard deviation $\sigma$ . At the receiver end the noisy observation Y of Eq. (2) is obtained. The goal is to obtain the image Z from noisy observation Y such that the MSE is minimum. Lifting Wavelet Transforms decomposes the image into different frequency subbands. Small coefficients in the subbands are dominated by noise while coefficients with large absolute value carry more image information than noise. Replacing noisy coefficients by zeros and an inverse lifting wavelet transform may lead to reconstruction that has lesser noise. Normally hard thresholding and soft thresholding techniques are used for denoising.

**Hard Thresholding**

$$\begin{aligned} D(X,T) &= X \text{ if } |\mathrm{X}| \rangle \mathrm{T} \\ &= 0 \text{ if } |\mathrm{X}| \langle \mathrm{T} \end{aligned} \tag{30}$$

**Soft Thresholding**

$$D(\mathrm{X}, \mathrm{T}) = \mathrm{Sign}(\mathrm{X}) * \max(0, |\mathrm{X}| - \mathrm{T}) \tag{31}$$

Where X is the input subband, D is the denoised band after thresholding and T is the threshold level. The denoising algorithms, which are based on thresholding suggests that each coefficient of every detail subband is compared to threshold level and is either retained or killed if its magnitude is greater or less respectively.

In lifting wavelet transform decomposes an image into one approximate (LL) and three details (LH, HL and HH) subbands. The approximate coefficients are not submitted in this process. Since on one hand they carry the most important information about the image, on the other hand the noise mostly affects the high frequency subbands. Hence the HH subband contains mainly noise.

For estimating the noise level we use the Median Absolute Deviation (MAD) as proposed by Donoho [23].

$$\sigma = \frac{Median\left|Y_{ij}\right|}{0.6745}, Y_{ij} \in LH, HL, HH \tag{32}$$

The factor 0.6745 in the denominator rescales the numerator so that $\sigma$ is also a suitable estimator for standard deviation for Gaussian white noise. Selecting an optimum threshold value (T) for soft thresholding is not an easy task. An optimum threshold value should be selected based on the subband characteristics. In lifting schemes subbands decomposition as the level increases, the coefficient of the subband becomes smoother. For example when an image is decomposed into 2 level LWT using Daubechies 4 tap lifting wavelet transform, we get four subbands figure (5), the HH subband of first level contains large amount of noise, hence the noise level is estimated for the HH subband using Eq (32).Once the noise level is estimated we select the threshold value T. The Threshold value T is

$$T = \sigma - \left(\left|HM - GM\right|\right) \tag{33}$$

Here $\sigma$ is the noise variance of the corrupted image. As given in [19], the Harmonic mean and geometric mean are best suited for the removal of Gaussian noise, hence we use the absolute difference of both the Harmonic Mean (HM) and Geometric Mean (GM) or either of the means also can be considered for denoising the image corrupted by Gaussian noise. The harmonic mean filter is better at removing Gaussian type noise and preserving edge features than the arithmetic mean filter. Hence we have considered harmonic mean than arithmetic mean. The process is repeated for LH and HL bands and threshold is selected for all the three bands once threshold is estimated, soft thresholding of Eq.(31) , is performed to denoise the image.

$$HM = \frac{M^2}{\sum_{i=1}^{M}\sum_{j=1}^{M}\frac{1}{g(i,j)}} \tag{34}$$

$$GM = \left[\prod_{i=1}^{M}\prod_{j=1}^{M} g(i,j)\right]^{\frac{1}{M^2}} \tag{35}$$

**5.3. Proposed Adaptive Interpolation for Super Resolution Reconstruction**

Once the image are denoised using our proposed soft thresholding technique, interpolation is performed to obtain an image of double, quadruple the size of the original image. Our proposed algorithm works in four phases: In the first phase the lifting wavelet transform based fused image is expanded. Suppose the size of the fused image is n x m. The image will be expanded to size N (2n-1) x (2m-1). In the figure (7) solid circles show original pixels and hallow circles show undefined pixels. In the remaining three phases these undefined pixels will be filled

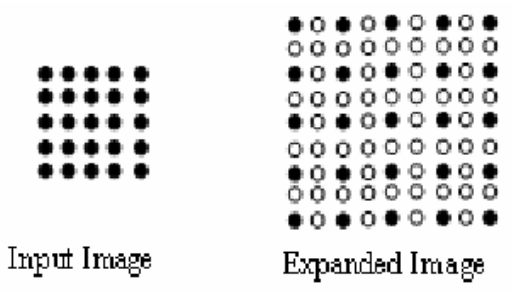


**FIGURE 7:** High Resolution Grid

The second phase of the algorithm is most important one. In this phase the interpolator assigns value to the undefined pixels

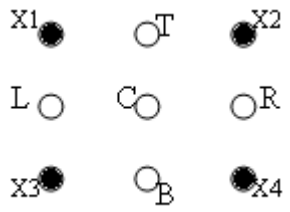


**FIGURE 8 :** HR unit cell with undefined pixels Top, Center, Bottom, Left, Right dented by T,C,B,L,R.

The undefined pixels are filled by following mutual exclusive condition.
Uniformity: select the $\text{range}(X_1, X_2, X_3, X_4)$ and a Threshold T.

$$\begin{aligned} &if\ \text{range}(X_1, X_2, X_3, X_4) < T\ \text{Then} \\ &\quad C = (X_1 + X_2 + X_3 + X_4)/4 \\ &if\ \text{there is edge in NW-SE Then} \\ &\quad C = (X_1 + X_2)/2 \\ &if\ \text{there is edge in NS Then} \\ &\quad T = (X_1 + X_2)/2 \text{ and } B = (X_3 + X_4)/2 \\ &if\ \text{there is edge in EW Then} \\ &\quad L = (X_1 + X_3)/2 \text{ and } R = (X_2 + X_4)/2 \end{aligned} \tag{36}$$

(37)

In this phase, approximately 85% of the undefined pixels of HR image are filled. In the third phase the algorithm scans magnified image line by line and looking for those pixels which are left undefined in the previous phase.

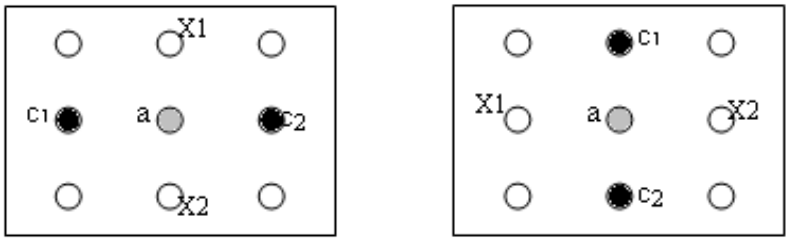


**FIGURE 9 :** Layout referred in the phase 3

In the third phase ,the algorithm checks for the layout as shown in Figure(9).

$$\begin{aligned} &\textit{if} \text{ there is edge } c_1c_2 \text{ then } a=(c_1+c_2)/2 \\ &\textit{else if} \text{ there is edge } X_1X_2 \text{ then } a=(X_1+X_2)/2 \end{aligned} \tag{38}$$

In the fourth phase all the undefined pixels will be filled. If there are any undefined pixels left then the median of the neighboring pixels is calculated and assigned. We call our interpolation method adaptive as the interpolator selects and assigns the values for the undefined pixels based on mutual exclusive condition.

## 6. PROPOSED ALGORITHM FOR SUPER RESOLUTION RECONSTRUCTION OF LOW RESOLUTION MAMMOGRAM IMAGES.

Our proposed novel super resolution reconstruction consists of following consecutive steps:

Step 1: Three input low resolution blurred, noisy, under sampled, rotated, shifted images are considered.

$$\text{i.e. } I_1(i,j),\ I_2(i,j),\ I_3(i,j) \text{ where } i=1\ldots N,\ j=1\ldots N \tag{39}$$

Step 2: The images are first preprocessed, i.e. registered using FFT based algorithm, as explained in section (5.1).

Step 3: The registered low resolution images are decomposed using LWT to a specified number of levels. At each level we will have one approximation i.e. LL sub band and 3 detail sub bands, i.e. LH, HL, HH coefficients.

Step 4: The decomposed images are fused using the fusion rule i.e. Maximum Frequency Fusion: "fusion by averaging for each band of decomposition and for each channel the wavelets coefficients of the three images is averaged". That is maximum frequencies of approximate and detail coefficients are fused separately

$$A_j^o I = \max(A_j^o I_1 + A_j^o I_2 + A_j^o I3)/3 \qquad D_j^c I = \max(D_j^c I_1 + D_j^c I_2 + D_j^c I_3)/3 \tag{40}$$

Step 5: The fused image contains LL, LH, HL and HH subbands.

a) Obtain the noise variance ( $\sigma$ ) using Eq.(32) for LH, HL and HH subbands of level one.
b) Compute Eq.(33) and select the threshold (T) for LH, HL and HH subbands of level 1.
c) Denoise all the detail subband coefficients of level one (except LL) using soft thresholding given in Eq.(31) by substituting the threshold value obtained in step (5b).

Step 6: Most of the additive noise will be eliminated during the fusion process by denoising using our proposed soft hresolding approach as explained in section (5.2.1), where as the image is deblurred using Iterative Blind Deconvolution Algorithm (IBD)[30] .

Step 7: Inverse LWT is applied to obtain a high resolution restored image.

Step 8: Finally in order to obtain a super resolved image, an image with double the resolution as that of the original image our proposed adaptive interpolation as explained in section (5.3) is applied.

### 6.1. Quality Measurement

**1) Improvement in Signal-to-Noise Ratio (ISNR)**

For the purpose of objectively testing the performance of the restored image, Improvement in signal to noise ratio (ISNR) is used as the criteria which is defined by

$$\text{ISNR} = 10\log_{10}\frac{\sum_{i,j}\left[f(i,j)-y(i,j)\right]^2}{\sum_{i,j}\left[f(i,j)-g(i,j)\right]^2} \tag{41}$$

Where j and i are the total number of pixels in the horizontal and vertical dimensions of the image; f(i, j), y(i, j) and g(i, j) are the original, degraded and the restored image.

**2) The MSE and PSNR of the Reconstructed Image is**

$$MSE = \frac{\sum[f(i,j)-F(I,J)]^2}{N^2} \tag{42}$$

Where f(i, j) is the source image F(I,J) is the reconstructed image, which contains N x N pixels

$$PSNR = 20\log_{10}\left(\frac{255}{RMSE}\right) \tag{43}$$

**3) Super Resolution Factor**

$$SRF = \frac{\sum_{i=1}^{M}\sum_{j=1}^{N}\left(F(i,j)-f(i,j)\right)^2}{\sum_{i=1}^{M}\sum_{j=1}^{N}\left(y(i,j)-f(i,j)\right)^2} \tag{44}$$

**4) MSSIM**

The structural similarity (SSIM) index is defined in [27] by equations

$$SSIM(f,F) = \frac{(2\mu_f\mu_F+C_1)(2\sigma_F+C_2)}{(\mu_f^2+\mu_F^2+C_1)(\sigma_f^2+\sigma_F^2+C_2)} \tag{45}$$

$$MSSIM(f,F)=\frac{1}{G}\sum_{p=1}^{G}SSIM(f,F) \quad (46)$$

The Structural SIMilarity index between the original image and reconstructed image is given by SSIM, where $\mu_f$ and $\mu_F$ are mean intensities of original and reconstructed images, $\sigma_f$ and $\sigma_F$ are standard deviations of original and reconstructed images, f and F are image contents of $p^{th}$ local window and G is the number of local windows in the image.

## 7. EXPERIMENTAL RESULTS AND DISCUSSIONS.

To evaluate the performance of the proposed algorithm we performed our experiments using MATLAB software. The tested images were selected from "**Geneva Foundation for Medical Education and Research**". The test data can be summarized as follows
**Case1**: Ductal carcinoma in Situ.
**Case 2**: Fat necrosis of breast- benign inflammatory
**Case 3:** Benign tubular adenomyoepithelioma
**Case 4**: clustered micro calcification masses.

Each data set consists of three to four LR mammographic images generated from a reference image. To simulate low resolution and low dosage conditions, each LR mammographic image is generated by applying a motion blur with an angel of (10, 20 and 30) and Gaussian white noise with SNR(5, 10,15 and 20 dB) is added to the blurred low resolution images. The goal is to generate a Super Resolution image of size 512 x512 and 1024x1024 from three noisy, blurred, under sampled and mis-registered images. In addition a comparative study has been made with well known algorithms like; Projection on to Convex Sets(POCS), Papoulis Gerchberg (PG) Algorithm, Iterative Back Projection(IBP) and DWT based SRR[3]. Figures (11 & 12) show two different cases of LR mammograms and the super resolution results of our proposed algorithm compared with POCS, Papoulis, IBP and DWT. To asses the performance of the super resolution model on test images, we used the above mentioned metrics to estimate the enhancement quality based on PSNR, ISNR, SRF and MSSIM measure. Table 1 and Table 2, show a comparative study of our algorithm with POCS, Papoulis Gerchberg(P.G), Iterative Back Projection(IBP) and DWT in terms of PSNR, ISNR and MSSIM values.

The results indicate that our proposed super resolution reconstruction have much more high frequency information than Projection on to Convex Sets, Papoulis Gerchberg Algorithm and Iterative Back Projection. To evaluate the performance of the proposed method in a quantitative manner , PSNR is computed for the resolution enhanced images obtained with tested algorithms, relative to the reference image used to generate the lo w resolution images. The PSNR results for all the test cases are summarized in Table 1. It can be observed that the PSNR values for the mammographic images generated using the proposed method are noticeably higher than those produced using the other methods. Case 1 and Case 2 are shown in figures (11 & 12) respectively.

case 1: is mammogram of Ductal carcinoma in Situ (DCIS), the carcinomas are difficult to interpret in the high resolution mammographic images obtained using POCS, PG and IBP. Both wavelet based SRR and LWT SRR method provide noticeably improved structural detail. The proposed LWT based SRR provides an improved structural contrast when compared to wavelet based SRR.

In case 2, mammogram of 69-year-old woman with benign tubular adenomyoepithelioma is considered, it's a Lateral oblique mammogram showing circumscribed mass lying inferiorly in left breast. Benign calcifications are also present. The calcification behind the dense tissues is very difficult to interpret in the high resolution mammographic images obtained using POCS, PG and IBP. But the wavelet based SRR and LWT based SRR provide noticeably improved structural

detail pertaining to the calcification. Lifting wavelet based SRR provides an improved contrast and a sharper image of the masses. The shape, boundaries and structure of the masses tend to be better defined in the high resolution image provided by the proposed method.

The MSSIM and ISNR results are summarized in Table 2, MSSIM which accounts well for texture changes introduced by super resolution process, has its value increased for the proposed lifting wavelet based approach. MSSIM was created to reflect the perceived visual quality by humans [27][33].
From the Table II , it is clear that the proposed LWT SRR algorithm increases the perceptual visual quality. Another interesting factor is that the proposed Lifting Wavelet based SRR have much more detail information than the results of Projection on to Convex Sets, Papoulis Gerchberg Algorithm and Iterative Back Projection.

From the Table (1 and 2) and Figures (11 & 12), we observe that the proposed algorithm outperforms the others, and we have a clearer and high resolution mammogram with a super resolution factor of 4, much better than the original one, which is very helpful for the radiologist to make proper decision whether it is benign or malignant characteristics of breast tumor. Once the exact location of the tumor is detected, radiation can be passed in the precise location, by which we can avoid the health risks of the patients and side effect of radiation therapy can be avoided.
And from the plots in figure(13) it's clear that our proposed approach has better ISNR and MSSIM when compared to other approaches.

.

| Image | POCS SRR | | Papoulis Gerchberg (P G) SRR | | IBP SRR | | DWT based SRR[3] | | Proposed LWT SRR | |
|---|---|---|---|---|---|---|---|---|---|---|
| | ***MSE*** | ***PSNR*** | ***MSE*** | ***PSNR*** | ***MSE*** | ***PSNR*** | ***MSE*** | ***PSNR*** | ***MSE*** | ***PSNR*** |
| **case 1** | 34.87 | 32.7 | 32.5 | 33.1 | 50.43 | 37.1 | 59.63 | 51.043 | 16.76 | 62.23 |
| **case 2** | 69.46 | 29.71 | 67.48 | 29.83 | 69.46 | 29.73 | 42.66 | 54.11 | 25.46 | 58.46 |
| **case 3** | 54.11 | 30.79 | 53.45 | 30.85 | 40.37 | 28.59 | 28.81 | 57.056 | 11.98 | 65.14 |
| **case 4** | 34.21 | 32.78 | 30.61 | 33.27 | 37.6 | 32.37 | 54.94 | 49.42 | 40.71 | 52.02 |

**TABLE I:** MSE and PSNR comparison of our proposed approach with other approaches

| Image | POCS SRR | | Papoulis Gerchberg (P G) SRR | | IBP SRR | | DWT based SRR[3] | | Proposed LWT SRR | |
|---|---|---|---|---|---|---|---|---|---|---|
| | ***ISNR*** | ***MSSIM*** | ***ISNR*** | ***MSSIM*** | ***ISNR*** | ***MSSIM*** | ***ISNR*** | ***MSSIM*** | ***ISNR*** | ***MSSIM*** |
| **case 1** | 2.41 | 0.67 | 2.78 | 0.69 | 2.82 | 0.68 | 6.82 | 0.897 | 13.61 | 0.99 |
| **case 2** | 3.7 | 0.63 | 3.49 | 0.67 | 3.61 | 0.67 | 6.78 | 0.890 | 13.61 | 0.985 |
| **case 3** | 2.98 | 0.66 | 3.21 | 0.71 | 3.23 | 0.69 | 6.83 | 0.912 | 9.46 | 0.971 |
| **case 4** | 3.7 | 0.73 | 3.17 | 0.68 | 3.56 | 0.71 | 7.12 | 0.870 | 8.29 | 0.984 |

**TABLE II:** ISNR and MSSIM comparison of our proposed approach with other approaches

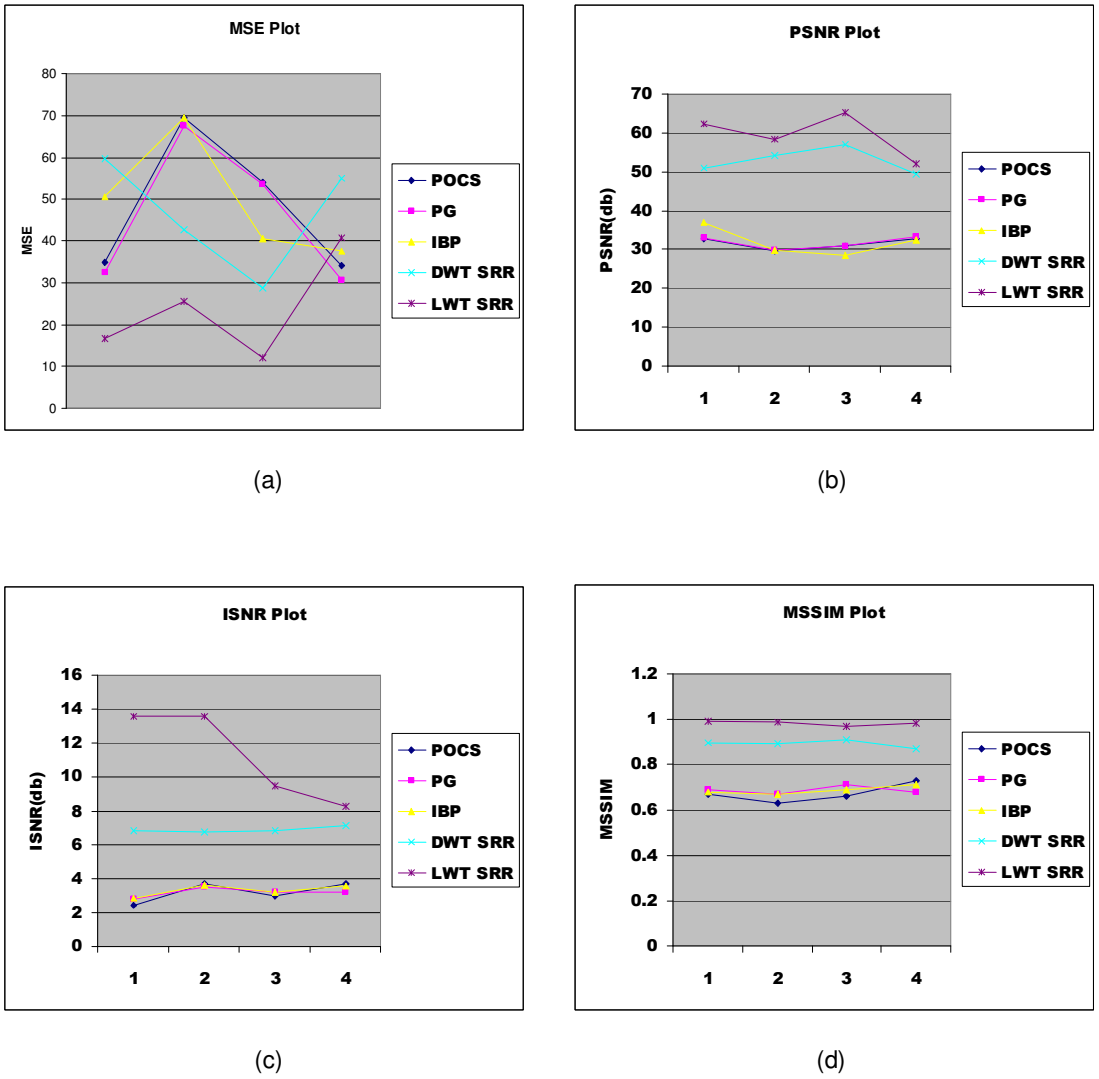


(a) (b)

(c) (d)

**FIGURE 10**: (a) Comparison graph of MSE at different blur and noise densities of LR mammogram images (b) Comparison graph of PSNR at different blur and noise densities of LR mammogram images. (c) Comparison graph of ISNR at different blur and noise densities of LR images (d) Comparison graph of MSSIM at different blur and noise densities of LR images

### 7.1 Simulation Results

Case 1: Ductal carcinoma in situ (DCIS) mammogram with a Super resolution factor of 2 (enlarged from 256x256 to 512 by 512 )

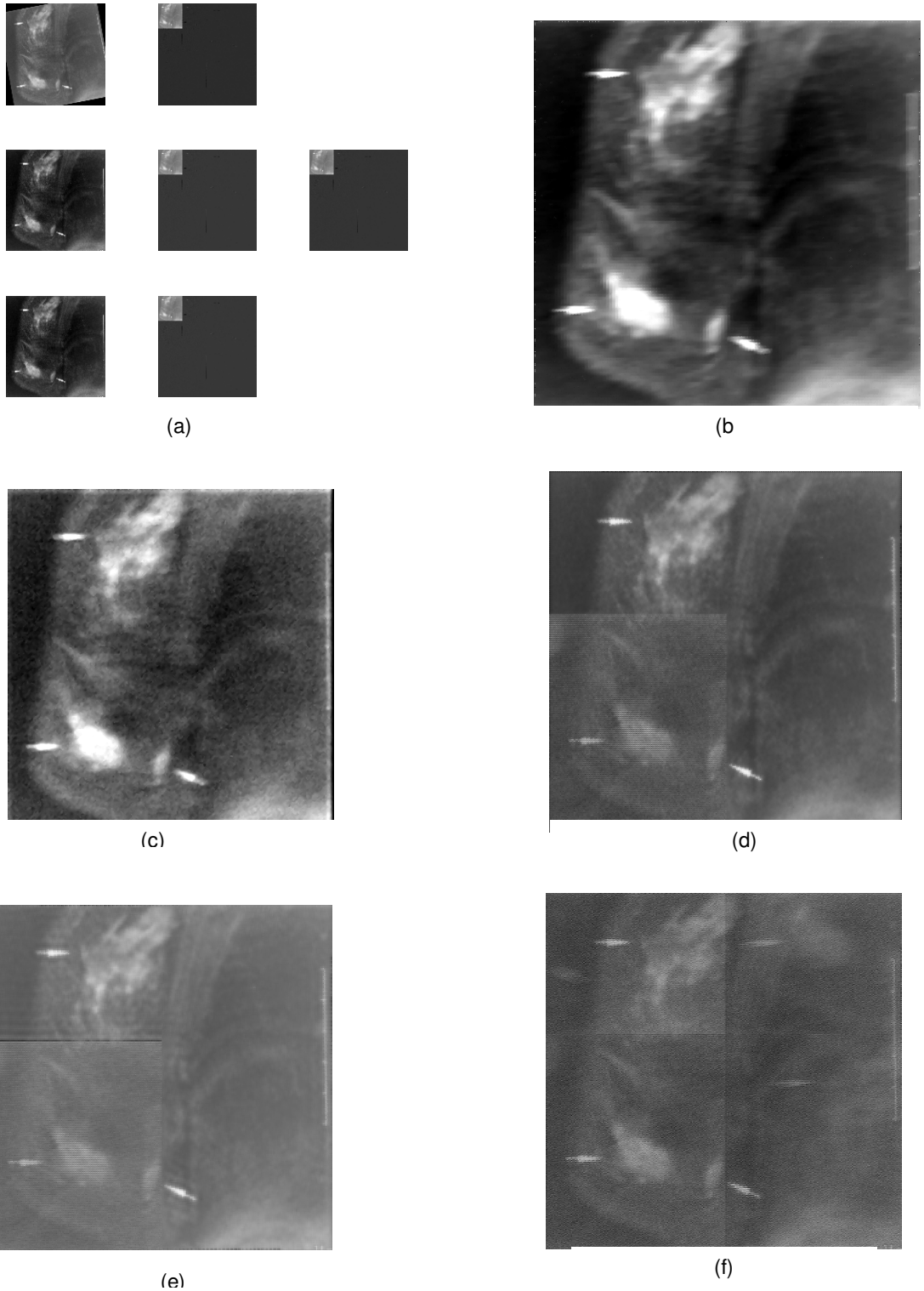

**FIGURE 11:** (a) Low Resolution Images (b) Proposed LWT based SRR (c) DWT based SRR (d) POCS SRR (e) Papoulis Gerchberg SRR (f) IBP SRR

Case 2: 69-year-old woman with benign tubular adenomyoepithelioma with a super resolution factor of 4(enlarged from 256 x 256 to 1024 x 1024)

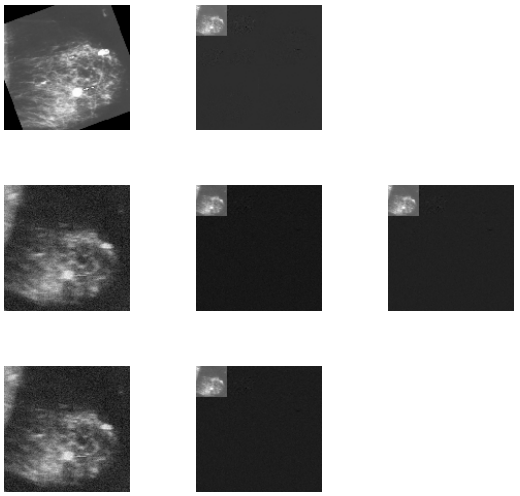

(a)

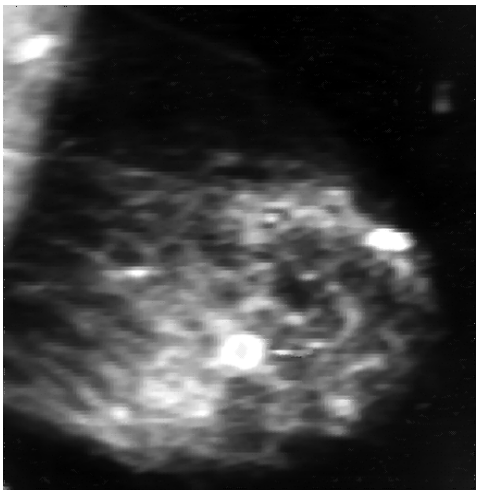

(b)

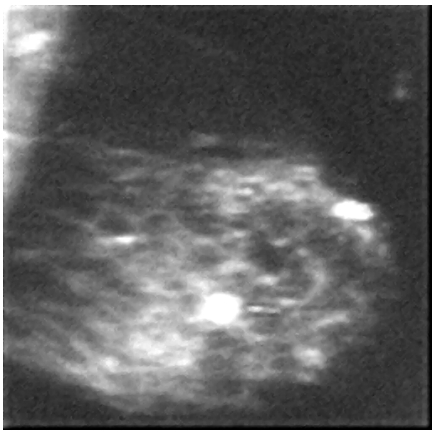

(c)

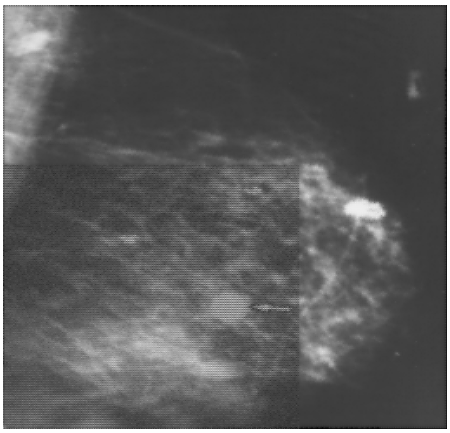

(d)

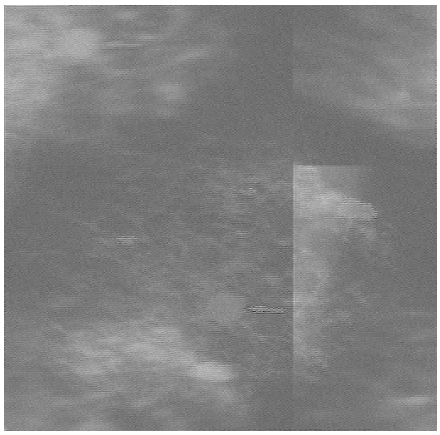

(e)

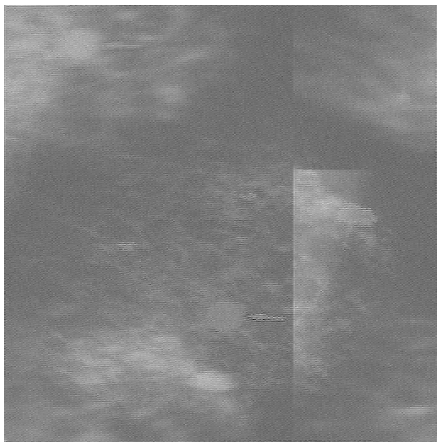

(f)

**FIGURE 12:** (a) Low Resolution Images (b) Proposed LWT based SRR (c) DWT based SRR (d) POCS SRR (e) Papoulis Gerchberg SRR (f) IBP SRR

## 8. CONCLUSION

In this paper we have proposed a novel and efficient lifting scheme based denoising for super resolution reconstruction of low resolution mammogram images. We have presented a new way to improve the quality of x-ray mammography images without having to use more radiations, which increases health risks of patients. The results indicate that the proposed system can facilitate the doctor to detect breast cancer in early stage of diagnosis process. Early detection tests for breast cancer can save many thousands of lives, with super resolution reconstruction the cancer can be diagnosed at an early stage and treated successfully. High resolution images give better visibility of the breast, particularly near the skin line, chest wall and in women with dense breast tissues. As medical imaging moves towards complete digital imaging and produces prohibitively large amounts of data, compression is necessary for storage and communication purposes. Our method has the potential for storage and communication purposes. Our method has the potential to eliminate the need to store images at full resolution, since they could be regenerated them from low resolution ones. Experimental results show that the proposed algorithm yields significantly superior image quality when it is compared to the other well known algorithms.

## REFERENCES

[1] Liyakathunisa and C.N.Ravi Kumar, “Advances in Super Resolution Reconstruction of Low Resolution Images" International Journal of Computational Intelligence Research ISSN 0973-1873 Volume 6, Number 2 , pp. 215-236,2010.

[2] Liyakathunisa, C.N.Ravi Kumar and V.K. Ananthashayana , “Super Resolution Reconstruction of Low Resolution Images using Wavelet Lifting schemes" in Proc ICCEE'09, 2nd International Conference on Electrical Computer Engineering", Dec 28-30TH 2009, Dubai, Indexed in IEEE Xplore.

[3] Liyakathunisa and C.N.Ravi Kumar, “A Novel and Robust Wavelet Based Super Resolution Reconstruction of Low Resolution Images Using Efficient Denoising and Adaptive Interpolation”, in International Journal of Image Processing-IJIP, CSC Journals Publications, Issue 4, Vol 4, pp 401-420, 2010.

[4] R.Gaughan, “New approaches to early detection of breast cancer makes small gains” ,Biophotonics Int. , pp 48-53, 1998.

[5] Smith R.A., “Epidemiology of breast cancer categorical course in physics”, Tech. Aspects Breast Imaging, Radiol. Sco. N. Amer., pp 21-33, 1993.

[6] S. Shapiro, W. Venet, P.Strax, L.Venet, and R. Roester, ” Ten-to Fourteen year Effect of screening on breast cancer mortality”, JNCL, vol 69, pp 349, 1982.

[7] M. Irani and S. Peleg, “Improving resolution by image registration", CVGIP: Graphical Models and Image Proc., vol. 53, pp. 231-239, May 1991.

[8] R.Y. Tsai and T.S. Huang, “Multiple frame image restoration and registration”, in Advances in Computer Vision and Image Processing. Greenwich, CT: AI Press Inc., pp, 317-339.

[9] P. Vandewalle, S. Susstrunk, and M. Vetterli, Lcav, “A frequency domain approach to registration of aliased images with application to Super resolution", EURASIP Journal on applied signal processing pp 1-14, 2006.

[10] S. C. Park, M. K. Park, and M. G. Kang, “Super-resolution image reconstruction: A technical review”, IEEE Signal Processing Mag., vol. 20, pp. 21-36, May 2003.

[11] H. Greenspan, G. Oz, N. Kiryati, and S. Peled, “Super-resolution in mri,” in Proceedings of IEEE International Symposium on Biomedical Imaging, pp. 943 -946, 2002.

[12] J. A. Kennedy, O. Israel, A. Frenkel, R. Bar-Shalom, and H. Azhari, “Super-resolution in pet imaging”, IEEE transactions on medical imaging, vol. 25, no. 2, pp. 137 - 147, February 2006.

[13] J. T. Hsu1, C. C. Yen, C. C. Li, M. Sun, B. Tian, and M. Kaygusuz, “Application of wavelet-based pocs super resolution for cardiovascular mri image enhancement ”, in Proceedings of the Third International Conference on Image and Graphics (ICIG04), pp. 572-575, 2004.

[14] Alexander wong and Jacob Scharcanski, “ Phase -adaptive Super Resolution of mammogram Images using complex wavelts ", 2009.

[15] Jun Zhang, olacFuentes and Ming-Yingleung, “Super resolution of Mammograms", 2010.

[16] A.Jensen, A.la Cour-Hardo, “Ripples in Mathematics” , Springer publications.

[17] Barbara Zltova, J.Flusser, “Image Registration: Survey”, Image and vision computing, 21, Elsevier publications, 2003.

[18] E.D. Castro, C. Morandi, “Registration of translated and rotated images using finite Fourier transform” , IEEE Transactions on Pattern Analysis and Machine Intelligence 700–703, 1987.

[19] Gonazalez Woods , “ Digital Image Processing”, 2nd Edition.

[20] S. Grace Chang, Bin Yu and M. Vattereli, “Adaptive Wavelet Thresholding for Image denoising and compression”, IEEE Transaction, Image Processing, vol. 9, pp. 1532-15460.

[21] S.K.Mohiden, Perumal,Satik, “Image Denosing using DWT”, IJCSNS, Vol 8, No 1, 2008.

[22] D. Gnanadurai, V.Sadsivam, “An Efficient Adaptive Threshoding Technique for Wavalet based Image Denosing” , IJSP, Vol 2, spring 2006.

[23] D.L.Donoho and I.M JohnStone, “Adapting to unknown smoothness via wavelet shrinkage “, Journal of American Association, Vol 90,no, 432, pp1200-1224 .

[24] Huang, X.S., Chen, Z, “A Wavelet-Based Image Fusion Algorithm" , In Proceedings of the IEEE Region 10 Conference on Computers, Communications, Control and Power Engineering (TENCON 2002), 602-605, Beijing 2002.

[25] T. Acharya, P.S. Tsai, “Image up-sampling using Discrete Wavelet Transform", in Proceedings of the 7th International Conference on Computer Vision, Pattern Recognition and Image Processing (CVPRIP).

[26] S. Grace Chang, Bin Yu and M. Vattereli, “Adaptive Wavelet Thresholding for Image denoising and compression", IEEE Transaction, Image Processing, vol. 9, pp. 1532-15460.

[27] Wang, Bovik, Sheikh, et al, “Image Quality Assessment: From Error Visibility to Structural Similarity”, IEEE Transactions of Image Processing, vol. 13, pp. 1-12, April 2004.

[28] S. Chaudhuri, Ed., “Super-Resolution Imaging”, Norwell, A: Kluwer, 2001.

[29] S.Susan Young, Ronal G.Diggers, Eddie L.Jacobs, “Signal Processing and performance Analysis for imaging Systems”, ARTEC HOUSE, INC , 2008.

[30] G.R.Ayer and J.C.Danity, “ Iterative Blind Deconvolution”, vol13, No 7, optics Letters, July 1988.

[31] G.K. Lemanur, Drocihe and J.Decoinck, “Highly Regular Wavelets for the Detection of clustered Micro calcification in Mammograms”, IEEE Trans on Medical Imaging, VOl.22, No. 3, March 2003.

[32] J.Kristin , McLoughlin, J.Philip , Bones, “Noise Equalization for Detection of Micro calcification Clusters in Direct Digital Mammogram Images”, IEE Trans on Medical Imaging, Vol 23, No 0 , March 2004.

[33] I. B´egin and F. P. Ferrie, “Comparison of super-resolution algorithms using image quality measures,” in Proceedings of the 3rd Canadian conference on computer and robot vision. Washington, DC, USA: IEEE Computer Society, pp. 72, 2006.

[34] B. Girod, “What’s wrong with mean-squared error?” in Digital images and human vision, MIT Press, Cambridge, MA. ISBN 0-262-23171-9, pp. 207–220, 1993.

# A Novel Biometric Technique Benchmark Analysis For Selection Of Best Biometric Modality And Template Generation Method

**Raikoti Sharanabasappa11** *sr.raikoti@gmail.com*
*Research Scholar Dravidian University*
*Kuppam, India*

**Dr Sanjaypande M. B.2** *rkroop99@gmail.com*
*Prof. and Head of Dept.*
*VVIET Mysore, India*

**Abstract**

A biometric security is a technique by means of which digital contents are protected by a cryptographic key generated from the biometric features of a person like Retina, Iris, Fingerprint, Face, Voice and so on. Normally the digital contents like documents are protected by a cryptographic key generated from a unique password. The process in irreversible, i.e the key can be generated from the password but not the vice versa. Passwords are relatively easy to hack as most of the users keep their personal information like date of birth as password and also password length has a limit as human beings cannot remember a password of significantly large length. Hence guessing the password of a user, whose significant information is available, is easier. Therefore off late lot of emphasis has been given to biometric features. Biometric features of no two people are same. For example the finger prints or the face of any two people differ. Hence if a template (alphanumeric or binary representation of features from a biometric data) is selected for the key generation than cracking them for accessing information becomes significantly difficult. But as with every advantage comes certain limitations also. The keys are not time invariant. Templates tends to change based on the data acquisition, or with time. For example the finger prints or palm prints changes with ages. Iris, retina and face features changes with change in light intensity during the acquisition phase. Fingerprint features changes with change in the orientation of the finger while scanning. In a classic authentication problem, such variability's can be easily dealt with by keeping a threshold for the acceptance of the features. Such acceptance threshold is not applicable for the case of biometric templates. Even slightest of the variability in the templates changes the generated key, therefore causing a high false rejection rate. Hence in this work we analyze the most accepted biometric features and techniques for key generation and propose the most invariable technique in terms of data acquisition invariability. The work analyzes Iris, Face, Fingerprint and Palm prints for analysis of the biometric template generation and key generation form the templates. Further a unique benchmark analysis technique is proposed for quantifying the quality of a biometric model or features.

**Keywords:** Template Quality Analysis, Biometric Security, Biometric Key Invariability.

## 1. INTRODUCTION

1.1 Public Key Cryptography

It is a means of exchanging digital data securely over a network or internet. If a peer wants to send a document to other peer by encrypting it, then the peers first exchange their secured keys. A key is unique number generated randomly using a key generation function with the help of a set of alphanumeric string and users identity (like user name). Hence the key is unique to each user. While peer A wants to send information to B, it encrypts the document with the public key of B. While decrypting, B needs to decrypt the document with its private key. Now even if there is an eavesdropping while the public keys are exchanged and unauthenticated user acquires the

public key of B, any encrypted document transmitted from A to B will not be decrypted by the unauthenticated entity because it is unaware of the private key of B. Now if the same entity had to decrypt the document successfully, it has to "guess" the private key of B. It requires a reverse engineering by means of which the unauthenticated entity first tracks the function through which this key might have been generated and then uses a trial and error method to guess the key. A decade ago, this technique was quite full proof because the amount of time required by any computer to guess the key through trial and error method or as commonly known brute force method would be significantly high and extend to weeks and months. But Over the period of time the processing capabilities of the computers are being increased by many a folds. Therefore the random guessing of the keys has become less time consuming and hackers are able to crack most sophisticated keys even with the help of a simple personal computer and without the aid of any super computer. Hence there was a need to come up with techniques which offers more randomness than the unique string which used to be use as a key generation base. Hence biometric templates got an edge and attention for public key cryptography over last decade or so.

**1.2 Biometric Templates**

For generating the key it is essential to select a password as discussed in the previous section. A password is a typical and known combination of numerals and characters that user can remember. Now every user has a limitation of remembering the length of the password. Hence number of permutations is finite even though it is huge. Whenever possible combinations of the key are finite the probability of generating the key from random combination is non zero. Considering that there are ten digits and twenty six characters (English alphabet) and that the password is of length ten, then total possible combinations are $^{35}P_{10}$.

Now let us consider that number of possible symbol is S and the length of the password is D then possible combination C is depicted as

$$C={}^{S}P_{D} \quad (1)$$

Hence the randomness of the key can be increased by increasing the both S and D. Number of characters are fixed and is a set of maximum 256( as used by modern computer systems). Still it does not guarantee an infinite set. Instead of the symbols if real number sets are used as the base for generating the key than S becomes a set of all real numbers and can be claimed computationally infinite. Hence even a fixed length of D ensures a virtually untraceable key. It is almost impossible for human beings to remember large set of real numbers. Therefore a simple solution to the problem is to generate this number each and every time from the identity of the user, for instance face or fingerprint or palm print or voice or retina and so on. These identities are called biometric identities. The identity is scanned to a digital format and features are extracted from the pattern. These features are unique and are commonly known as biometric templates. A common technique for using these templates is to store them either centrally in a server or locally in the form of a smart card.

Hence a biometric template is a finite length set of either real numbers or symbols representing the unique identity of a person and can be used to generate unique key for public key cryptography [1].

Hence it can be said that biometric templates are set of measurable features which can be either used for public key cryptography or authenticating the person.

**1.3 Problem formation**

The biometrics features must be selected in such a way that it produces a unique and finite set for the user identity [2].

The overall process of data security can be elaborated in figure 1.

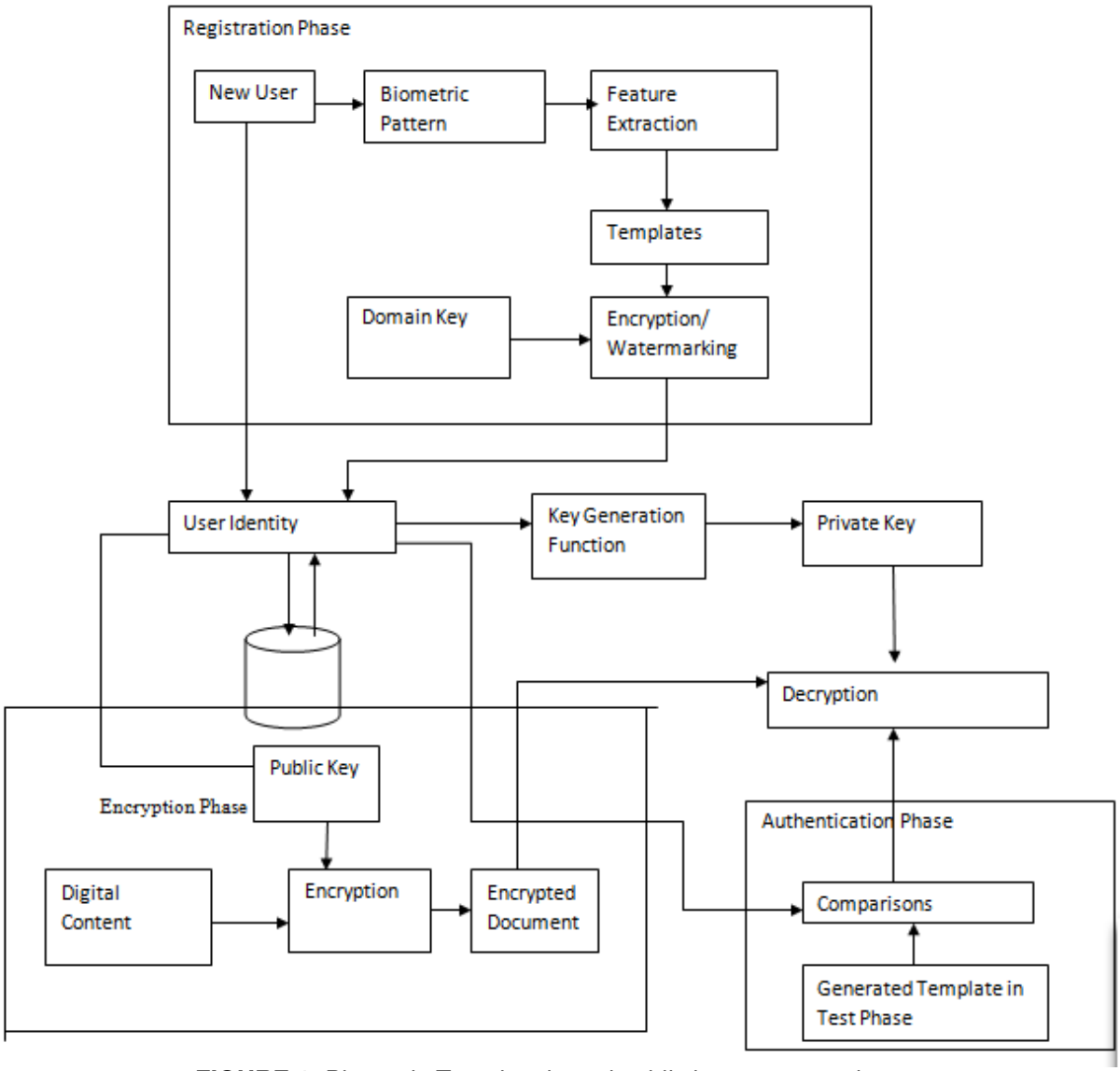


**FIGURE 1:** Biometric Template based public key cryptography.

When the user is registered for the first time, biometric template is extracted and stored in a database. When user receives an encrypted document which he needs to decrypt, he needs to get authenticated first. In authentication process biometric template of the user is regenerated and is compared with the features of the database and if they match the private key is generated from the stored features because every time new features are generated, they will not be 100% same as that of the stored templates. In key generation even deviation of a symbol out of a matrix of size say 1024, will result in generating wrong key. Hence the best method is to generate the key from the stored vector rather than the new vector. Further the stored vectors are protected using either watermarking techniques or are encrypted by a common domain key and are stored. Therefore if an unauthenticated intruder can track the domain key, he can easily temper with the stored key. Therefore the strength of the technique is considered to be dependent on the techniques of protecting the templates themselves, which interns minimizes the strength of the biometric templates itself.

A possible alternative to this problem is to device a mechanism by means of which it is not required to store the key in the database. Every time a document arrives, user's biometric

template is generated and a private key is generated from recently generated template rather than the existing stored template.
The solution is depicted in simple block diagram in figure 2.

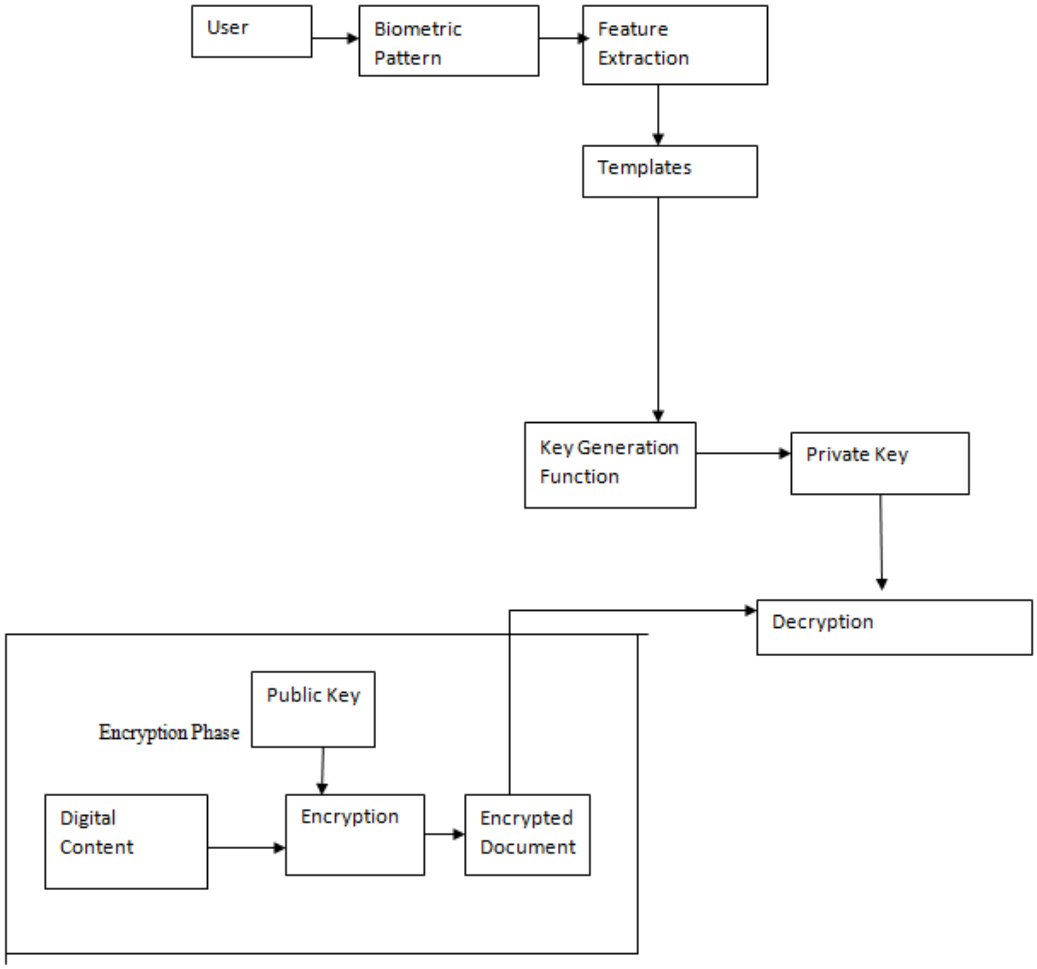


**FIGURE 2:** Proposed solution for Biometric security of the digital document.

Figure 2 clearly elaborates that there are no stored element to temper with. Therefore theoretically the key generated out of this technique is temper proof.
The main challenge with this technique is the variability of the features. Every time biometric data is acquired, it must be unique and the selected function must be such that it produces the exact key at every instance. Thus the first step is to find out the most invariant biometric features and template generation methods.

## 2. BENCHMARK ANALYSIS OF BIOMETRIC TEMPLATE SECURITY AND INVARIABILITY

### 2.1 Similarity With Self (SS)[2]

It is the average of the similarity scores obtained in the comparison between the user and the different access he has made. The greater the value, the more accurate is the biometric trait. A large value indicates similarity between the different stored versions of the user's biometric trait. This large similarity score overcomes the threshold. Maximization of this value reduces the false non match rate (FNMR).

SS must be very high and ideally 100% for every instance of template generation in order to ensure a unique key generation every time. Though with the current systems, it is not yet being achieved, this work towards identifying the biometric features and techniques to generate invariant features is to achieve this objective.

Let $s(x, y)$ be the matching similarity score between users $x$ and $y$, given $N$ genuine users, $G_1, G_2, ..., G_n$ and $P(i)$ successful and genuine access of user $i$, $A(i)_1, A(i)_2, ..., A(i)_{P(i)}$ we define $SS(Gi)$ as:

$$SS(Gi) = \frac{\sum_{j=1}^{j=P(i)} s(Gi, A(i)\,j)}{P(i)} \quad ...(2)$$

**2.2 Similarity With Others(SO)[2]**

Similarity with the other users *(SO – Similarity Others)*: is the average of the similarity scores obtained in the comparison between the user and the rest of the users stored in the database and the users found in the impostor access list. The smaller the value, the more accurate is the biometric trait. A small value indicates a great distinction with the rest of the users stored in the database and potential impostors. This small similarity score doesn't overcome the threshold. Minimization of this value reduces the false match rate (FMR). Even though the objective of this work is study the invariability amongst the templates of a users subsequent template acquisition and not authentication, Similarity with others gives a benchmark for analyzing how strong a particular technique is. The more the value of SO, the stronger the technique is considered.

Let $s(x, y)$ be the matching similarity score between users $x$ and $y$, given $N$ genuine users, $G_1, G_2, ..., G_n$ and $M$ impostors $I_1, I_2, ..., I_m$, we define $SO(Gi)$ as:

$$SO(Gi) = \frac{\sum_{j=1.\,j\neq 1}^{j=N} s(Gi, Gj) + \sum_{k=1}^{k=M} s(Gi, Ij)}{N + M} \quad ...(3)$$

**2.3 Entropy Based Measures [3] and Guessing Distance**

One of the most analytical measures for the quality of the biometric key is Strong Biometric Privacy (SBP) analysis. This explains that if an adversary learns no useful information about a biometric, given auxiliary information, the template used to derive the key, and the key itself. For instance, no computationally bounded adversary should be able to compute any function of the biometric.

This is a direct function of Key Randomness (KR). This elaborates the randomness of the generated keys to any adversary who has access to auxiliary information and the template used to derive the key. For instance, we might require that the key be statistically or computationally indistinguishable from random.

Randomness can further be analytically defined as the probabilistic variations in keys generated from user to user. Such probabilistic measures are elaborated by entropy measures.

Theoretical approaches begin by assuming that the biometrics has high adversarial min-entropy (i.e., conditioned on all the auxiliary information available to an adversary, the entropy of the biometric is still high) and then proceed to distill this entropy into a key that is statistically close to uniform.

However, in practice, it is not always clear how to estimate the uncertainty of a biometric. In more practical settings, guessing entropy [7] has been used to measure the strength of keys.
It is shown that the average number of successive guesses, $E(G)$ , required with an optimum Strategy until one correctly guesses the value of a discrete random $X$ , is under bounded by the entropy H(X) in the manner

$$E[G] \geq \frac{1}{4} 2^{H(x)} + 1 \ldots (4)$$

Provided that $H(x)$ 2 bits, this bound is tight within a factor of (4/e) when $X$ is geometrically distributed. It is further shown that $E[G]_q$ may be arbitrarily large when $H(x)$ is an arbitrarily small positive number EO that there is no interesting upper bound on $E[G]$ in terms of $H(x)$.

We assume that a specific user u induces a distribution U over a finite, n-element set Ω. We also assume that an adversary has access to population statistics that also induce a distribution, P, over Ω. P could be computed from the distributions of other users u'!= u. We seek to quantify how useful P is at predicting U.

Let $\omega^* = \arg\max_{\omega \in \Omega} u(\omega)$. Let $L_P = (\omega_1, ..., \omega_n)$ be the elements of Ω ordered such that $P(\omega_i) \geq P(\omega_{i+1}) for\ all\ i \in [1, n-1]$. Define $t^-$ and $t^+$ to be the smallest index and largest index i
such that $|P(\omega_i) - P(\omega^*)| \leq \delta$. The Guessing Distance between $U$ and $P$ with tolerance δ is defined as:

$$GD_\delta(u, p) = \log \frac{t^- + t^+}{2} \ldots (5)$$

### 2.4 Distance Measurement Techniques

#### 2.4.1 Euclidian Distance

Most common and widely used distance measurement technique is Euclidian distance and is

given by

$$d_{Eucl} = \|v - c\|^2 \ldots (6)$$

Where is the test vector and is the template vector corresponding to class . The Euclidean distance treats all elements of the feature vector as equally important and uncorrelated.

#### 2.4.2 Posterior Probability

In [9], it is claimed that decisions that are based on the posterior probability densities are optimal, where optimality means minimal error rates. An error rate can be calculated based on either a single user scenario or a multi user scenario. In this context, optimality is defined as the lowest FAR for a given FRR or alternatively the lowest FRR for a given FAR. Where FAR and FRR are the most common measures of the performance of biometric authentication system and are defined by Rate of (or Percentage of) False authentication for a worng user and rate of False non authentication or rejection of a correct user. Thus posterior probability measures elaborates wheather it is feasible to obtain certain desired optimality for the system.

The posterior probability density of class $W$ given observed feature vector is given by

$$p(wv) = \frac{p(v \mid w).p(w)}{p(v)} \ldots (7)$$

where $p(v,w)$ is the probability density of the feature vectors given class $w$, $p(w)$ is the probability density of the class , and $p(v)$ is the prior probability density of the feature vectors. The feature vector is accepted as member of the template class if its posterior probability density exceeds a threshold $t \in [0, t_{\max}]$.

Thus it is important to define the rejection mechanism of a pattern along with its acceptance criteria.
It is known [l0] that the optimum rule is to reject the pattern if the maximum of the a posteriori probabilities is less than some threshold. More explicitly, the optimum recognition rule is given as
$\delta(d_k \mid v) = 1 \quad (k \neq 0)$
i.e., to accept the pattern v for recognition and to identify it as of the k[th] pattern class whenever
$p_k F(v \mid k) \geq p_i F(v \mid j)$ for all j=1,2,...,n (8)

And

$$p_k F(v \mid k) \geq (1-t)\sum_{i=1}^{n} p_i F(v \mid i) \ldots \quad (9)$$

To reject a pattern

$$\max_i [p_i F(v \mid i)] < (1-t)\sum_{i=1}^{n} p_i F(v \mid i) \ldots (10)$$

where $v$ is the pattern vector, $n$ is the number of classes, $(p_1, p_2, ..., p_n)$ is the a priori probability distribution of the classes, $F(v \mid i)$ is the conditional probability density for v given the i[th] class, $d_i (i != 0)$ is the decision that $v$ is identified as of the i[th] class while $d$, is the decision to reject, and t is a constant between 0 and 1 $(0 \leq t \leq 1)$.

**2.4.3 Quantization Error and Log Likelihood Ratio[4]**
There bound be the difference amongst the templates generated from one instance to another instance. Therefore under no way practically invariable templates can be generated. In order to minimize this variability, a quantization based technique is adopted by different works. According to this system, rather than using the values generated from the templates to generate the key, the template values can be quantized to set of values.
In a one-dimensional feature space V the likelihood ratio of user is defined as:

$$L_\omega = \frac{G(v, \mu_\omega, \sigma_\omega)}{G(v, \mu_0, \sigma_o)} \ldots (11)$$

Where the numerator defined the background probability density function and the denominator defines the actual probability density function of a user.
In simple terms, The generated pattern from the biometric features are Quantized to their nearest values and the likihood probability defines the fraction of probability of the quantized set to the probability distribution function of the actual set.

**2.4.4 Normalized Hamming Distance**
The formulated templates are converted into zeros and ones and are matched and similarity scores are calculated. Bit-wise comparison of the templates is made and Hamming distance is calculated for every such comparison. This is achieved by doing successive bit wise “X-OR”ing and “AND”ing. To account for the rotational inconsistencies the maximum matched value is chosen. The mask templates are used to ignore the noisy parts of the image. The formula for finding out the hamming distance is given as

$$HD = \frac{(codeA \otimes codeB) \cap maskA \cap maskB}{maskA \cap maskB} \quad \textbf{(12)}$$

**2.5 Ratio of Bit Error Rate v/s Template Length[5]**

It is fundamentally impossible to avoid noise during biometric data acquisition, because "life means change". For example, faces age and iris patterns are not perfectly invariant to a contraction of a pupil. More noise is introduced by changes in the environmental conditions, which is again an unavoidable circumstance. Finally noise often finds its way into the sensor, during transmission or in the data processing process ("algorithmic noise").

Thus noise removal from the templates must be considered an essential stage of biometric key generation.

The error corrected template is a *"bit identical" unique data set that can be derived repeatedly from the different noisy biometric templates of a user*.

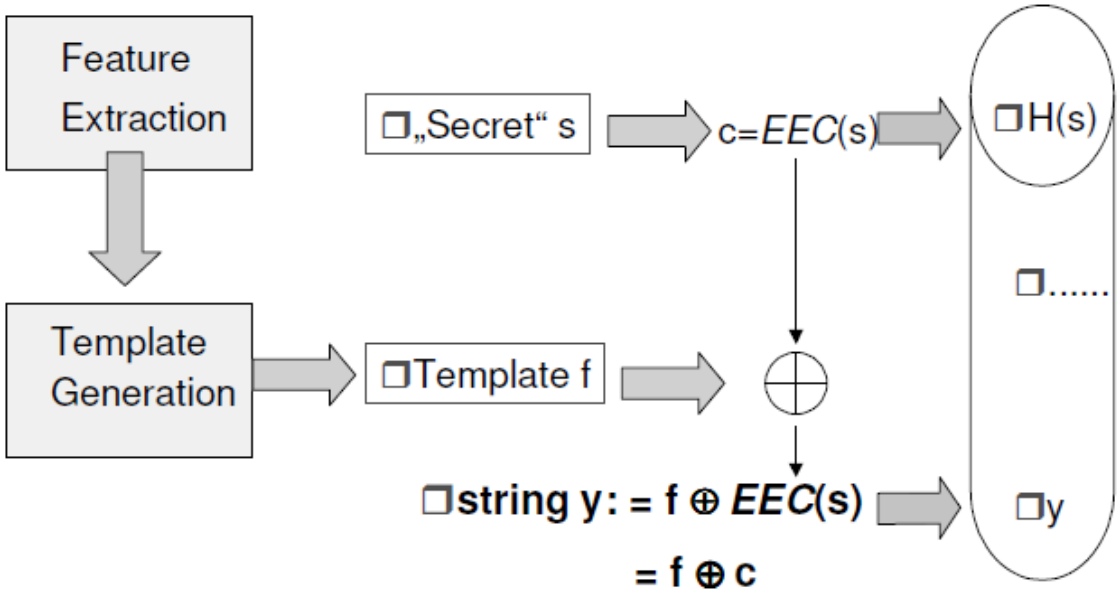


**FIGURE 3:** Biometric Key generation technique as par[11]

Juels and Wattenberg [18] proposed a very simple scheme based on any binary (not necessarily linear) [*n, k, 2t* +1] error correcting code *C* (+) GF(q)*n* for the Hamming distance with generator matrix G, where GF(q)*n* denotes the finite field with q elements. The encoding function transforms messages consisting of k symbols into n symbol code words (n>k), that can be retransformed into the original messages even if up to t symbols of the received codeword are corrupted due to error.

During enrolment, a random codeword, i.e. *c = G(s)* for a random *s* (+) GF(q)*k*, is bitwise added (XOR) to the biometric template *f* and the result is stored in the database as:

*y = c* (+) *f* *(13)*

Furthermore, the secret s is hashed with a cryptographic hash function H and H(s) is stored in the database. This scheme is sketched in symbolical form in figure 3.

For authentication, the template *f**, presented by the user, is added to the value y stored in the database. The result is *f**(+) *y = f** (+) *c* (+) *f.* If the hamming distance between *f** and *f* is at most

t, *c = G(s)* and hence s can be recovered. If the hash value of the recovered s matches the one stored in the database, the user is authenticated. This approach extracts a secret key from the biometric template presented and the corresponding public string. No information about this key shall be extractable from the public string without the corresponding biometric template.

Thus an error correction code must be device from the template and needs to be stored in a database. This code does not reveal any information about generating the template, rather can change the generated template such that the error with corresponding to the actual template from which the error correction code is derived is zero.
Thus we measure the bit error rate ratio as bit wise difference between the actual template and the generated template when the templates are converted into a binary bit stream. We adopt local binary patter generation technique for achieving the same.

**2.6 Related Work**
[1] Elaborates the various techniques for biometric data security by proposing a matching environment based on smart cards. It also elaborates the mechanism of generating a hash from the fingerprint biometric data and encrypting data through this hash.

Authors in [2] deal with the variability in the biometric templates. According to the finding of the author, every matching for authentication must also measure the quality of the just generated template and periodically must update the template in order to maintain high accuracy in biometric authentication process. The paper also presents matrices for biometric template quality analysis which is used in the proposed benchmark analysis work.

Authors in [3] elaborate the main problem with the conventional password based security techniques and emphasizes on the facts as to why the biometric keys are better than conventional keys. The work defines the technical steps associated with the keys and also discusses the properties of good biometric keys.

For biometric key generation from biometric features like faces and fingerprints, first image specific features must be extracted which is called templates. A quantization is applied on the template to generate the key. As real number range is infinity, if a key is generated without quantization, matching becomes a difficult process. Hence authors in [4] elaborate the mechanism for the quantization process for key generation. They also suggest a log likelyhood based technique for the same.

Even though biometric keys are strong technique for cryptographic key generation, because they are stored in the database, there remains a chance for the keys to be eavesdropped by unauthenticated users which makes the system vulnerable. Therefore techniques must also be adopted for such key generation. Hence authors in [5] proposes the techniques for securing the biometric key itself.

[6] proposes an Iris recognition technique with the help of bio orthogonal wavelets. But most importantly the authors in [6] proposes an encoding technique for the templates for ease in matching.

The strength of a biometric key is defined from the inability of a propoer guessing of a key using brute force technique. A biometric key appears random to any intruder. Therefore how he guesses the key depends upon the entropy information of a random variable that generates the key. [7] defines a mathematical relationship of probability of successful guess of a key with the entropy information of the templates and hence quantifies the fact that entropy analysis of any template is an important step in deciding the strength of the key.

The closeness of a template with the stored template depends upon the distance between the templates. This distance can be represented in various mathematical forms as proposed by the

authors of [8]. The authors also proves experimentally that log likelyhood measure is one of the better way of representing the closeness of two templates.

Whenever a mechanism is selected for biometric template matching for authenticating purpose, it invariably presents a false rejection and false acceptance on the biometric data and the mechanism itself. The authors in [9] presents a unique way to select the appropriate tradeoff between the rejection and acceptance tradeoff so that the adopted technique is acceptable and efficient. The author also presents a benchmark analysis for optimality for any recognition technique in [10] and illustrate the proposed theory with the help of character recognition system. Gabor based techniques are widely adopted for biometric feature representation or generation of templates. But the size of such initial vectors is so high that it presents a practical problem of storage. Thus biometric template reduction becomes an important aspect for biometric key generation or authentication technique. [12] presents a technique for minimizing the number of feature vectors for template generation.

Out of all the possible attacks on biometric keys the most severe attack is on the stored keys. This findings of [13] forms a base for our assumption that if a system can be deviced without the necessatiy for the key to be saved, a biometric system can be made un-attackable. Even though the authors present multi biometric model for hardening the security of a biometric system, the system still remains vulnerable against the attacks.

For any biometric like face or fingerprints or iris, templates will differ from one instance to the other instance of acquisition. Therefore out of N number of aquistion of the templates of a single feature type of a person there would certainly exist a variability amongst the templates. Therefore authors in [14] presents a systematic way of extracting the best template out of all the templates. This paper also presents an important step for biometric feature benchmark analysis by proposing a clustering technique for seggegating the biometric features by their average distance measures.

As against most widely used gabor convolve methods, authors in [15] proves that biorthogonal wavelets achieve higher accuracy with low FAR and high FRR. Thus Biorthogonal wavelet based template generation is selected as one of the methods for testing the quality of a biometric template for experiments in this paper.

[16] classifies the type of attack on the stored biometric systems and proposes a unique mechanism for minimizing the risk emerging from such attack. But the authors presents an important finding that encrypting the biometric keys or appending more security layer for protecting the biometric data leads to more complicated processing in the recognition phase which delays the overall time for recognition. This findings also strengthens the need for a system which can empirically analyze the quality of a biometric system before adopting it.

[17] presents a technique to remove the need of a centralize storage for biometric data with the help of smart cards. But the authors also emphesis that even such a card based system cannot guarantee a perfect un attackable system as the user information can be eavesdropped from the card itself.

[18] discusses various techniques by means of which the biometric data itself ( not the templates) can be acquired , forged and can be used. It also presents a wide verity of attacks and describes at which instance and which data sets the attacks can affect.

In [19] authors describes a technique for generation of digital signature from biometric template. Such signatures can be used in public key cryptography for encryption and decryption of digital documents shared across a network.

[20] analyzes the technique proposed by [11] to rectify the errors in generated template by using Reed Solmon code. The authors also proposes a unique mechanism for protection of biometric

key by storing the checksum rather than the key in the database. The authors also show that a key generation from biometric template and subsequent correction using the checksum improves the system security to a great deal. This work has adopted the elaborated model for error correction in biometric template.

In [21] authors have used irreversibility and revocability of the templates as a measurement for biometric key security and shows the technique of biometric matching in the secured environment. The authors present another significant observation here interms of feature selection. [21] finds that lower order features like means and standard deviation can not reveal the actual information of any feature set and higher order spectra is better suited for the representation of the features. Hence in our benchmark analysis, we have used a higher order spectra for determining the closeness of the templates.

[22] proposes an alternative method for biometric security through intronization. It is a process of adding extra feature systematically in the biometric template to increase the randomness of the template and also demonstrates that even after intronization, the achieved results are satisfactory.

[23] discusses one of the most least talked possible attacks on the biometric templates. The author here finds out a technique through which the image itself can be interpolated or reconstructed from leaked template. Therefore this image can be subsequently used to obtain un authorized information through hill climbing attack. Thus the findings demonstrates that not only the randomness of the templates are enough to provide security to the biometric system but at the same time it is also important to ensure that the inverse process of reconstruction of images should not be possible from the templates.

[24] elaborates a new technique called biometric template transformation be menas of which direct mathematical transformation can be achieved on the templates to extract more information from the templates. This important transformation is the answare for the following severe problem. Whenever a biometric key is encrypted, it can not be used for direct matching at the time of verification. The key needs to be decrypted before matching which invariably exposes the key. But with the help of direct transformation on the biometric templates, key matching can be performed over the encrypted keys, minimizing the requirement for a decryption stage prior to verification.

In [25] authors proves that presence of noise in the biometric data actually improves the security of the data itself. This claim is supported through entropy analysis of the generated key from the template and the relationship of energy and the entropy of the information.

[26] discusses various mathematical transformation related to guessing of a biometric key and presents a fish-bone model for categorization of the attacks on biometric data. The model helps in identifying various areas which must be considered for ensuring the security of biometric data.

[27] proposes a mechanism for mixing a biometric template with biometric key for biometric key protection.

[28] discusses about possible technique for face biometric and is used for selection of the techniques for the current work.

Merely ensuring a strong key generation technique is not sufficient for biometric technique adaptation. It must be checked for the feasibility of adaptation. [29] presents various means of feasibility check for biometric techniques.

[30] proposes an indexing scheme through binning to index the biometric images in a large database into groups for better classification and representation.

Authors in [31] discusses a unique technique for secured biometric mechanism by introduction of N-template system. The authors clasim and proves that if more than one template is generated from the same biometric feature like iris and a similarity measurement function can be deviced to find the similarity between the templates than, the empirical value of similarity can be used to authenticating the users rather than the template itself.

The method of selecting best templates or function that generates best templates are always result driven tests. Thus it is quite difficult to select the best templates out of available templates. [32] accesses this problem partially and presents a score based mechanism for template selection. In this work, the prototype of [32] is extended for selecting not only the best templates but for selecting the mechanism itself which can generate most acceptable templates.

[33] discusses various non technical issues alongside the technical issues for acception a biometric access control technique.

Improving the biometric recognition with 0% FAR and 0% FRR is considered to be ideal theoretical biometric system which is not yet achieved. Authors in [34] observe that most widely used technique for enhancing the security of a biometric system is through combining more than one modality like combining face and iris. But this needs the user to expose his features twice before two different sensors. Instead [34] proposes a mechanism to extract two different types of features from the same modality to enhance the recognition efficiency.

## 3. ALGORITHMIC APPROCH FOR BIOMETRIC TEMPLATE QUALITY BENCHMARK ANALYSIS

For analysis the quality of a specific biometric type and the template generated from the specific feature set of the template for time invariance analysis must be carried out with the following Model

i) First select d different type of biometric features like face, fingerprint, iris, Retina, Palm Print etc. We define D={Face,Iris,Fingerprint}---(14) as a set of different biometric types.

ii) U is a finite set of N users.

$$U = \{u_1, u_2, ..., uN_u\} \qquad (15)$$

iii) Select feature selection method for each type of D and let us consider that the feature

selection set is $F$

$$F = \{C_1, C_2, ..., C_{nc}, I_1, I_2, I_3, ..., I_{ni}, P_1, P_2, ...P_{np}\} \quad (16)$$

Where I,C,P represents feature selection methods for Iris, Face and Fingerprints respectively.

iv) Let T be a set of all the templates generated from all the feature selection technique from (14) with all the feature generation methods from (16) for all the users from (15).

$$T_i = \{T_{i1}, T_{i2}, T_{i3}, ..., T_{\text{int}}\} \quad (17)$$

Where nt is total number of templates and are given by

$nt = nu \text{ x } ni \text{ x } np \text{ x } nc$ (18) and i is used to denote independent users.

$T = \{T_i\}$ where i=1,2,….nu (19)

Now let us consider that templates of separate instances of the same users are taken over the time and is represented by j.

Then (19) is redefined as

$T = \{T_{ij}\}$ (20) where j=1,2,3….t where t is the maximum number of instances.

The objective is to find best F for which

$T_{ij} EQ T_{i(j-1)}$

$T_{i(j-1)} EQ T_{i(j-2)}$

$T_{i(j-t)} EQ T_{i(j-t-1)}$ for all $i$ (21)

(21) must also satisfy the constraints low SO and high SS as par equation (2) and (3).

Equal operator $EQ$ is defined as the set of distance measurement techniques.

$EQ = \{D_1, D_2, D_3, ..., D_m\}$ (22)

Where m are different types of distance measurement.

From (18) it is clear that as number of users increases, total number of analysis step also increases. Therefore rather than checking for (21) after generating all the features we need to minimize the selected features such that total number of comparison does not increase with number of instances and user.
In order to process the number of processing in (21) we define following steps
a) Generate two instances of feature vectors from each user for every technique to form the set $T_{ij}$ as in (20) for t=2.
b) For every user i, take the uncorrelated Euclidian distance E between template Ti1 and Ti2.

If($E_{ik}$>95%) where k represents template generation method F from (16), then

Delete Fk.

Therefore at the end of step (b) $F_1$ will be a reduced length set of techniques nf2 where nf2<nf, the standard set of all techniques F of length nf. These are the techniques which produces most similar templates after two instance comparison.
c) Now divide the users into two categories $C_1$ the set of all genuine user and $C_2$ a set of all imposters. $C_1$ and $C_2$ are constructed randomly with any user having equal probability to be in the set C1 or C2.

Calculate average SSf and SOf with all templates from every independent Feature generation technique where suffix f represents a particular feature or template generation technique.
Find out average SSf and SOf as Assf and Asof.
Omit all the f for which following condition is false.
(SSf<Assf)&&(SOf>Asof).

Hence after step C, we obtain a new set of feature generation technique F3 where nf3 or the length of feature selection technique is less than $nf_2$.

d) Now construct independent set $I_3$,$C_3$ and $P_3$ as set of techniques generating Iris features, face features and fingerprint features respectively.

Let the new length of the sets be $n_{i3}, n_{c3},$ and $n_{p3}$ respectively.

Select the Biometric feature set B as the maximum of $n_{i3}, n_{c3},$ and $n_{p3}$.

Hence $B = \max(n_{i3}, n_{c3}, n_{p3}) \in D$ (23).

Omit all F3 other than those belonging to B.
Thus finally F4 is the set of a feature generation techniques with High SO and low SS of either face or fingerprint or Iris.

e) Regenerate Template set $T_{ij}$ as in (20) for t=2. Now $T_{ij}$ must be further optimized to find out the techniques which satisfies the posterior probability principal calculated as (7) through (8) (9) and (10).

f) Finally after step e) we have all the template generation techniques which presents high autocorrelation with same class, low self similarity, high other similarity and high posterior probability. Thus the biometric key generated using these set of methods are better suited for proposed method as in finger 2.

g) Finally a bit stream is generated by using local binary patterns and the error correction code is saved as in section 2.5

h) Equation (20) is now checked by considering t where t>>2. Here Operator EQ is defined as the hamming distance between current Binary template and the previous binary template. At this step we can select the technique or set of techniques which are best suited to generate most time invariant templates.

## 4. TESTING AND RESULTS

For Face database, Yale face database B is used which contains 5760 single light source images of 10 subjects each seen under 576 viewing conditions (9 poses x 64 illumination conditions). For every subject in a particular pose, an image with ambient (background) illumination was also captured.

The IIT Delhi Iris Database is used for testing the iris images. The currently available database is from 224 users, all the images are in bitmap (*.bmp) format. All the subjects in the database are in the age group 14-55 years comprising of 176 males and 48 females. The database of 1120 images is organized into 224 different folders each associated with the integer identification/number. The resolution of these images is 320 x 240 pixels and all these images were acquired in the indoor environment.

FVC2004 Fingerprint database with DB1 and DB2 with both seta and setB are considered for testing the algorithms on the fingerprint images. Each database is 150 fingers wide and 12 samples per finger in depth i.e., it consists of 1800 fingerprint images.
Result Tables are developed by aggregating the results of images from independent classes.

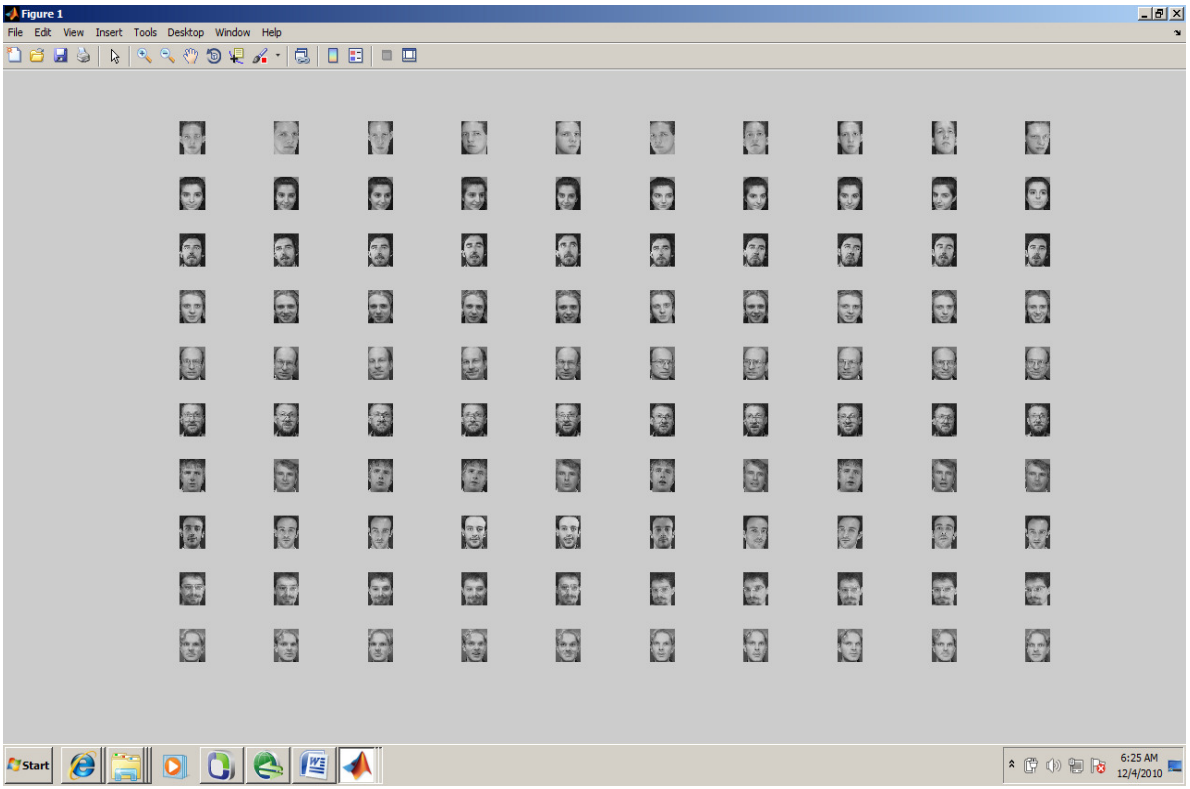


**FIGURE 4:** Face Database

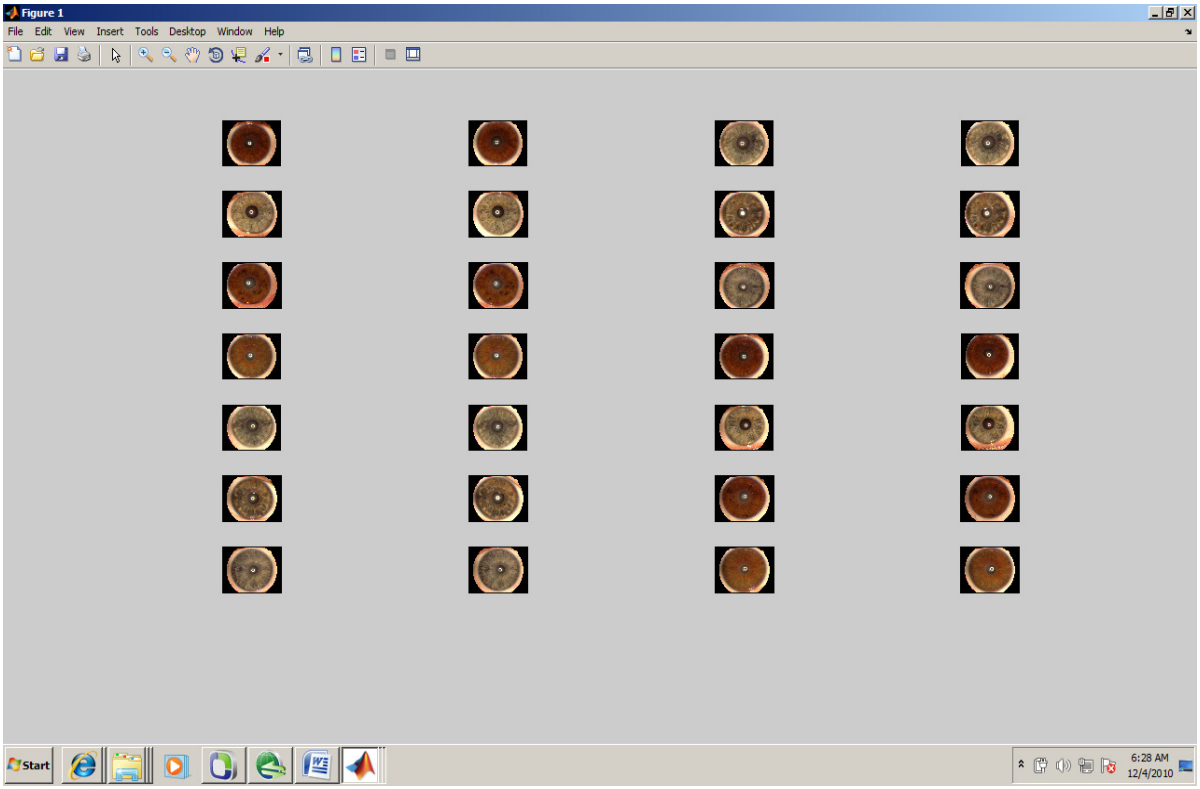


**FIGURE 5:** IRIS database

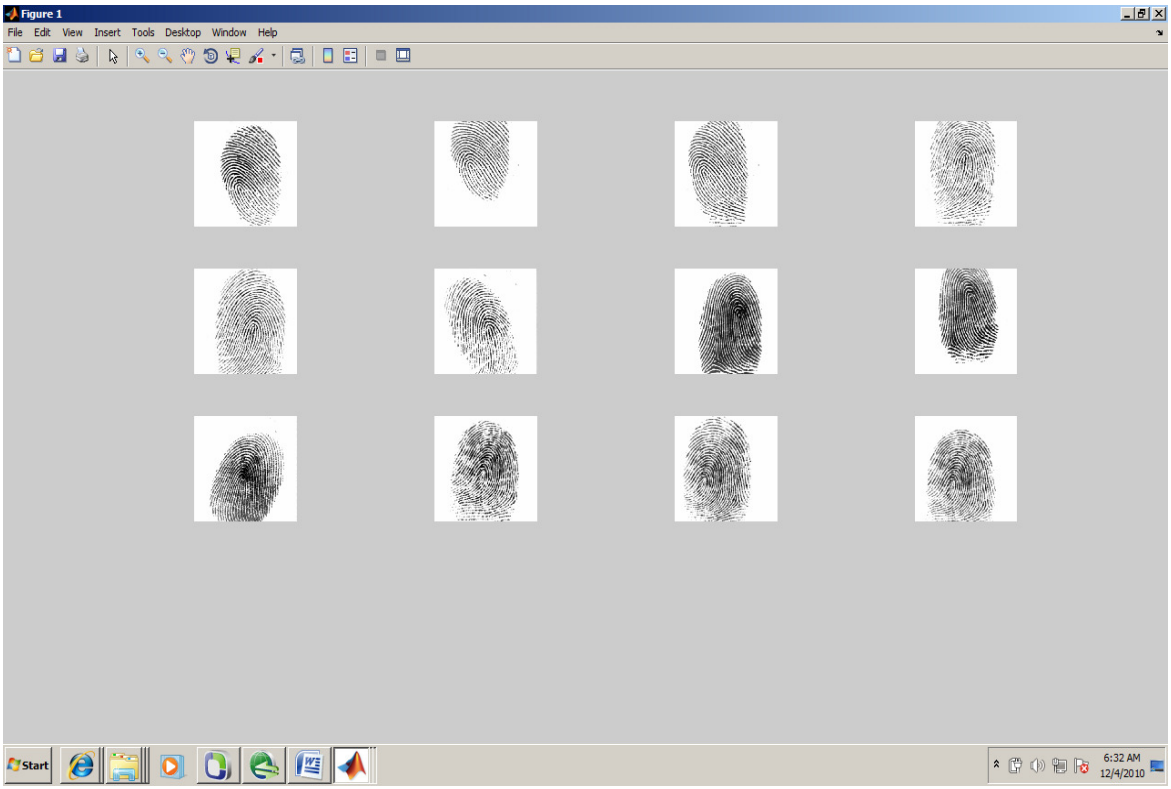


**FIGURE 6 :** Fingerprint Database

| Method | Hx | Gd | Average Ed | SS | SO | BER |
|---|---|---|---|---|---|---|
| GLCM | .12 | 11.63 | 1.03 | 1e-3 | 5291.35 | .2e-11 |
| Wavelet | .471 | 21.57 | 1.11 | .7e-3 | 588.334 | 16e-11 |
| Gabor Convolve | .14 | 29.519 | .0071 | .3e-4 | 2181.0 | 1.9e-19 |
| PCA | .11 | 29.6 | .031 | .000132 | 2664.1 | 1e-20 |
| ICA | .663 | 13.64 | 4.34 | .0096 | 998.03 | 1e-8 |
| BEST | PCA | GABOR/PCA | GABOR | GABOR | PCA | PCA |

**TABLE 1:** Sample Face Statistics Summery

| Method | Hx | Gd | Average Ed | SS | SO | BER |
|---|---|---|---|---|---|---|
| GLCM | .29 | 1.761 | 2.17 | .009 | 471.55 | 1e-9 |
| Wavelet | .27 | 4.17 | 9.11 | .003 | 426.334 | 1e-10 |
| Gabor Convolve | .22 | 19.0085 | 3.21 | .0001 | 1781.76 | 1e-19 |
| PCA | .19 | 16.6 | 1.61 | .00087 | 1864.122 | 1e-19 |
| ICA | .263 | .64 | 7.64 | .056 | 1011.03 | 1e-14 |
| BEST | PCA | GABOR | PCA | GABOR | PCA | PCA/GABOR |

**TABLE 2:** Sample summery of Fingerprint based methods

| Method | Hx | Gd | Average Ed | SS | SO | BER |
|---|---|---|---|---|---|---|
| GLCM | .45 | .0761 | 12.33 | .049 | 176.55 | 1e-8 |
| Wavelet | .21 | .0017 | 6.34 | .003 | 526.14 | 1e-12 |
| Gabor Convolve | .12 | .00083 | 2.21 | .0001 | 1271.76 | 1e-13 |
| PCA | .16 | .0016 | 4.61 | .00027 | 1464.882 | 1e-17 |
| ICA | .31 | .064 | 8.64 | .051 | 1011.03 | 1e-14 |
| BEST | GABOR | GABOR | GABOR | GABOR | PCA | PCA |

**TABLE 3:**Summary of performance of IRIS biometric templates

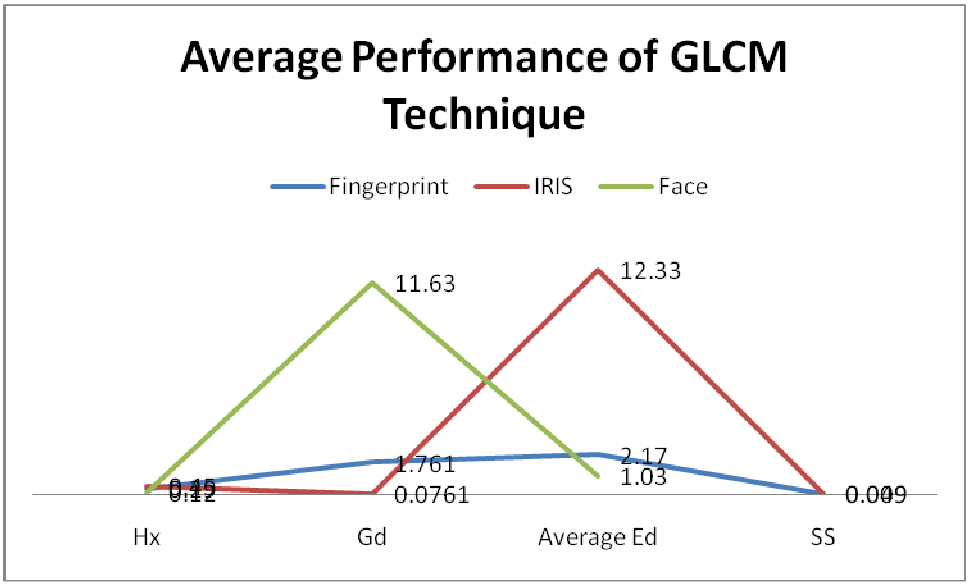


**FIGURE 7:** Avergare Performance of The GLCm technique

It is clear from Figure 7 that GLCM is a suitable technique for IRIS and Fingerprint due to low SS,HX and High GD. Though for face recognition system presents a very high Ed which makes it not a good choice for Face Recognition.

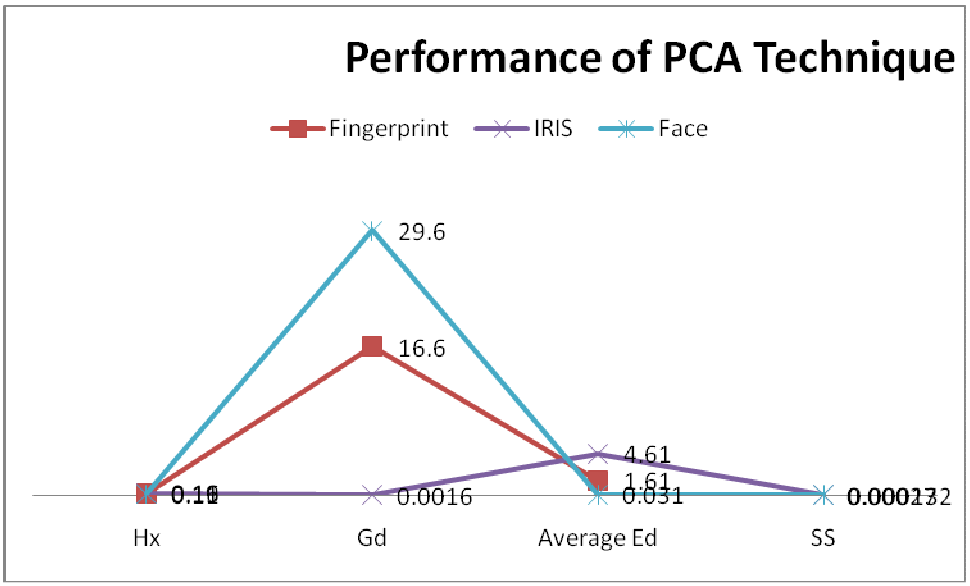


**FIGURE 8:** Performance of PCA with respect to all the techniques
The result demonstrate that PCA for classification of face , IRI and Fingerprint provides the desired properties of low Hx, High Gd, low SS and Hence can be adopted as universal biometric feature for any of the three biometrics with optimum result.

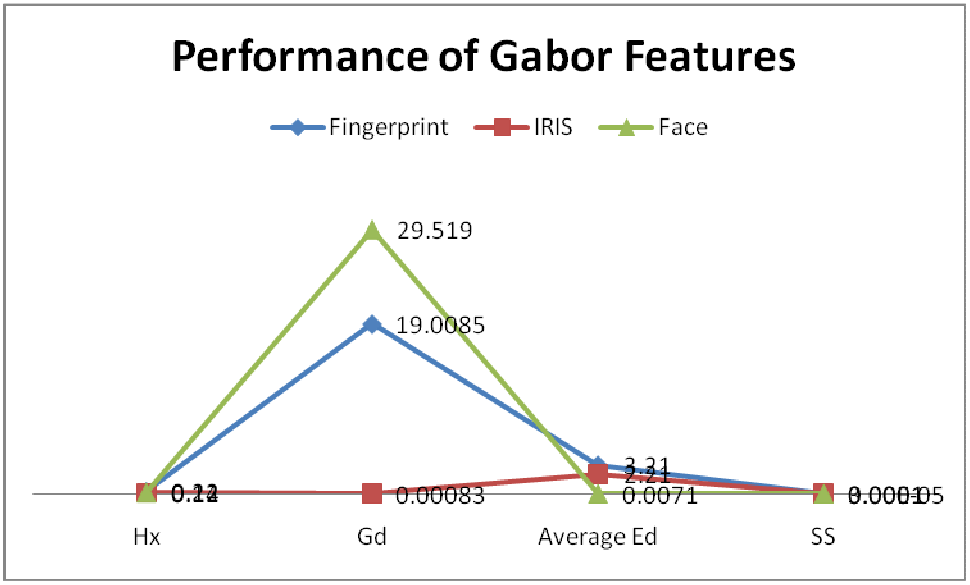


**FIGURE 9:** Performance of Gabor features for various biometrics also shows desireable result for all the biometrics.

In comparision to other techniques, Gabor convolve features and PCA features are more universially suitable for biometric recognition.

Hence it can be claimed that both of these features are more invariable and are more suited to biometric recognition.

**5. CONCLUSION**

Selecting an appropriate biometric model is an important step towards achieving high performance solutions. A lot of factors like scalability, usability and invariability must be analyzed amongst the models and the feature selection type for the template before finalizing the selection. Many work is proposed towards improving the efficiency of particular biometric technique as reviewed in related work. But there has not been any standard benchmark which offers a systematic analysis of benchmark of the performance of the system. In this work an entirely new approach of benchmark analysis for the quality of the selected biometric model and the technique is proposed based on invariability analysis of the templates from instance to instance. Results shows that IRIS has better invariability from both face and fingerprints and also offers better SO and SS values desired for high accuracy classification. The result also suggests that once time and instance invariant templates are generated, binarization process will always contain least bit error. Hence before any biometric model and technique is adopted, if the techniques available for the models are analyzed using this method, it can give an assurance of performance over the use. Further the proposed technique can be tested with many different other algorithms developed over the years for all the considered biometric model to present the proof of acceptance.

## 3. REFERENCES

[1] Magnus Pettersson, “The Match On Card Technology”, *Precise Biometrics White Paper*

[2] Ricardo García Noval, Francisco Perales López, “Poster: Adaptative Templates In Biometric Authentication”

[3] Lucas Ballard, Seny Kamara, Michael K. Reiter, “The Practical Subtleties of Biometric Key Generation”, *17th USENIX Security Symposium*

[4] C. Chen, R.N.J. Veldhuis, T.A.M. Kevenaar, A.H.M. Akkermans, “Multi-Bits Biometric String Generation based on the Likelihood Ratio”, *DOI: Multi-Bits Biometric String Generation based on the Likelihood Ratio,IEEE, 2007*

[5] U. Korte, R. Plaga, “Cryptographic Protection of Biometric Templates: Chance, Challenges and Applications”

[6] Aditya Abhyankar , Stephanie Schuckers, “Novel Biorthogonal Wavelet based Iris Recognition for Robust Biometric System”, *International Journal of Computer Theory and Engineering, Vol. 2, No. 2 April, 2010 1793-8201*

[7] James L. Maseey, “Guessing and Entropy”,*DOI: 0 - 7803-2015-8/94, IEEE,1994*

[8] Asker M. Bazen and Raymond N. J. Veldhuis, “Likelihood-Ratio-Based Biometric Verification”, *Ieee Transactions On Circuits And Systems For Video Technology, Vol. 14, No. 1, January 2004, 1051-8215/04,Ieee, 2004*

[9] C. K. CHOW, “On Optimum Recognition Error and Reject Tradeoff”, *IEEE Tr.4nsactions On Information Theory, Vol. It-16, No. 1, January 1970*

[10] C. K. CHOW, “An Optimum Character Recognition System Using Decision Functions”, *PGEC, June 3, 1957*

[11] Juels A. and Wattenberg M., "A Fuzzy Commitment Scheme", ACM Conference on Computer and Communications Security", 1999, p.28-36

[12] Daniel Gonz´alez-Jim´enez and Jos´e Luis Alba-Castro, “Modeling Marginal Distributions of Gabor Coefficients: Application to Biometric TemplateReduction”, *project PRESA TEC2005-07212*

[13] V. S. Meenakshi and Dr G. Padmavathi, “Securing Revocable Iris and Retinal Templates using Combined User and Soft Biometric based Password Hardened Multimodal Fuzzy Vault”, *IJCSI International Journal of Computer Science Issues, Vol. 7, Issue 5, September 2010 ISSN (Online): 1694-0814*

[14] Anil Jain, Umut Uludag and Arun Ross, “Biometric Template Selection: A Case Study in Fingerprints”, *Proc. of 4th Int'l Conference on Audio- and Video-Based Person Authentication (AVBPA), LNCS 2688, pp. 335-342, Guildford, UK, June 9-11, 2003.*

[15] Aditya Abhyankar and Stephanie Schuckers, “Novel Biorthogonal Wavelet based Iris Recognition for Robust Biometric System”, *International Journal of Computer Theory and Engineering, Vol. 2, No. 2 April, 2010 1793-8201*

[16] Abhishek Nagar, Karthik Nandakumar, and A. K. Jain, “Biometric template security”, *SPIE, 10.1117/2.1200911.001590*

[17] Julien Bringer, Herve Chabanne, David Pointcheval, and Sebastien Zimmer, “An Application of the Boneh and Shacham Group Signature Scheme to Biometric Authentication”, *Springer-Verlag 2008*

[18] Qinghan Xiao, “Security Issues in Biometric Authentication”, *Proceedings of the 2005 IEEE,Workshop on Information Assurance and Security, United States Military Academy, West Point, NY*

[19] Yunsu Chung, Kiyoung Moon, Hyung-Woo Lee, “Biometric Certificate based Biometric Digital Key Generation with Protection Mechanism”, *Frontiers in the Convergence of Bioscience and Information Technologies 2007*

[20] Andrew Beng Jin Teoh, Thian Song Ong, “Secure Biometric Template Protection via Randomized Dynamic Quantization Transformation”, *1-4244-2427-6/08,IEEE*

[21] Brenden Chen and Vinod Chandran, “Biometric Template Security Using Higher Order Spectra”, *978-1-4244-4296-6/10, IEEE,2010*

[22] Qinghai Gao, Xiaowen Zhang, and Michael Anshel, “Experiments on Matching Intronized Fingerprint Minutiae Templates”, *IJCSNS International Journal of Computer Science and Network Security, VOL.8 No.9, September 2008*

[23] Andy Adler, “Vulnerabilities in biometric encryption systems”, *IST-044-RWS-007*

[24] Michael Braithwaite, Ulf Cahn von Seelen, James Cambier,, “Application-Specific Biometric Templates”

[25] E. Verbitskey,D. Denteneer, P. tuylys, “Reliable biometric authentication with privacy protection.”

[26] Anil K. Jain, Karthik Nandakumar, and Abhishek Nagar, “Biometric Template Security”, *EURASIP Journal on Advances in Signal Processing Volume 2008, Article ID 579416, 17 pages, doi:10.1155/2008/579416*

[27] Shih-Wei Sun¤*y*, Chun-Shien Lu¤, and Pao-Chi Chang*y,* "Biometric Template Protection: A Key-Mixed Template Approach", *1-4244-0763-X/07, IEEE, 2007*

[28] Morpho, "Automatic Facial Recognition: A review", *SAFRON*

[29] Tony Mansfield, Marek R. G., "Feasibility study on the use of biometric in an Entitlement scheme, Biometric Feasibility Study", *Version 3, 2003*

[30] Srinivasa Palla, Sharat S. Chikkerur, Venu Govindaraju, Pavan Rudravaram, "Classification and Indexing in Large Biometric Databases"

[31] Tarachand Verma, Prof. Richa Jindal, Prof. Sonika Jindal, "A Security Algorithm For Iris Based Biometric System", *International Journal Of Engineering Science And Technology, Vol. 2(06), 2010, 2316-2320*

[32] Yong Li, Jianping Yin, En Zhu, Chunfeng Hu, Hui Chen, "Score Based Biometric Template Selection", *978-1-4244-2175-6/08/, IEEE, 2008*

[33] Luisa Riccardi, Bruno Peticone and Mario Savastano, "Biometrics for massive access control Traditional Problems and Innovative Approaches", *Proceedings of the 2005 IEEE Workshop on Information Assurance and Security United States Military Academy, West Point, NY*

[34] C.Lakshmi Deepika, A.Kandaswamy, "An Algorithm for Improved Accuracy in Unimodal Biometric Systems through Fusion of Multiple Feature Sets", *ICGST-GVIP Journal, ISSN 1687-398X, Volume (9), Issue (III), June 2009*

# Content Based Image Retrieval Approaches for Detection of Malarial Parasite in Blood Images

**Mohammad Imroze Khan** *imroze786@gmail.com*
*Lecturer/Department of Electronics & Telecommunication*
*National Institute of Technology Raipur,*
*Raipur, 492010, India*

**Bibhudendra Acharya** *bacharya.etc@nitrr.ac.in*
*Assistant Professor/Department of Electronics & Telecommunication*
*National Institute of Technology Raipur,*
*Raipur, 492010, India*

**Bikesh Kumar Singh** *bsingh.bme@nitrr.ac.in*
*Assistant Professor/Department of Electronics & Telecommunication*
*National Institute of Technology Raipur,*
*Raipur, 492010, India*

**Jigyasa Soni** *jigyasha2006_elex@yahoo.com*
*M. Tech Student/Department of Electronics & Telecommunication*
*Shri Shankracharya College of Engineering & Technology,*
*Bhilai, 490020, India*

**Abstract**

Malaria is a serious global health problem, and rapid, accurate diagnosis is required to control the disease. An image processing algorithm to automate the diagnosis of malaria in blood images is proposed in this paper. The image classification system is designed to positively identify malaria parasites present in thin blood smears, and differentiate the species of malaria. Images are acquired using a charge-coupled device camera connected to a light microscope. Morphological and novel threshold selection techniques are used to identify erythrocytes (red blood cells) and possible parasites present on microscopic slides. Image features based on colour, texture and the geometry of the cells and parasites are generated, as well as features that make use of a priori knowledge of the classification problem and mimic features used by human technicians. A two-stage tree classifier using back propogation feed forward neural networks distinguishes between true and false positives, and then diagnoses the species (Plasmodium Falciparum, P. Vivax, P. Ovale or P. Malariae) of the infection. Malaria samples obtained from the various biomedical research facilities are used for training and testing of the system. Infected erythrocytes are positively identified with two measurable parameters namely sensitivity and a positive predictive value (PPV), which makes the method highly sensitive at diagnosing a complete sample, provided many views are analyzed.

**Keywords:** Falciparum, Vivax, Ovale, Malariae and Giemsa

## 1. INTRODUCTION

This guideline is used for all journals. These are the manuscript preparation guidelines used as a Malaria is caused by parasites of the species Plasmodium that are spread from person to person through the bites of infected female mosquitoes. It can also be transmitted through blood transfusions. If an infected person donates blood, the blood will contain malaria parasites. If the blood is put into another person's body, the parasites will also flow into his or her bloodstream. For the most serious form of malaria, the incubation period is eight to twelve days. In some rare forms of malaria, the incubation period can be as long as ten months.

### 1.1 Facts and Figures

Approximately, 40% of the world's population, mostly those living in the world's poorest countries, is at risk of malaria. A child dies of malaria every 30 seconds. Every year, more than 500 million people become severely ill with malaria. [1]. Between 300 million to 500 million people in Africa, India, Southeast Asia, the Middle East, the South Pacific, and Central and South America have the disease. The worldwide annual economic burden of malaria, calculated to include spending on prevention and treatment as well as loss of productivity due to illness, was estimated at US$ 500 million in 2005[2].

### 1.2 Diagnosis of Malaria

The definitive diagnosis of malaria infection is done by searching for parasites in blood slides (films) through a microscope. In peripheral blood sample visual detection and recognition of Plasmodium spp is possible and efficient via a chemical process called (Giemsa) staining.

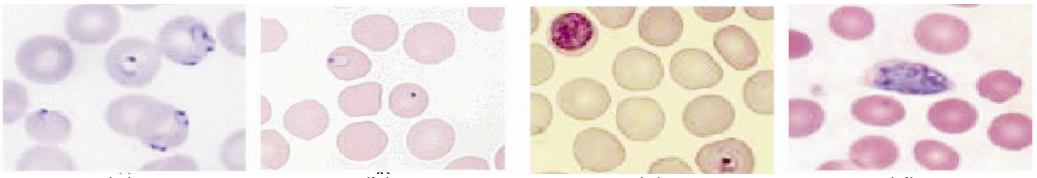


**FIGURE 1:** (a) P. Falciparum (b) P. Vivax (c) P. Malariae (d) P. Ovale

The staining process slightly colorizes the red blood cells (RBCs) but highlights Plasmodium spp parasites, white blood cells (WBC), and platelets or artifacts. The detection of Plasmodium spp requires detection of the stained objects. However, to prevent false diagnosis the stained objects have to be analyzed further to determine if they are parasites or not. [1]

In the Fig.1:, there are four types of human malaria – Plasmodium Falciparum, P. Vivax, P. Malariae, and P. Ovale. P. Falciparum and P. Vivax are the most common. P. Falciparum is by far the most deadly type of malaria infection.

### 1.3 Clinical Presumptive Diagnosis

The appearance of clinical symptoms is usually the reason that urges the ill patient in industrialized non endemic countries to turn to the physician. Clinicians in western countries need to be well aware of the possibility of imported malaria cases. Diagnosis in these cases may be made difficult by the possibility that the exposure to the infective bite may date back to a long time before clinical symptoms appear, especially in the case of P. vivax or P. malariae infections. The accurate geographical history should be a routine in every interrogation of every patient even in the malaria-free world. Finally, it is to be stressed that P. falciparum malaria in non immune subjects coming from non endemic western countries may be extremely severe, with high case fatality rates if correct diagnosis and treatment is not carried out promptly.

### 1.4 Laboratory Diagnosis

Once malaria is suspected on clinical grounds, it is mandatory to obtain the laboratory confirmation of the presence of malaria parasites in the patient's organism, whenever possible. The diagnosis of malaria may in fact be pursued by the direct demonstration of the parasite whole cell or of parasite's nucleic acid or products in the blood (direct diagnosis) or by the demonstration of the patient's immune response to the infection (indirect diagnosis or immune diagnosis).

Direct diagnosis: The Laboratory material needed for light microscopical observation of thin and thick films for malaria diagnosis are given below:

- Optic microscope with 100x oil immersion objective

- Electric supply of adequate mirrors for sun light
- Stain stock solution
- Buffered distilled/de-ionized water
- Graduated cylinders
- Staining recipients
- Clean glass slides
- Cover slips (optional)
- Disinfectant alcoholic solution
- Sterile pricking needles
- Gauze or cotton

### 1.5 Light Microscopic Observation

The direct microscopic observation of stained blood specimens requires specific instrumentation and reagents (microscope, microscopic slides, pricking needle, staining reagents, water, electric or solar light, etc. and a trained professional to obtain to a correct diagnosis. Information on basic microscopy, the basic staining procedures and on the most common mistakes is given together with the morphological clues to make an adequate qualitative (stage and species diagnosis) and quantitative (parasitaemia) diagnosis of malaria infection at the district level.

### 1.6 Fixation and Staining Procedures

Thin and thick films may be allowed to dry in the air protected by dust, or actively dried by waving it. It is important to avoid abrupt exposure to heath (fire, sunlight) that may lead to fixation and fissure the preparations. Fixation may be achieved by heat and alcoholic solutions. Methanol (methyl alcohol) is the most widely used fixative for malaria thin films. Contact with methanol should be maintained for 10-20 seconds. If both thin and thick films are on the same slide, it is mandatory to avoid the contact of methanol (or even of its fumes!) with the thick film to avoid fixation.

*Giemsa staining procedure:* To achieve optimal results, it is important that the Giemsa staining solution is prepared with distilled or de-ionized water buffered to pH 7.2. The Giemsa staining solution is prepared by diluting Giemsa stain with buffered water. A ratio 1:10 and 1:20 is usually used for staining thin and thick films respectively, that is 2 to 1 drops of Giemsa per ml of buffered water. Grossly, 5 ml of the solution is necessary to stain each single slide. The Giemsa stain is then poured onto the slide (or the slide is immersed in the staining trough) and contact is maintained for 30-40 minutes depending on the local climatic conditions. The staining solution is then removed by gentle but accurate rinsing with buffered distilled water and the slide is then drained on filter paper and allowed to dry in air. When the clinical situation requires immediate action, thick films may be stained with a Giemsa accelerate procedure. The qualitative morphological results are however far worse than the usual ones. Briefly, the thick smear is allowed to dry under a heat source of up to 50°C (even sunlight is suitable if slides are protected from dust) and then stained for 8 minutes with a 10% Giemsa solution (2 drops/ml) before rinsing and drying. Giemsa staining is the most commonly used method for both thin and thick films all over the world for the quality of the stain and, of greater importance, its stability in tropical climates.

### 1.7 Basic Microscopy

The microscope is an essential component of the malaria diagnostic laboratory, even in field condition. The care and maintenance of the microscope is thus of the outmost importance. A basic knowledge of the main features of a microscope is also required (World Health Organization, 1991). A monocular microscope is best suited for a natural solar light source, but the quality and the ease of observation is greatly improved when a binocular microscope (requiring electric light supply) is used. A routine microscope usually has three objectives (10x, 40x, 100x magnifications). The 100x objective is also referred to as an “immersion objective” and has to be used to observe blood smears. The binoculars also have their own magnification (6x or

7x are preferred for malaria diagnosis), the total magnification resulting from the multiplication of both lenses. The following practical suggestions may be of help for a better use of this invaluable diagnostic tool:

- Place the slide on the stage;
- Keep the diaphragm completely open and raise the condenser to reach the brightest field;
- Using the coarse adjustment lower the stage (or lift the objective, depending on the microscope used) to the maximum distance from the objective revolver;
- Place one drop of immersion oil on the slide;
- Using the coarse adjustment, lift the stage to allow the oil drop to touch the lens of the objective;
- Using the fine adjustment, sharply focus by slightly lowering the stage again;
- Modulate iris diaphragm to obtain optimal illumination;
- Clean the objective lenses with soft gauze or lens tissue.
- Use Xylene (always avoid strong alcohol solutions or acetone as these substances may dissolve the glue used to fix the objective lenses) only from time to time to remove traces of dried oil.

### 1.8 Morphological Species and Stage Diagnosis [6]

Complete knowledge of the morphological features of the different blood stages of the different Plasmodia species represents the essential basis of a correct laboratory diagnosis confirmation of malaria infection. It is to be stressed that a correct diagnosis may be done only after attentive and careful observation of a number of microscopic fields (at least 100 microscopic fields should be observed before a thick film may be classed as negative) and of a number of different morphologic characteristics that draw a well defined picture of the species. A crescent-shaped gametocyte in peripheral blood does not obligatorily mean that a P. falciparum infection is the cause of the actual clinical complaint and, however, does not rule out the possibility of mixed infection.

## 2. TEST ALGORITHM

The design is essentially an image classification problem, and thus takes the form of a standard pattern recognition and classification system in Fig. 2:. It consists of five stages:

1. Image Acquisition (Done using high resolution Digital Camera)
2. Image Analysis
3. Image Segmentation
4. Feature Generation
5. Classification of Parasite and result verification

### 2.1 Image Analysis

Image analysis usually starts with a pre-processing stage, which includes operations such as noise reduction.

#### 2.1.1 Test Algorithm Using Filtering Approach

Different test algorithms using filter approach are describe below.

##### 2.1.1.1 Median Filtering: [15]

In microscopic image processing, it is usually necessary to perform high degree of noise reduction in an image before performing higher-level processing steps, such as edge detection. The median filter is a non-linear digital filtering technique, often used to remove noise from images or other signals. The idea is to examine a sample of the input and decide if it is representative of the signal. This is performed using a window consisting of an odd number of samples. The values in the window are sorted into numerical order; the median value, the sample in the center of the window, is selected as the output. The oldest sample is discarded, a new sample acquired, and the calculation repeats.

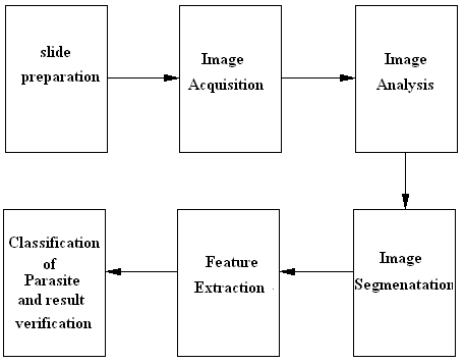


**FIGURE 2:** Block schematic of the parasite detection system

Algorithm: The median filter considers each pixel in the image in turn and looks at its nearby neighbors to decide whether or not it is representative of its surroundings. Instead of simply replacing the pixel value with the mean of neighboring pixel values, it replaces it with the median of those values. The median is calculated by first sorting all the pixel values from the surrounding neighborhood into numerical order and then replacing the pixel being considered with the middle pixel value. (If the neighborhood under consideration contains an even number of pixels, the average of the two middle pixel values is used.)

#### 2.1.1.2. Non Linear Filtering: SUSAN

For a real time system using time varying image sequences, speed is an important criterion to be considered. Also there has to be a compromise between maximizing signal extraction and minimizing output noise: the so-called “Uncertainty Principle” of edge detection. I have implemented a new approach to low-level image processing - SUSAN (Smallest Uni-value Segment assimilating Nucleus) Principle [16], which performs Edge and Corner Detection and Structure Preserving Noise Reduction. Canny edge detector, which has become one of the most widely used edge finding algorithms, is found to be ten times slower than this SUSAN approach. The results are stable for Canny but the edge connectivity at junction is poor and corners are rounded. The fact that SUSAN edge and corner enhancement uses no image derivative, explains why the performance in the presence of noise is good. The integrating effect of the principal together with its non-linear response gives strong noise rejection.
Algorithm: The following steps are performed at each image pixel:

- Place a circular mask around the pixel in question.
- Calculate the number of pixels within the circular mask which have similar brightness to the nucleus. These define the USAN.
- Subtract USAN size from geometric threshold to produce edge strength image.
- Use moment calculations applied to the USAN to find edge direction.
- Apply non-maximum suppression thinning and sub-pixel estimation, if required.

Hence SUSAN allows image edges, corners and junctions to be accurately and quickly found and a related method for reducing noise whilst preserving image structure. The localization of the features is independent of the mask size used and noise suppression is shown to be good.

### 2.1.2 Test Algorithm Using Edge Detection Approach

Edge detection is one of the most commonly used operations in image analysis. An edge is defined by a discontinuity in gray level values. In other words, an edge is the boundary between an object and the background. The shape of edges in images depends on many parameters: The geometrical and optical properties of the object, the illumination conditions, and the noise level in the images. The importance of the classification is that it simplifies several problems in Artificial Vision and Image Processing, by associating specific processing rules to each type of edges. The classification is based on the behavioral study of these edges with respect to the following differentiation operators. From each category in the classification, at least one algorithm has been chosen for implementation.[15]

Gradient edge detectors: This contains classical operators and uses first directional derivative operation. It includes algorithms such as: Sobel (1970), Prewitt (1970) etc.
Zero Crossing: This uses second derivative and includes Laplacian operator and second directional derivative.
Laplacian of Gaussian (LoG): This was invented by Marr and Hildreth (1980) who combined Gaussian filtering with the Laplacian. This algorithm is not used frequently in machine vision.
Gaussian Edge Detectors: This is symmetric along the edge and reduces the noise by smoothing the image. The significant operator here is Canny that convolves the image with the derivative of Gaussian for Canny.

### 2.2 Image Segmentation

For the actual recognition stage, segmentation should be done before it to extract out only the part that has useful information. The goal of the segmentation process is to define areas within the image that have some properties that make them homogeneous. The definition of those properties should satisfy the general condition that the union of neighboring regions should not be homogeneous if we consider the same set of properties. After segmentation, the discontinuities in the image correspond to boundaries between regions can be easily established.

#### 2.2.1 Test Algorithm Using Thresholding

Thresholding can be applied locally, i.e. within a neighborhood of each pixel, or globally. Due to highly varying defect sizes, it will be impossible to find one neighborhood size that works for all. Thus, following global thresholding techniques are implemented to test their achievability.
Otsu: Otsu's method is still among the most referenced methods in segmentation [17]. It is based on minimizing within-class variances of foreground and background pixels.
Entropy: Kapur et al. explained foreground and background of an image as different signals [18]. Therefore, optimal threshold is the one maximizing the sum of the two class entropies as shown in following (1).

$$H = max\left[ -\sum_{i=0}^{T_{opt}} p_i log(p_i) - \sum_{i=T_{opt}+1}^{255} p_i log(p_i) \right] \quad (1)$$

#### 2.2.2 Test Algorithm Using Region Based Segmentation

Different test algorithms using Region based segmentation approaches are describe below.

##### 2.2.2.1 Watershed Segmentation [15]

Separating touching blood cells in an image is a difficult issue in the project. The watershed transform could minimize this problem. The watershed transform finds "catchment basins" and "watershed ridge lines" in an image by treating it as a surface where light pixels are high and dark pixels are low.
In watershed based segmentation, each local minima of a gray-scale image I is regarded as a surface has a hole and the surface is immersed out into water. Then, starting from the minima of lowest intensity value, the water will progressively fill up different catchment basins of image (surface) I. Conceptually the algorithm then builds a dam to avoid a situation that the water coming from two or more different local minima would be merged. At the end of this immersion process, each local minimum is totally enclosed by dams corresponding to watersheds of image (surface) I.

##### 2.2.2.2 Marker-Controlled Watershed Segmentation [15]

Watershed transform can separate touching cells but not overlapping cells. For this Marker-controlled watershed segmentation is used instead. It follows this basic procedure:

1. Compute a segmentation function. This is an image whose dark regions are the object one is trying to segment.
2. Compute foreground markers. These are connected blobs of pixels within each of the objects.
3. Compute background markers. These are pixels that are not part of any object.

4. Modify the segmentation function so that it only has minima at the foreground and background marker locations.
5. Compute the watershed transform of the modified segmentation function

**2.2.3 Test algorithm Using Morphology**
Different test algorithms using Morphology approach are describe below.

**2.2.3.1. Morphological Granulometry and Gradient [20]**
Here gray scale granulometries based on opening with disk shape elements are used. Non flat disk shaped structural element are used to enhance the roundness and compactness of the red blood cells and flat disk shaped structural element are used to segment overlapping cells. The method makes use of the knowledge of size of the red blood cells making use of granulometries.

**2.2.3.2. Top-Hat and Bottom-Hat Transforms [15]**
The Top-hat is defined as the image minus the opening of the image. The Bottom-hat is defined as the closing of the image minus the image.

**2.3 Feature Extraction**
Feature selection is one of the most important tasks in data mining area, with methods which allows determining the most relevant features for pattern recognition. A suitable subset of features is found when it permits synthesizing the similarity of the pattern within its class and dissimilarity amongst other different classes. The goal of feature selection is to reduce the dimensionality of vectors associated to patterns selecting a subset of attributes smaller than the original. The classifier performance is often improved eliminating redundant features. Hence the purpose of feature generation is to compute new variables from the image array that concentrate information to separate classes. The classifier has two functions: it must determine whether or not a detected cell is truly positive for malaria, and what the species of the infection is. Features are created with these functions in mind. They provided information with which the classifier distinguished between parasites and other artifacts in the blood, and allowed the classifier to differentiate between parasites of different species. The final performance of the classifier directly depended on the success of the feature generation stage. Two sets of features had been chosen for development. The first set is based on image characteristics that have been used previously in biological cell classifiers, which include geometric features (shape and size), colour attributes and grey-level textures [18, 19].

**2.3.1 Test Algorithm Using First Order Features (Mean, Standard Deviation, Skewness, Kurtosis, Energy and Entropy) [15]**
Texture is generated from the grayscale image matrices of the red, green and blue components, as well as the intensity component from the hue-saturation-intensity image space. First order features, based on the image histograms are used.

1. Average gray level or mean
2. Average contrast or standard deviation
3. Third moment or skewness
4. Kurtosis
5. Energy
6. Entropy or Randomness

$$\text{Mean:} \qquad S_M \equiv \bar{b} = \sum_{b=0}^{L-1} bP(b)$$

$$\text{Standard Deviation:} \quad S_D = \left[ \sum_{b=0}^{L-1} (b-\bar{b}) \right]^{1/2}$$

$$\text{Skewness:} \qquad S_S = \frac{1}{\sigma_b^3} \sum_{b=0}^{L-1} (b-\bar{b})^3 P(b)$$

$$\text{Kurtosis:} \quad S_K = \frac{1}{\sigma_b^4}\sum_{b=0}^{L-1}(b-\bar{b})^4 P(b) - 3$$

$$\text{Energy:} \quad S_N = \sum_{b=0}^{L-1}[P(b)]^2$$

$$\text{Entropy:} \quad S_E = -\sum_{b=0}^{L-1} P(b)\log_2[P(b)]$$

Where, P (b) is the first-order histogram estimate, Parameter b is the pixel amplitude value. L is the upper limit of the quantized amplitude level. Finally, σ is the standard deviation. Geometric features like size information such as the area and equivalent radius are also utilized.

**2.3.2. Test Algorithm Using Moment Invariant Features [21]**

Moment invariants have been frequently used as features for image processing, remote sensing, shape recognition and classification. Moments can provide characteristics of an object that uniquely represent its shape. Invariant shape recognition is performed by classification in the multidimensional moment invariant feature space. Several techniques have been developed that derive invariant features from moments for object recognition and representation. These techniques are distinguished by their moment definition, such as the type of data exploited and the method for deriving invariant values from the image moments. These moment invariant values are invariant with respect to translation, scale and rotation of the shape.

Seven of these shape descriptor values are computed from central moments through order three that are independent to object translation, scale and orientation. Translation invariance is achieved by computing moments that are normalised with respect to the centre of gravity so that the centre of mass of the distribution is at the origin (central moments). Size invariant moments are derived from algebraic invariants but these can be shown to be the result of a simple size normalisation. From the second and third order values of the normalised central moments a set of seven invariant moments can be computed which are independent of rotation. The moments used to construct the moment invariants are defined in the continuous but for practical implementation they are computed in the discrete form. Given a function f(x, y), these regular moments are defined by the following (2).

$$M_{pq} = \iint x^p y^q f(x,y)\,dx\,dy \tag{2}$$

Where, Mpq is the two-dimensional moment of the function f(x,y). The order of the moment is (p + q) where p and q are both natural numbers. For implementation in digital from this becomes (3):

$$M_{pq} = \sum_x x^p \sum_y y^q f(x,y) \tag{3}$$

To normalise for translation in the image plane, the image centroids are used to define the central moments. The co-ordinates of the centre of gravity of the image are calculated using the previous equation and are given by (4):

$$\bar{x} = \frac{M_{10}}{M_{00}} \quad \text{and} \quad \bar{y} = \frac{M_{01}}{M_{00}} \tag{4}$$

The central moments can then be defined in their discrete representation as (5):

$$\mu_{pq} = \sum_x (x-\bar{x})^p \sum_y (y-\bar{y})^q \tag{5}$$

The moments are further normalised for the effects of change of scale using the following (6):

$$\eta_{pq} = \mu_{pq} / \mu_{00}\lambda \quad (6)$$

Where the normalisation factor: $\gamma = (p + q / 2) + 1$. From the normalised central moments a set of seven values can be calculated and are defined as:

$\phi 1 = \eta 20 + \eta 02$

$\phi 2 = (\eta 20 - \eta 02)2 + 4\eta 211$

$\phi 3 = (\eta 30 - 3\eta 12)2 + (\eta 03 - 3\eta 21)2$

$\phi 4 = (\eta 30 + \eta 12)2 + (\eta 03 + \eta 21)2$

$\phi 5 = (3\eta 30 - 3\eta 12)(\eta 30 + \eta 12)[(\eta 30 + \eta 12)2 - 3(\eta 21 + \eta 03)2] + (3\eta 21 - \eta 03)(\eta 21 + \eta 03) \times [3(\eta 30 + \eta 12)2 - (\eta 21 + \eta 03)2]$

$\phi 6 = (\eta 20 - \eta 02)[(\eta 30 + \eta 12)2 - (\eta 21 + \eta 03)2] + 4\eta 11(\eta 30 + \eta 12)(\eta 21 + \eta 03)$

$\phi 7 = (3\eta 21 - \eta 03)(\eta 30 + \eta 12)[(\eta 30 + \eta 12)2 - 3(\eta 21 + \eta 03)2] + (3\eta 12 - \eta 30)(\eta 21 + \eta 03) \times [3(\eta 30 + \eta 12)2 - (\eta 21 + \eta 30)2]$

These are the seven invariant moments, $\phi I$, $1 \leq I \leq 7$. Results of these moment calculations are given in the result section. The images are cropped, rotated and subjected to noise results show that the values of these moments do not vary. Hence any microscopic image that has not captured the image properly will not affect the features calculated for those images because moment s are invariant to rotation, translation and convolution, but are highly sensitive to local variation.

## 3. TEST ALGORITHM

The design follows the same steps as that of a pattern recognition problem. But the best part of the algorithm is the usage of the most appropriate algorithm for each stage. The test algorithms illustrated above give an insight about the algorithm to be used for each stage. The process is given below.

1. Image Acquisition and database collection
2. Image Analysis
3. Image Segmentation
4. Feature Generation
5. Classification of Parasite and result verification

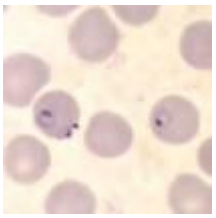

**FIGURE 3:** Plasmodium Falciparum

### 3.1 Image Acquisition and Database Collection

Oil immersion views (10x1000), of Giemsa stained blood films were captured using a binocular microscope mounted with a digital camera. Captured images were 460 pixels X 307 pixels bitmap images. Fig. 3 shown above the sample slide of P. Falciparum. The database consists of 110 images.

### 3.2 Image Analysis

Out of the all specified image filtering based approaches, it is found hat median filtering gives the most appropriate results. Hence the image is first filtered using a 5×5 median filter [15], followed by a morphological area closing filter using a disk-shaped structuring element (SE) of radius 6

pixels. The morphological filter removes some parasite detail from the image, and so the morphologically-filtered image is only used for functions where parasite detail is not important, such as erythrocyte segmentation. In all other cases, the median-filtered image is used.

### 3.4 Image Segmentation

Techniques have been proposed earlier that make use of thresholding or morphology to segment an image. In this section we have presented a technique that takes benefit of morphological operation and thresholding at appropriate positions in the whole process to maximize the productivity of the algorithm. In order to use morphological methods for image segmentation, the shape and size of the objects in the image must be known. The most commonly used morphological procedure for estimating size distribution of image components is the Granulometry. The size and eccentricity of the erythrocytes are also required for the calculation of some feature values (as these can be indicative of infection). The shape of the objects (circular erythrocytes) is known a priori, but the image must be analyzed to determine the size distribution of objects in the image and to find the average eccentricity of erythrocytes present. A pattern spectrum showing the size distribution of objects in a sample can be calculated using Granulometry [15]. The next stage of the process identifies and segments potential parasites and erythrocytes from the image background. To extract the infected erythrocytes, it is first necessary to identify them from the combination of parasites and erythrocytes in the image, and then segment them from the background. This algorithm relies primarily on thresholding. The key to successfully segmenting an image using thresholding is threshold selection. The histogram of the complemented, green component of the sample image (fig.4) is a bimodal distribution typical of all the images considered.

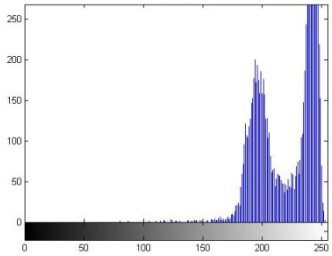


**FIGURE 4:** Bimodal histogram of Plasmodium Falciparum

The threshold level is automatically selected using a modified version of the method that maximizes the separability of the resultant classes of the grey-level histogram [17]. The principle mode is due to the grayscale intensities of the image background, and the second mode is due to those of the erythrocytes in the image. Two threshold levels need to be determined from the histogram: one for erythrocytes, and one for parasites. The first threshold is selected to separate the erythrocytes from the background of the image. This essentially means separating the two modes of the image histogram. The first threshold is selected to separate the erythrocytes from the background of the image. This essentially means separating the two modes of the image histogram. The resulting thresholded binary mask of erythrocytes then has all holes with an equivalent radius less than an empirically determined average erythrocyte radius removed. A morphological opening using a disk-shaped SE with a radius 40% of the mean erythrocyte radius is applied to smooth the objects in the image, and any objects with an equivalent radius of less than half the mean erythrocyte radius are removed. The problem with this binary image of erythrocytes is that clusters of cells are not separated. The next step is to select the second threshold to find parasites present in the image. A global threshold level, taking the threshold as the first local minimum in the histogram after the mode due to erythrocytes, is not sensitive enough. This is a common problem experienced with global threshold selection, caused by inconsistent intensities in the image. The solution is to find local threshold levels. The erythrocytes, having already been identified, provide excellent image regions in which to find these, especially since valid parasites are only found inside erythrocytes. The threshold is then found by taking the first minimum after the principal mode of the histogram incorporating only the

erythrocytes. While this method has greater sensitivity, it is at the expense of a reduced specificity. There are also cases, particularly with P. Ovale, where the global threshold is able to detect parasites that are missed by the local thresholds. This is due to colorization of the infected cells, which shifts the principle mode of the local histograms of the affected cells. For this reason, both local and global thresholds are used, and the union of the two binary images is used as the parasite marker image. Invalid objects in the marker image (objects detected with the global threshold that lie outside any erythrocyte) are removed by taking the intersection of the parasite marker image with the binary mask of erythrocytes. The erythrocyte mask is dilated first, to ensure that 'blister' forms of the parasites, that appear to bulge out of the edge of the cells, are not removed. Other artifacts in the blood containing nucleic acid, particularly white blood cell nuclei, are also detected by this thresholding. They are removed by excluding all objects greater than an empirically determined size (chosen to exclude all objects greater than the largest trophozoite that one would expect to find.) The infected cells are identified by morphologically reconstructing the erythrocyte mask with the valid parasite marker. Binary reconstruction simply involves extracting the connected components of an image (the mask) that are marked by another image (the marker), where cells are clustered together, if an infected cell forms part of the group, then the entire aggregation is reconstructed.

To separate these clusters so that the infected cell can be isolated and extracted, a modification of the morphological technique used in Di Ruberto et al. [20] is used. A morphological opening filter, using a disk-shaped SE with radius equal to the mean erythrocyte radius less the standard deviation, is applied to the grayscale, morphologically filtered green component of the image to remove any objects smaller than an erythrocyte. The morphological gradient—the difference between a dilation and erosion of the image—is then calculated using a diamond-shaped SE with unity length.

The segmentation method is applied to each object in the reconstructed binary image of erythrocytes individually. Those objects that do not exceed the area of a circle with radius equal to the mean erythrocyte radius plus the standard deviation are regarded as being single cells, and are unmodified.

Unlike the method in Di Ruberto et al. [20], where the morphological gradients are used to generate marker images for the watershed algorithm, the objects deemed to be overlapping erythrocytes are segmented as follows. First, the intersection of the morphological gradient image and the dilated cell cluster is taken. This image is then transformed to a binary image by thresholding any value greater than zero. A series of morphological operations, namely a closing operation, thinning, and spur-removal are then applied to generate a contour of the segmented erythrocytes. The contours are filled, and the segmented mask is again reconstructed with the valid parasite marker image to result in a segmented mask of infected cells.

The erythrocytes that have been identified as possibly infected are then extracted from the image and passed to the next stage of the algorithm for feature generation. The binary mask of the erythrocyte, as well as a binary mask (obtained by local threshold selection based on the image histogram as detailed above) of parasite-like objects present in the cell, is also passed to the next stage.

## 4. FEATURE GENERATION AND CLASSIFICATION

Feature generation and classification are done as follows.

### 4.1 Feature Generation

Two sets of features are used for development. The first set will be based on image characteristics that have been used previously in biological cell classifiers, which include geometric features (shape and size), color attributes and grey-level textures. It will be advantageous to apply expert, a priori knowledge to a classification problem. This will be done with the second set of features, where measures of parasite and infected erythrocyte morphology that are commonly used by technicians for manual microscopic diagnosis are used. It's desirable

to focus on these features, because it is already known that they are able to differentiate between species of malaria.

### 4.2 Feature Classification

The final classification of an erythrocyte as infected with malaria or not, and if so, the species of the parasite, falls to the classifier. The classifier is a two-stage tree classifier, with an infection classified as positive or negative at the first node, and the species assigned at the second node as shown in fig. 5. The design of a tree classifier has the following steps: the design of a tree structure (which has already been assigned), the selection of features to be used at every node, and the choice of decision rule at each node [22]. The same type of classifier is used at both nodes. Taking into account the fact that there is no guarantee that the classes are linearly separable, back propagation feed forward (BFF) neural networks is selected. The features selected for the first classifier are those that describe the colour and texture of the possible parasites. The features used by microscopists to differentiate malaria species are selected for the second classifier. The training goal is to minimize squared errors, and training is stopped when the error of a validation set increased. This is done to avoid overtraining.

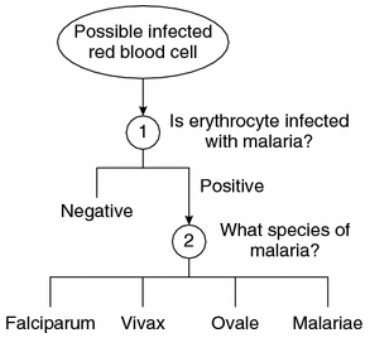


**FIGURE 5:** Structure of the tree classifier

## 5. RESULTS AND ANALYSIS

The performance and accuracy of the algorithm are analyzed using two measures: sensitivity, the ability of the algorithm to detect a parasite present; and positive predictive value (PPV), the success of the algorithm at excluding non-infected cells. These values are expressed in terms of true positives (TP), false positives (FP) and false negatives (FN) as stated in equation 7:

$$Sensitivity = \frac{TP}{TP + FN}$$

$$\& \quad PPV = \frac{TP}{TP + FP} \tag{7}$$

The algorithm has been tested on various malaria parasites. The results are summarized in the table no. 1 at various stages of Image Processing as shown in fig. 6.

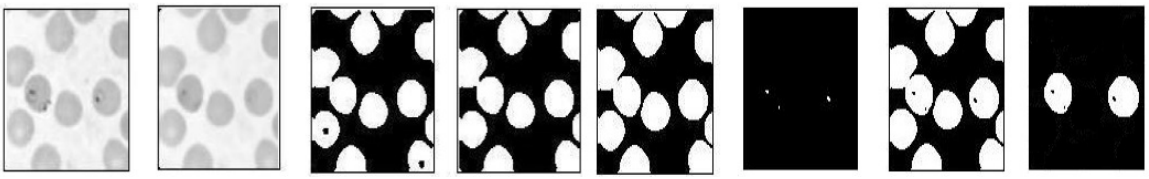


**FIGURE 6:** The algorithm results. (a)Grayscale image,(b)Filtered image, (c)Threshold RBC image, (d)Holes removed image, (e)Smoothed and dilated image, (f)Detected parasite image, (g)Infected RBC group, (h)Separated parasite affected RBC

| Test Image | Algorithm 1 | | Algorithm 2 | | Plasmo - Vision | | Manual microscopy | |
|---|---|---|---|---|---|---|---|---|
| | RBC | Parasites | RBC | Parasites | RBC | Parasites | RBC | Parasites |
| 1 | 18 | 21 | 16 | 0 | 10 | 0 | 15 | 0 |
| 2 | 18 | 1 | 21 | 0 | 13 | 0 | 12 | 0 |
| 3 | 7 | 10 | 9 | 3 | 6 | 9 | 12 | 9 |
| 4 | 15 | 4 | 14 | 2 | 8 | 4 | 9 | 4 |
| 5 | 39 | 5 | 40 | 3 | 36 | 3 | 36 | 3 |
| 6 | 15 | 72 | 13 | 3 | 9 | 2 | 17 | 2 |
| 7 | 21 | 114 | 13 | 2 | 11 | 2 | 11 | 2 |
| 8 | 44 | 3 | 17 | 2 | 12 | 2 | 13 | 2 |
| 9 | 23 | 86 | 22 | 2 | 14 | 2 | 14 | 2 |
| 10 | 29 | 16 | 43 | 10 | 20 | 10 | 19 | 10 |

**TABLE 1:** Results of 10 blood images consisting of 158 Red blood cells

| Algorithm | Sensitivity (%) | PPV | Average Execution time (sec) |
|---|---|---|---|
| Algorithm 1 | 74 | 88 | 11.02 |
| Algorithm 2 | 90 | 80 | 30 |
| Plasmo - Vision | 85.5 | 81 | 3.44 |

**TABLE 2:** The results of all the algorithms tested

## 6. CONCLUSION

The proposed automated parasite detection algorithm has many advantages compared to other diagnostic techniques. It avoids the problems associated with rapid methods, such as being species-specific and having high per-test costs, while retaining many of the traditional advantages of microscopy, viz. species differentiation, determination of parasite density, explicit diagnosis and low per-test costs. Apart from overcoming the limitations of conventional methods of parasite detection, the proposed algorithm is optimized to overcome limitations of image processing algorithms used in the past. Among the tested test algorithms, 'SUSAN edge detection technique' gave good localization of edges but formed a thick border making cell separation difficult. 'Otsu's algorithm' gave accurate separation of RBCs where as local and global thresholding segmented the parasites. Touching cells were separated successfully using 'Marker controlled watersheds', while it did not work for overlapping cells. 'Clump splitting algorithm' solved the difficulty. Results prove that the algorithm developed in this project has better sensitivity than the algorithm proposed by Di Ruberto and has far better execution speed than the algorithm proposed by Silvia and is applicable to many other blood cell abnormalities other than malaria in contrast to the algorithm developed by Jean Phillipe. This is because the percentage of pathological differences in various diseases has very less effect on this robust algorithm. The algorithm detects the species of parasite and also gives the count of RBCs and the parasites with a sensitivity of 85.5% and a positive predictive value of 81%.

## 7. REFERENCES


[1] World Health Organization. What is malaria? Facts sheet no 94. http://www.who.int/mediacentre/factsheets/fs094/en/.

[2] Foster S, Phillips M, Economics and its contribution to the fight against malaria. Ann Trop MedParasitol 92:391–398, 1998.

[3] Makler MT, Palmer CJ, Alger AL, "A review of practical techniques for the diagnosis of malaria". Ann Trop Med Parasitol 92(4):419–433, 1998.

[4] Bloland PB (2001) Drug resistance in malaria, WHO/CDS/CSR/DRS/ 2001.4. World Health Organization, Switzerland, 2001.

[5] Gilles H.M. "The differential diagnosis of malaria. Malaria. Principles and practice of malariology (Wernsdorfer W.H., McGregor I eds)", 769-779, 1998.

[6] F. Castelli, G.Carosi, Diagnosis of malaria, chapter 9, Institute of Infectious and Tropical Diseases, University of Brescia (Italy).

[7] Baird J.K., Purnomo, Jones T.R. Diagnosis of malaria in the field by fluorescence microscopy of QBC ® capillary tubes. Transactions of the Royal Society of Tropical Medicine and Hygiene; 86: 3-5, 1992.

[8] Anthony Moody, Rapid Diagnostic Tests for Malaria Parasites, Clinical Microbiology Reviews,0893-8512/02/$04.00_0 DOI: 10.1128/CMR.15.1.66–78.2002, p. 66–78, Jan. 2002.

[9] Brown A.E., Kain K.C., Pipithkul J., Webster H.K. "Demonstration by the polymerase chain reaction of mixed Plasmodium falciparum and P. vivax infections undetected by conventional microscopy". Transactions of the Royal Society of Tropical Medicine and Hygiene; 86: 609-612, 1992.

[10] Jean-Philippe Thiran, Benoit Macq, "Morphological Feature Extraction for the Classification of Digital Images of Cancerous Tissues". IEEE Transaction on Biomedical Engineering, Vol. 43, no. 10, October 1996.

[11] Di Ruberto, A. Dempster, S. Khan, and B. Jarra. "Automatic thresholding of infected blood images using granulometry and regional extrema". In ICPR, pages 3445–3448, 2000.

[12] Silvia Halim, Timo R. Bretschneider, Yikun Li, "Estimating Malaria Parasitaemia from Blood Smear Images". 1-4244-0342-1/06/$20.00 ©IEEE, ICARCV 2006.

[13] Selena W.S. Sio, Malaria Count, "An image analysis-based program for the accurate determination of parasitaemia, Laboratory of Molecular and Cellular Parasitology", Department of Microbiology, Yong Loo Lin School of Medicine, National University of Singapore. May 2006.

[14] F. Boray Tek, Andrew G. Dempster and Izzet Kale, "Malaria Parasite Detection in Peripheral Blood Images", Applied DSP & VLSI Research Group, London, UK, Dec 2006.

[15] Rafeal C. Gonzalez, Richard E. Woods, Digital Image Processing, 2nd Edition, Prentice Hall, 2006.

[16] S. M. Smith, J. M. Bardy, "SUSAN - A New Approach to Low Level Image Processing", International Journal of Computer Vision, Volume 23, and Issue 1 Pages: 45 – 78, may 1997.

[17] N. Otsu, "A threshold selection method from gray-level histograms". IEEE Transactions on Systems, Man and Cybernetics, 9(1):62.66, 1979.

[18] J.N. Kapur, P.K. Sahoo, and A.K.C. Wong, "A new method for gray-level picture thresholding using the entropy of the histogram". Graphical Models and Image Processing, 29:273.285, 1985.

[19] T.W. Ridler and S. Calvard, "Picture thresholding using an iterative selection method". IEEE Transactions on Systems, Man and Cybernetics, SMC-8:630.632, 1978.

[20] Di Ruberto C, Dempster A, Khan S, Jarra B, "Analysis of infected blood cell images using morphological operators". Image Vis Comput 20(2):133–146, 2002.

[21] M. K. Hu, "Visual pattern recognition by moment invariants"," IRE Trans. Information Theory, vol. 8, pp. 179{187, 1962

[22] Mui JK, Fu K-S, "Automated classification of nucleated blood cells using a binary tree classifier". IEEE Trans Pattern Anal Machine Intell 2(5):429–443, 1980

# Vancomycin Resistance Genes in Various Organisms- An *Insilico* Study

**Rajeshwari D Sanakal** *rajkbio@rediffmail.com*
*Bioinformatics Infrastructure Facility Centre*
*Post-Graduate Department of Biotechnology and Microbiology*
*Karnatak University,Dharwad- 580003*
*Karnataka, India*

**Basappa B Kaliwal** *b_kaliwal@yahoo.com*
*Professor,Bioinformatics Infrastructure Facility Centre,*
*Post-Graduate Department of Biotechnology and Microbiology*
*Karnatak University,Dharwad – 580003*
*Karnataka, India*

## Abstract

Vancomycin, a glycopeptide antibiotic is widely used to treat many serious infections caused by gram positive bacteria particularly, methicillin resistant Enterococci and Staphyllococcus sp. Emergence of commonly acquired resistance in bacterial pathogens has lead to clinical complications and threat to human health. The resistance in these organisms is conferred by several vancomycin resistance genes (Van) like VanA, VanB, VanD, VanC and VanM. Knowledge of presence of Van genes in various organisms was felt necessary prior to molecular investigation. Therefore, in this *insilico* study screening was carried out for presence of Van gene like sequences using the DNA sequence information available in biological databases. Results indicated that many pathogenic and non-pathogenic bacteria, fungal, viral and protozoan pathogens, other organisms like fishes, mammals possess Van like sequences. The present findings provide first hand information on extent of presence of Van sequences in many organisms and their phylogenetic relationship with each other. Further investigation on the significance of these genes is emphasized using molecular and bioinformatics tools to help minimize acquired resistance in antibiotics.

**Keywords** : Van Gene, Similarity, Sequence Analysis, Antibiotics, Enterococci, Phylogenetic Analysis

## 1. INTRODUCTION

The post surgical and hospital acquired infections have become life threatening diseases and lead to many clinical complications [1]. The development of antibiotic resistance in community acquired bacterial pathogens has become matter of great concern. Some opportunistic human pathogens like Entrococci, Staphylococci, and Clostridium sp. cause many diseases like skin infections, cellulitis, folliculitis, pneumonia, meningitis, endocarditis, bacteremia and sepsis. Infections that occur during hospitalization are called as nosocomial infections. These infections are dangerous as they exhibit resistance to methicillin and glycopeptide antibiotics.

Vancomycin and teicoplanin are glycopeptide antibiotics effective against majority of gram positive bacteria, particularly against multiple drug resistant Enterococci and Staphylococci which are resistant to β-lactum antibiotics [2]. These pathogens have acquired resistance to these compounds by virtue of their intrinsic property especially in clinical isolates. This leads to severe complications in immuno compromised as well as surgical patients. vancomycin resistance enterococci (VRE) was first reported in 1988 in Europe [3,4] and USA [5]. In Asia nosocomial infections in hospitals have been reported from China, Japan, South Korea. Taiwan and Thailand [6,7,8,9]. Similarly, resistance to glycopeptides have been reported in *S. aureus* in Japan [10] and

USA [11]. In India emergence of vancomycin resistance *S.aureus* was analysed [12] and the Vancomycin resistant gene in *S.aureus* was detected first time [13].

Vancomycin binds with the C-terminal D-alanyl-D-alanine (D-Ala-D-Ala) residue of pentapeptide and blocks the addition of precursors by transglycosylation to peptidoglycan chain and inhibits cross linking of cell wall by transpeptidation[14]. Resistance to vancomycin is caused by synthesis of precursors with low affinity for these antibiotics conferred by operons present on Van gene clusters that encode enzymes which synthesize low affinity precursors wherein C-terminal D-Ala residue is replaced by D-lactate (D-Lac) or D-serine (D-Ser) that modify vancomycin binding site. These genes confer high or low level resistance to vancomycin and teicoplanin which may be inducible or constitutive. VanA type gene confers inducible high levels of resistance to vancomycin and teicoplanin. Inducible various levels of resistance to vancomycin and susceptibility to teicoplanin is conferred by type VanB [15]. VanC confined to *Enterococcus gallinarum* is intrinsically resistance to low levels of vancomycin but susceptible to teicoplanin [16]. VanC resistance expressed constitutively or inducibly by production of peptidoglycan precursor ending in D-Ser [17]. VanD type confers resistance to intermediate levels of vancomycin and low levels of teicoplanin that is expressed constitutively. VanD is not transferable to other Enterococci and that distinguishes it from VanA and VanB [18,19].

Van A has a Tn3-like transposon with a cluster of seven genes (VanR, vanS, VanH, Van A, VanX, VanY and VanZ) [20]. VanA is ligase of broad substrate specificity [21] responsible for production of dipeptidase which is incorporated in peptidoglycan precursor in place of D-alanyl – D alanine. VanA is produced by VanH dehydrogenease [22]. The VanR and VanS genes encode VanR-VanS regulatory system which activate transcription of VanH, VanA, VanX in presence of vancomycin. These proteins are necessary for vancomycin resistance where the vancomycin binding site is altered. VanY encodes an accessory resistance protein D, D-carboxypeptidase, insensitive to the activity of β-lactams like penicillin G that hydrolyses the C-terminal residue thereby preventing the translocation of D-Ala D-Ala containing precursors to cell surface [23]. VanZ-is likely teicoplanin resistant protein encoding gene [2].VanB ligase gene cluster is divided in to three sub types $VanB_1$, $B_2$, $B_3$ located on transposon $T_n$ 5382 resulted from conjugation of plasmids [24,25]. Another glycopeptide resistance gene ,VanM reported from China [8] encodes D-Alanine:D-Lactase ligase and is related to VanA, VanB and VanD gene and transferred by conjugation.

As there is increase in emergence and rapid dissemination of resistance to vancomycin that has become challenge to treat human diseases, it was felt necessary to screen presence of vancomycin resistance or vancomycin resistance like DNA sequences that are present in various organisms prior to carry out molecular characterization. Therefore, in this *Insilico* study presence and extent of Van genes has been analysed with the sequence information available in biological databases and also by construction of phylogenetic tree. Possibly, this would provide important clues before initiating any treatment with glycopeptide or other antibiotics and understand the nature of dissemination of antibiotics resistance in various organisms.

## 2. PRELIMINARIES

### 2.1 Methodology

Vancomycin resistance genes from *Enterococcus faecalis* viz.,VanA (VanR, VanS, VanH, VanA, VanX, VanY and VanZ), VanB, VanC, VanD and VanM were selected using National Centre for Biotechnology Information (NCBI) genome search with following accession numbers. VanA (VanR, VanS, VanH, VanA, VanZ, VanY)-M97297.1 and (for VanY &VanZ) -AB563188.1, Van B-U00456, VanC - AF162694.1, VanD-AF130997.1, and VanM-FJ349556. The individual genes were screened using Basic Local Alignment Search Tool (BLASTn) tool [26] against NCBI's nonredundant nucleotide database for pairwise alignment in the month of December, 2010 (BLASTn is nucleotide sequence similarity search algorithm that aligns matches with query sequence with the existing nucleotide sequence database). The sequences produced with significant alignments with higher score, percent identity ≥ 70% and percent query coverage ≥

4% were considered for the study. Further, the sequence information of *E.faecalis* and *S.aureas* were mainly used for comparison. The vancomycin resistance like gene sequences found in various organisms were selected after pairwise alignment with help of BLASTn tool [27].

Phylogenetic analysis is an evolutionary investigation to carry out comparison in various sequences especially during the evolution among different organisms. The closely related sequences are placed in neighboring branches while distantly related sequences are placed far in phylogenetic tree. In our present study,a total of 28 sequences from various organisms were used for the analysis. (Only few organisms representing from various groups, that were significantly homologous to van resistance genes were considered for analysis). Hence the selected sequences of all organisms were analyzed phylogenetically to determine how Van genes have been associated during evolution and compared. The Phylogenetic tree was constructed using distance based Neighbor-Joining method using percent identity through CLUSTALW tool[28]. Flow chart (Fig.1) depicts the method of screening of vancomycin genes in various organisms.

**2.2 Results and Discussion**

Results of screening of all the Van genes is presented in Table No.1-5 ,Graphs 1-5 and Fig.2. The results indicated that there were around 37 various organisms that were homologous to Van genes. Most of the genes were identical in around 7 organisms around (93-100% identity) in *Streptococcus sp.*, *Bacillus sp.* and *Paenibaillus sp., Eggerthella lenta, Clostridium sp., Ruminococcus sp*. apart from *E.faecalis and S.aureus*. Van R found homologous in around 11 species viz., (Table -1-4, Graphs-1- 5). VanA, VanH, VanS, VanX, VanY and VanZ which are components of VanA gene clusters individually were homologous (70-100%) in different organisms like *Streptococcus gallolyticus*, *S.haemolyticus, Paenibacillus thiaminolyticus, Paenibacillus apiaris*, *Bacillus cereus, B.circulans, B.thurungiensis, B.clausil, Eggerthella lenta,* and *Ruminococcus sp.*. VanC and VanD recorded homologousness only in 4 species. Van M was recorded in 14 organisms apart from Enterococcus species while *Streptococcus suis, Lactococcus lactis, Lactococcus garvieae, Lactobacillus salivarius, Tetragenococcus halophilus* displayed homology with VanY and VanM genes (Table- 1-4, Graphs-1,2 and 3). Further, VanC, VanD and VanZ showed comparatively lesser similarity with VanA and VanB genes. Interestingly, VanZ was present in *Mus musculas, Rattus norvegicus,* Human Immuno deficiency virus-1(HIV-1) isolates from Belgium and USA envelope glycoprotein and *Schistsoma masoni* (Table-4-5,Graphs 4-5). Surprisingly, the part of DNA sequences of various organisms which were homologous to Vancomycin genes also ranged from Thermopiles to *Aspergillus sp.*, *Haemophilus influenzae*, *Plamodium vivax* and *P.falciparam, Trypanosoma brunie*, *Salmonella enterica* and *Danio verio* (zebra fish), *Taeniopygia guttata* (zebra finch), *Gallus gallus* (domesticated fowl) and *Monodelphis domestica* (marsupial).

Clostridium species, Streptococcus sp., *Paenibacillus thiaminolyticcus, Paenibacillus apiarius, Paenibacillus popillae, Ruminococcus sp, Eggerthealla lenta, Bacillus circulans, Staphylococcus gallolyticus* showed identity with VanA, VanB, VanM and VanD genes(Table- 3-4, Graphs 3-4). Other organisms like *Monodelphis domestica, Rattus novegicus, Mus musculas, Aspergillus nidalans, Gallus gallus, Staphylococcus bovis, Anophelis gambaei, Trypanosoma brunei gambiense, Plasmodium falcipuram, P.Vivox, Salmonella enterica, Haemophilus influenzae, Schistosoma masoni, Bacillus thuringiensis*, (Table- 3-5, Graphs 3-5 ) showed similarity with VanA, VanY, VanZ and VanB. Presence of VanC was limited only to Streptococcus sp. and clostridium sp. apart from Enterococcus sp. (Table- 1and 3, Graphs- 1and 3 ).

The phylogenetic tree (Fig.2) of vancomycin resistance gene is categorized into 8 major clads on the basis of their evolutionary distances by Neighbor-Joining (NJ) method using percent identity. It is depicted in the NJ evolutionary tree that first clad has monoclad of VanC of *Enterococcus gallanarium* with a evolutionary distance of 1.27 (gi-AF162694) which is distantly related to VanA of *Enterococcs faecalis*. clad 2 is divided into two sub-clads with distance of 1.25 and 2.75 consisting VanZ of *Enterococcus faecalis* (gi-M97297.1) and *Lactococcus lactis* (gi-2467210) respectively that are closely related to each other.Further, clad 3 is sub divided into two

branches with one branch having VanS (gi-M97297.1) with evolutionary distance of 2.42 and VanZ from Taiwan(gi-312836941) with distance of 0.64.The other branch is depicted with VanR and VanY with 1.83 and 3.17 distance values respectively (gi-M97297.1). Clad 4 is represented by three subclads with evolutionary distance of 0.39,1.71, and 2.95 by HIV-1(gi-308743091), *Haemophilus influenzae* (gi-CP000671.1) and VanM (gi-220901852) respectively.

The internal clad 5 is sub grouped into A and B . Group A has 6 branched sub-clads with highly homologous VanA (gi-M97297.1) and S.aureus (AE017171.1) with distance of 0.41. Further, it is branched into sub-clads having *Bacillus circulans* (gi-6448487,distance-0.49), *P.thiaminolyticus* (gi-AY926880.2, distance-0.58), *P.apiarius* (gi-50082942,distance-0.84) *and Staphylococcus haemolyticus* (gi- 222159958, distance-0.33). Group B is sub divided into 5 clads with *Eggerthella lenta* (gi-AY655718.2) highly homologous with Ruminococcus sp.(gi-56123451) and clostridium sp.(gi-56123455) with evolutionary distances of 0.25 and VanB (gi-U00456.1)with 0.32 and *S.bovis*(gi-1262410) with 0.76 respectively. Clad 6 has monoclads VanD (gi-M97297.1) with 2.24 value of distance.

Later, clad 7 has subdivided into 4 clads comprising of VanX (gi-M97297.1), VanH(gi-M97297.1), *Salmonella enterica* (gi-M97297.1)., and *Danio rerio* gene(gi-197333707) with distance of 0.59,2.35, 0.42 and 2.90 respectively. Lastly, clad 8 is having two sub-clads with *Bacillus thurungiensis* and Asperigillus sp. with distance of 0.89 and 3.08.It is indicated in the phylogenetic tree (Fig.2) that VanA, VanB are more homologous with various organisms like Streptococcus sp. Staphyllococcus sp., Bacillus sp., Paenibacillus sp., Ruminococcus sp., Clostridium sp. compared to VanD. HIV-1, *Haemophilus influenzae* and Lactococcus sp. are homologous to VanS, VanY VanZ and VanM. Further, VanX, VanH are homologous to *Salmonella enterica* and *Danio rerio*(Zebra fish) further corroborating the pairwise comparison. Moreover, VanC Asparigillus sp. and *Bacillus thurungiensis* showed distant relationship with VanA and VanB.

The presence and significance of Van genes in various species is discussed as follows.

**Streptococcus sp**

Table-1 and Graph-1 show *Streptococcus gallolyticus, Streptococcus pneumonia, Streptococcus thermophilus, Streptococcus suis, and S. bovis* organisms' sequences that have identity of 75-95% with VanA, VanB, VanC, VanD and VanM genes of *Entercoccus sp.. Streptococcus pnemoniae, S. bovis, S.gallolyticus* cause acute sinusitis, meningitis, bacteremia, sepsis, endocarditis in humans while *S.thermophilus* is non pathogenic. Antibiotics like pencillin G or Centrixone are administrated to treat these diseases. However, these have shown to have acquired glycopeptide resistance in our study [29] .

**Staphylococcus and Lactococcus sp**

It is known that *S.aureus* has already acquired vancomycin resistance[10] and hence under present investigation it is identical with Van genes (Fig.2) . Further it is depicted that *S.aureus* is not similar to VanC type, indicating VanC has quite different capacity of resistance than VanA and VanB. Further, *S.haemolyticus* (VanA-100% and VanM-84% identity) has homologies with Van gene (Table-2, Graph-2). It is pathogenic as it causes endocarditis , and also methicillin resistant. This resistance may be due to Insertion Sequences (ISs) homologous to *S.aureus. S.haemolyiticus* showing resistance to Van gene may be a difficult to treat case of nosocomial infections [30].

In *Lactococcus sp*. VanY and VanM type genes are found (Table-2,Graph-2). *Lactococcus sp*. are used in food processing and dairy industry and also as probiotics (Lactococcus lactis,*Tetragenococcus halophilus).* While some are animal pathogens (*Lactococcus garviae*), some also opportunistic pathogens causing endocarditis and cholangitis in immunocompetent patients [31,32] and have been isolated from clinical samples of blood, skin lesions and urine [33].These are administered with extended spectrum beta-lactam antibiotics like tazobactum. However, in our study it is indicated that both *Lactococcus lactis* and *Lactococcus garviae* have

VanY and VanM sequence homologies. Perhaps, it indicates that there may be possible synergism towards resistance in presently administered antibiotics.

**Paenibacillus sp**

Paenibacillus strains have been reported to have VanA and VanB operons [34]. Further, the results (Table-3,Graph-3) obtained in our findings corroborate the report and indicate that all the three species of Paenibacillus viz *P.thiaminolyticus, P.apiaris and P.popillae* are having identity of 80-87% with the newly reported vanM gene. Perhaps the soil bacterium and pest control pathogens of this class that have Van comparable genes may be derived from common ancestor or may be integrated through conjugation [8]. Though *P.thiaminolyticus* is environmental bacteria it is reported to cause human disease in hemodialysis patients [35]. Therefore great care has to be taken by clinicians while prescribing vancomycin in haemodialysis patient as *Paenibacillus* sp. have acquired Van resistance gene.

**Baccillus sp**

*B. cereus, B. Clausil* , *B. Circulans, Baccillus thurungiensis, B. and Weihenstephanesis* have identity with VanA, VanD and VanM and VanY genes in the results (Table-3, Graph- 3). Usually these species are harmless, beneficial as pest control agents, food processing agents, and used as probiotics [36]. However, *B. cereus* causes vomiting and diarrhea due to food contamination and also skin infections [37]. *B. Clausil* causes gastrointestinal infections and is reported as methicillin resistant, [38]. Further, *B. circulans* has more number of Van resistance genes, which is marine pathogen [39]. Perhaps, the findings at hand provide clue that through the water bodies contaminated with human waste may synergistically disseminate the antibiotic resistance to many pathogens. Hence, there should be proper management of human waste.

**Clostridium sp**

The Clostridium sp. have shown greater similarity with most of the Van genes in our findings. The antibiotics which is effectively used to control clostridium is metronidazole. vancomycin is second line therapy if there is no response to metronidozole. But, the similarity results observed with all the Van genes in this sp. (Table-4, Graph-4) indicate that clostridium too has acquired resistance to vancomycin gene. The diseases and deaths due to Clostridium species (*C. difficle, and C. Sordellii)* infections are associated with wide antibiotics usage [40,41]. VanR, VanS ,VanA ,VanX, VanY and ,VanB, and VanM genes have identity (70-95%) with Ruminococcus sp. (Table-4,Graph 4). The Ruminococcus sp. are anaerobic, cellulytic bacteria found usually in the rumen of cattle, sheep, goats and human large intestine. Presently, these do not seem to pose any threat to human as these are non pathogenic.

**Other Microorganisms**

Van resistance genes from VanS, VanA, VanH, VanX, VanZ, VanB, and VanM are having similarity with *Eggerthella lenta*(Table-4,Graph-4) sequences. It is anaerobic organism present in human intestinal flora found to cause anaerobic spondylodiscitis [42] which is infection of intervertebral disc and adjoining the vertebral bones. Besides, it is also responsible for polymicrobial blood stream infection and bacteremia [43]. Eggerthella sp. are reported to be sensitive to penicillin [44]. But, in this study *Eggerthella lenta* has shown similarity up to 72-95% with VanA, VanB, and VanM genes that are responsible for vancomycin resistance. *E. lenta* also infectious in following cases of post gynecological surgery, chrrioamniotitis, appendicitis and cutaneous abscess. Therefore, clinicians should carefully advice the antibiotics wherein *E. lenta* may also pose threat to life of patient. Further, similarity of VanZ gene with pathogenic HIV-1 isolate from Belgium and USA envelope glycoprotein and *Schistosoma masoni* is depicted in our study (Table-1,Graph-4). It is noted that VanZ may confer resistance to teicoplanin antibiotics where the functions of VanZ are not clearly revealed [45]. Surprisingly, results under present investigation also indicated the presence of VanR, VanH,VanY type genes in (Table-4,Graph– 4) *Haemophilus influenzae* (influenza virus), *Salmonella enterica* (a gram negative bacteria), *Asperigillus sp.*(pathogenic fungi) and VanY type in *Trypanosoma Brunei. Plasmodium vivax and P.falciparum* are reported to account for 65% of malaria cases in Asia and south America. Interestingly, in this study *P.vivax* and *P.falciparum* show homologies to VanB (100% identity)

and VanY (93% identity, Table-5, Graph-5) respectively. This is probably related to modification in host-parasite interaction mechanism. As the pathogen is protozoan and transfer of resistance genes from bacteria cannot be expected [14]. However, *P.vivax and P.falciparum* have been mysterious and posing resistance to commonly used antimalarial drug chloroquinine, which is increasing problem around the world [46].

**Higher Organisms**

Higher organisms viz., *Anophelis gambiae* (malaria spreading mosquito), *Danio verio* (Zebra fish),*Mus musculas*[rodent), *Rattus norvegius* (rat), *Taeniopygia guttata* (zebra finch), *Gallus gallus* (domesticated fowl), *Monodelphis domestica* (marsupials) have presented higher homologies with VanB, VanR ,VanH, VanX ,VanY and VanZ genes up to 80-94% identity of sequences (Table-5, Graph-5). Presence of single gene from Van gene clusters in any organisms may not contribute for resistance to vancomycin. The presence of glycopeptide resistance gene sequences in all above diverse organisms is unclear and need to unmask behavior of organisms towards the important antibiotics. Perhaps, drug pressure is believed to be responsible for the emergence of drug resistance in pathogens.

In our results, the observation of similarity with Van resistance genes in unrelated [non Enterococci sp.) organisms and as well as in the organisms where glycopeptides are not administered, may be attributed for having common ancestral origin with Van gene clusters, that might have evolved independently [8] (Fig.2). Further, it is also reported that biopesticide, *P.popillae* widely used for agricultural purposes already has Van gene and might have served as donor of Van gene and has impact on bacterial resistance [47,1] in human pathogens. Genetic variations are responsible for different glycopeptide resistance types, which are present on transferable elements in Enterococcus and Staphylococcus sp. This has lead to emergence of several types of Van resistance genes . Dissemination of glycopeptide resistance to other bacteria has been evident with example of *E.faecalis to S.aureus* [48] because of absence of barriers for heterospecific expression of genes [14]. Further the phylogenetic analysis of Van genes has also justified BLAST (Pairwise alignment) results.

It may be noted that some of the organisms have Van resistance gene even though vancomycin is not administered. It is observed that vancomycin resistance was inducible to *Enterococcus faecalis* when exposed to vancomycin [49]. Probably presence of Van genes may be attributed to this fact .In our investigation presence of Van like sequences in other organisms may indicate change in the nature of their cell wall. Studies made in *S.aureus* have provided evidence that glycopeptide resistant organisms have thicker, more irregular cell walls than the glycopeptides susceptible ones [50].Probably this would pose resistance to frequently used different antibiotics.

## 2.3 Conclusion

Our findings indicate presence of vancomycin resistance like DNA sequences in various organisms irrespective of species and which may be pose synergistic resistance to presently used antibiotics. Hence the need of molecular characterization and detailed bioinformatics investigation of glycopeptide resistance genes in pathogenic, commercially important organisms and animals is emphasized. A continuous surveillance can be warranted to check the emergence of glycopeptide resistance in various organisms. Probably this would facilitate to minimize indiscriminate use of many antibiotics all over the world and pave new ways to find alternative measures to combat the human diseases.

**Acknowledgement**

The authors are grateful to Department of Biotechnology, Ministry of Science and Technology, Government of India, New Delhi, for funding the Bioinformatics Infrastructure Facility project and granting the Research Associateship(RA) and Karnatak University,Dharwad for providing the facilities.

## 3. REFERENCES


1. S.Mendez-Alvarez,Xiomara, Perez-Hernandez,F.Claverie-Martín, "Glycopeptide resistance in Enterococci" , Internatl Microbiol , Vol. 3,pp.71–80, 2000.

2. Reynolds. P.E, "Structure, Biochemistry and Mechanism of Action of glycopeptide antibiotics",Eur.J.clin.Microbiol.Infect.Dis., Vol. 8(11),pp.943-950,1989.

3. R.Leclercq, E.Derlot., J.Duval, P.Courvalin, "Plasmid-mediated resistance to Vancomycin and teicoplanin in *Enterococcus faecium".* N Engl J Med. Vol. 21,319(3),pp157–161, 1988.

4. A.H.Uttley, C.H.Collins, J .Naidoo, and R.C.George., "Vancomycin resistant enterococci", Lancet , Vol. 1, no. 8575-76, pp. 57-58. 1988**.**

5. D.F.Sahm, J.Kissinger, M.S.Gilmore, P.R.Murray, R. Mulder, J. Solliday, and B. Clarke, "In vitro susceptibility studies of Vancomycin resistant *Enterococcus faecalis"* , Antimicrob. Agents Chemother, Vol.33,pp.1588-1591, 1989.

6. N.Fujita, M. Yoshimura, T. Komori, K.Tanimoto, and Y. Ike, "First report of the isolation of high-level Vancomycin-resistant *Enterococcus faecium* form a patient in Japan",Antimicrob Agents Chemother., Vol.42(8),2150, 1998.

7. Y.Ozawa, K .Tanimoto ,T Nomura, M.Yoshinaga, Y.Arakawam, and Y. Ike, "Vancomycin-resistant Enterococci in humans and imported chickens in Japan". Appl. Environ. Microbiol., Vol.68, pp.6457-6461, 2002.

8. X.Xu , D.Lin., G.Yan., X.Ye, S.Wu., Y .Guo., D.Zhu, F.Hu, Y.Zhang, F.Wang., G.A.Jacoby and M.Wang, "VanM, a New Glycopeptide Resistance Gene Cluster Found in *Enterococcus faecium*", Antimicrobial Agents and Chemotherapy, pp.4643-4647, Vol.54, No. 11. 2010.

9. B.H. Zheng, Y.H.Tomita, S .Xiao,.Y.Wang. Y.Li and Y.Ike. "Molecular characterization of Vancomycin-resistant *Enterococcus faecium* isolates form mainland China," J.Clin. Microbiol , Vol.45, pp.2813-2818,2007

10. K.Hiramatsu, H.Hanaki, T.Ino, K .Yabuta, T.Oguri and F.C .Tenover, "Methicillin-resistant S*taphylococcus aureus* clinical strain with reduced Vancomycin susceptibility", J.Antimicrob. Agents chemother, Vol. 40,pp.135-136, 1997.

11. F.D.Lowry,"*Stophylococcus aureus* infections",New Engl J Med.,Vol. 339,pp.520-532, 1998.

12. H.K.Tiwari and M.R.Sen , "Emergence of Vancomycin resistant *Staphylococcus aureus(*VRSA) from tertiary care hospital from northern part of India",BMC Infectious diseases, Vol.6,156, 2006.

13. C.G.Unkal and B.B.Kaliwal, "Vancomycin resistant Staphylococcus aureus containing Van A gene isolated from clinical samples of community health care centres of North Karnataka,India".,In Proceedings of ISBT held at Shillong, India,pp.464-469, 28$^{th}$- 30, Dec 2008.

14. P.Courvalin,"Vancomycin resistance in gram-positive cocci", Clin Infect.,Dis Vol. 42(suppl 1),pp.S25-S34, 2006.

15. R.Quintiliani, Jr., S. Evers, and P. Courvalin, "The Van B confers various levels ofself-transferable resistance to Vancomycin in enterococci".J.Infect.Dis., Vol. 167,pp.1220-1223, 1993.

16. R.S Leclercq, J.Dutka-Malen , Duval and P Courvalin., "Vancomycin resistance gene VanC is specific to *Enterococcus gallinarum",*Antimicrob. Agents Chemother. , Vol.36,pp 2005-2008, 1992.

17. P.E.Reynolds and P. Courvalin , "Vancomycin resistance by synthesis of precursor terminating in D-alanyl D-alanine". Antimicrobial Agents and chemother., Vol.49,pp.21-5,2005.

18. F.Depardieu, P.E.Reynolds and P.Courvalin, "VanD type Vancomycin resistance *Enterococcus faecium* 10/96A.A", Antimicrob. Agents chemother, Vol.47,pp.7-18 ,2003

19. B.Perichon, P.Reynolds and P.Courvalin, "VanD type glycopeptide resistant *Enterococcus faecium* B M 4339", Antimicrob. Agents chemother, Vol. 41,pp.2016-2118, 1997.

20. M.Arthur and P. Courvalin, "Genetics and Mechanisms of glycopeptides resistance in enterococci", Antimicrob Agents chemother, Vol.37,pp.1563-1571,1993.

21. T.D. Bugg , H.S. Dutka- malen , M. Arthur, P.Courvalin, and C.T. Walsh, "Identification of Vancomycin resistance protein vanA as a D-alanine ligase of altered substrate specificity", Biochemistry , Vol.30, pp. 2017-2021, 1991.

22. M.Arthur, C.Mlinas, S. Dutka-Malen and P. Courvalin, "Structural relationship between the Vancomycin resistance protein VanH and 2-hydroxycarboxylic acid dehydrogenasesGene" , Vol.103 ,pp.133-134, 1991.

23. L.D.Gutmann, S.Billot-Klein, I.Al-Obeid,S.Klare,E.Francoual,Collatz and J van Heijenoort, "Inducible carboxypeptidase activity in Vancomycin–resistant enterococci",Antimicrob. Agents Chemother, Vol.36,pp.77-80 ,1992 .

24. L. L.Carias, S D Rudin, C.J. Donskey and L.B. Rice, "Genetic linkage and cotransfer of a novel Van B-containing Transposon (Tn 5382) and alow-affinity penicillin-binding protein gene in a clinical Vancomycin resistant *Enterococcus faecium* is late" ,J. Bacteriol , Vol.180,pp.4426-4434,1998.

25. K.H.Dahl, G.S. Simonsen, O.Olsvik and A.Sundsfjord, "Heterogeneity in the vanB gene cluster of genomic ally diverse clinical strains of Vancomycin-resistant enterococci", Antimicrob Agents Chemother, Vol.43,pp.1105-1110, 1999.

26. S.F. Altschul, W. Gish, W. Miller, E.W.Myers and D.J. Lipman, "Basic local alignment search tool". J. Mol. Biol. Vol.215,pp.403-410, 1990.

27. http://www.ncbi.nlm.nih.gov/blast(December,2010)

28. http://www.ebi.ac.uk/clustalw (February,2011)

29. D.L. Headings, A.Herrera, E. Mazzi, and M. A. Bergman. "Fulminant neonatal septicemia caused by *Streptococcus bovis".* J. Pediatr. , Vol.92,pp.282-283, 1978.

30. M.Falcone, F.Campanile ,M.Giannella ,S.Borbone,S.Stefani ,M.Venditti, "*Staphylococcus haemolyticus* endocarditis: clinical and microbiologic analysis of 4 cases", Diagn.Microbiol. Infect .Dis. ,Vol.57(3),325-31, 2007.

31. J.M.Davies, D. Burkitt and A.Watson, "Ascending cholangitis presenting with *Lactococcus lactis cremoris* bacteraemia: a case report",*Journal of Medical Case Reports*, 3:3doi:10.1186/1752-1947-3-3,2009.

32. J.J.Fefer, K.R.Ratzan, S.E.Sharp and E.Saiz, *"Lactococcus garvieae* endocarditis: report of a case and review of the literature",Diagnostic Microbiology and Infectious Disease, Vol.32, 2, pp. 127-130 ,1998.

33. R.Facklam and J.A.Elliott, "Identification, classification, and clinical relevance of catalase-negative, gram-positive cocci, excluding the streptococci and enterococci", *Clin Microbiol Rev.* ,Vol.8(4),pp.479–495,1995.

34. G.Luca, B.Perichon,J. V.Heijenoort, D .Blanot and P.Courvalin, "Glycopeptide Resistance *vanA* Operons in *Paenibacillus* Strains Isolated from Soil", Antimicrobial Agents and chemotherapy, 49 (10),pp. 4227-4233, 2005.

35. J.Ouyang, Z.Pei,L.Lutwick, S.Dalal, L.Yang ,N.Cassai, K.Sandhu ,B.Hanna, R.L.Wieczorek, M.Bluth and M.R.Pincus, "*Paenibacillus thiaminolyticus:* A New Cause of Human Infection, Inducing Bacteremia in a Patient on hemodialysis", Annals of Clinical & Laboratory Science, Vol.38,pp.393-400,2008.

36. K .V. Tilak and B.R.Srinivasa Reddy , "*Bacillus cereus* and B. *circulans* –novel inoculants for crops", Current Scince, Vol.90 (5),pp.642-644, 2006.

37. A. Kotiranta, K.Lounatmaa , M.Haapasalo , "Epidemiology and pathogenesis of *Baccillus cereus* infections" , Microbes Infect Vol. 2 (2),pp.189-198,2000.

38. http://www.genome.jp/kegg/ (December,2010)

39. M.Thangaraj , P.Vishruth , T.Ramesh and A.P.Lipton, "RAPD Fingerprinting and Demonstration of Genetic Variation in Three Pathogens Isolated form Mangrove Environment" ,Asian Journal of Biotechnology, Vol.3(3),pp.269-274, 2011.

40. E.Meites,S.Zane,C.Gould, "Fatal Clostridium sordellii infections after medical abortions",N Engl J Med. , Vol.30,363(14),pp.1382-3,2010.

41. B.E.Murray.,"Diversity among multidrug-resistant entrococci", Emerg.InfectDis, Vol.4,pp.37-47,1998.

42. C.W.Bok and Y.S.Ng, "*Eggerthella lenta* as a cause of anaerobic Spondylodiscitis, Singapore", Med .J , Vol.50(12), e393-e396, 2009.

43. K.Liderot, M. Larsson, S.Borang and V.Ozenci, "Polymicrobial Bloodstream Infection with *Eggerthella lenta* and Desulfovibrio desulfuricans",Journal of Clinical Microbiology, Vol. 48,pp.3810-3812, 2010.

44. W.G.Wade, J.Downes, D.Dymock, S.J.Hiom, A.J.Weightman, F.E.Dewhirst, B.J. Paster, N.Tzellas, B.Coleman, "The family *Coriobacteriaceae*: reclassification of *Eubacterium exiguum*(Poco et al., 1996) and *Peptostreptococcus heliotrinreducens* (Lanigan 1976) as *Slackia exigua* gen. nov., comb. nov. and *Slackia heliotrinireducens* gen. nov., comb. nov., and *Eubacterium lentum* (Prevot 1938) as *Eggerthella lenta* gen. nov., comb. Nov" . *Int J Syst Bacteriol*, Vol. 49,595-600,1999.

45. M.Arthur, C.Molinas, F.Depardieu and P.Courvalin,"Characterization of Tn/546,aTn3-related Transposon conferring glycopeptide resistance by synthesis of depsipeptide peptidoglycon precursors *Enterococcus faecium* BM4147",J. Bacteriol., Vol. 175,pp.117-127, 1993.

46. K.S.Lee,T.H.Kim,E.S.Kim, H.S.Lim, J.S.Yeom, G.Jun and J.W.Park, "Chloroquine-resistant *Plasmodium vivax* in the Republic of Korea", Am. J. Trop. Med.Hyg.,80(2),pp.215-217,2009.

47. R.K.Patel,.K.Piper, F.R Cockerill III, J.M Steckelberg and A.A.Yousten., "The biopesticide *Paenibacillus popillae* has a Vancomycin resistance gene cluster homologous to the enterococcal VanA Vancomycin resistance gene cluster", Antimicrob. Agents chemother, Vol. 44,pp.705-709,2000.

48. W.C. Noble, Z.Virani, R.G .Cree, "Co-transfer of Vancomycin and other resistance genes from *Enterococcus faecalis* NCTC 12201 to *Staphylococcus aureus"*. ,FEMS Microbiol Lett., 1, Vol. 72(2),pp.195–198,1992 .

49. N.Woodford , A.P.Jhonson,D.Morrison and D.C.Spellar, "Current perspectives on Glycopeptide Resistance", Clinical Microbiology Reviews, Vol. 8,pp.585-615,1995.

50. R.S.Daum,S.Gupta,R.Sabbagh,W.M.Milewski, "Characterization of S*taphylococcus aureus* isolates with decreased susceptibility to vancomycin and teicoplanin: isolation and purification of a constitutively produced protein associated with decreased susceptibility", J Infect Dis., Vol.166(5),pp.1066–1072,1992.

**TABLE 1:** Percent identity of Vancomycin resistant gene sequences in Enterococcus and Streptococcal sp.

| Sr. No | Organisms | Percent identity(%) | | | | | | | | | | |
|---|---|---|---|---|---|---|---|---|---|---|---|---|
| | **Enterococcus and Streptococcal sp.** | **Van R** | **Van S** | **Van H** | **Van A** | **Van X** | **Van Y** | **Van Z** | **Van B** | **Van C** | **Van D** | **Van M** |
| 1. | *Enterococcus faecium (Van A)* | 100 | 100 | 100 | 100 | 100 | 99 | 100 | 73 | -- | 70 | 81 |
| 2. | *Enterococcus faecium (Van B)* | 75 | 99 | 74 | 75 | 72 | -- | -- | 100 | -- | 69 | 73 |
| 3. | *Enterococcus faecium v583* | 94 | 96 | 71 | 74 | 73 | 94 | -- | 99 | -- | -- | 72 |
| 4. | *Enterococcus faecium (Van D)* | 72 | 69 | 71 | 75 | 71 | -- | -- | 68 | -- | 100 | -- |
| 5. | *Enterococcus gallinarum (Van C)* | -- | -- | 67 | 99 | -- | -- | -- | 69 | 100 | 78 | -- |
| 6. | *Streptococcus gallolyticus* | 89 | 100 | -- | 75 | -- | -- | 92 | 95 | -- | -- | -- |
| 7. | *Streptococcus pneumoniae* | -- | -- | -- | -- | -- | -- | -- | -- | 90 | -- | -- |
| 8. | *Streptococcus thermophilus* | -- | -- | -- | -- | -- | -- | -- | -- | 85 | -- | 100 |
| 9. | *Streptococcus suis* | -- | -- | -- | -- | -- | -- | -- | -- | -- | -- | 99 |
| 10. | *Streptococcus bovis* | -- | -- | -- | 74 | -- | -- | -- | 96 | -- | -- | -- |

Note:VanR,VanS, VanH,VanA, VanX,VanY, VanZ are components of VanA gene

**TABLE 2:** Percent identity of Vancomycin resistant gene sequences in Staphylococcus and Lactococcus sp.

| Sr.No | Organisms | Percent identity (%) | | | | | | | | | | |
|---|---|---|---|---|---|---|---|---|---|---|---|---|
| | **Staphylococcus and Lactococcus sp.** | **Van R** | **Van S** | **Van H** | **Van A** | **Van X** | **Van Y** | **Van Z** | **Van B** | **Van C** | **Van D** | **Van M** |
| 1. | *Staphylococcus aureus* | 100 | 100 | 100 | 100 | 100 | 99 | 100 | 75 | -- | 70 | 81 |
| 2. | *Staphylococcus haemolyticus* | -- | -- | -- | 100 | -- | -- | -- | -- | -- | -- | 84 |
| 3. | *Lactococcus lactis* | -- | -- | -- | -- | -- | 71 | -- | -- | -- | -- | 100 |
| 4. | *Lactococcus garvieae* | -- | -- | -- | -- | -- | -- | -- | -- | -- | -- | 99 |
| 5. | *Tetragenococcus halophilus* | -- | -- | -- | -- | -- | -- | -- | -- | -- | -- | 100 |

Note:VanR,VanS, VanH,VanA, VanX,VanY, VanZ are components of VanA gene

**TABLE 3:** Percent identity of Vancomycin resistant gene sequences in Paenibacillus and Bacillus species.

| Sr. No | Organisms | Percent identity(%) | | | | | | | | | | |
|---|---|---|---|---|---|---|---|---|---|---|---|---|
| | **Paenibacillus and Bacillus sp.** | **Van R** | **Van S** | **Van H** | **Van A** | **Van X** | **Van Y** | **Van Z** | **Van B** | **Van C** | **Van D** | **Van M** |
| 1. | *Lactobacillus salivarius* | -- | -- | -- | -- | -- | -- | -- | -- | -- | -- | 100 |
| 2. | *Paenibacillus thiamino-lyticus* | 99 | 91 | 91 | 91 | 93 | 84 | -- | 74 | -- | -- | 83 |
| 3. | *Paenibacillus popillae* | -- | -- | 74 | 77 | 80 | 73 | -- | 70 | -- | -- | 79 |
| 4. | *Paenibacillus apiarius* | 94 | 90 | 79 | 91 | 84 | 81 | -- | -- | -- | -- | 87 |
| 5. | *Bacillus cereus* | 88 | -- | -- | 97 | -- | 73 | -- | -- | -- | -- | -- |
| 6. | *Bacillus clausil* | 96 | -- | -- | -- | -- | -- | -- | -- | -- | -- | -- |
| 7. | *Bacillus circulans* | 91 | -- | 91 | 93 | -- | 94 | 91 | -- | -- | 70 | 82 |
| 8. | *Bacillus thuringiensis* | -- | 86 | -- | 97 | -- | 70 | -- | -- | -- | -- | 93 |
| 9. | *Bacillus weihenste-phanensis* | -- | -- | -- | -- | -- | 93 | -- | -- | -- | -- | 93 |

Note:VanR,VanS, VanH,VanA, VanX,VanY, VanZ are components of VanA gene

**TABLE 4:** Percent identity of Vancomycin resistant gene sequences in Clostridium sp. and other microorganisms

| Sr. No | Organisms | Percent identity(%) | | | | | | | | | | |
|---|---|---|---|---|---|---|---|---|---|---|---|---|
| | **Clostridium sp. and other microorganisms** | **Van R** | **Van S** | **Van H** | **Van A** | **Van X** | **Van Y** | **Van Z** | **Van B** | **Van C** | **Van D** | **Van M** |
| 1. | *Clostridium sp.* | 95 | -- | -- | -- | 72 | 90 | 71 | 99 | 72 | -- | 90 |
| 2. | *Ruminococcus sp.* | 76 | 70 | -- | 75 | 70 | 84 | -- | 95 | -- | -- | 73 |
| 3. | *Eggerthella lenta* | -- | 72 | 71 | 75 | 72 | -- | 85 | 95 | -- | -- | 74 |
| 4. | *HIV-1 isolate* | -- | -- | -- | -- | -- | -- | 96 | -- | -- | -- | -- |
| 5. | *Schistosoma masoni* | -- | -- | -- | -- | -- | -- | 92 | -- | -- | -- | -- |
| 6. | *Aspergillus sp.* | 100 | -- | | -- | -- | -- | -- | -- | -- | -- | -- |
| 7. | *Haemophilous influenzae* | -- | -- | 71 | -- | -- | -- | -- | -- | -- | -- | -- |
| 8. | *Salmonella enterica* | 85 | -- | -- | -- | 71 | -- | -- | -- | -- | -- | -- |
| 9. | *Trypanosoma brunei* | -- | -- | -- | -- | 82 | 82 | -- | -- | -- | -- | -- |
| 10. | *Plasmodium vivax* | -- | -- | -- | -- | -- | -- | -- | 100 | -- | -- | -- |
| 11. | *Plasmodium falciparum* | -- | -- | -- | -- | -- | 93 | -- | -- | -- | -- | -- |

Note:VanR,VanS, VanH,VanA, VanX,VanY, VanZ are components of VanA gene

**TABLE 5:** Percent identity of Vancomycin resistant gene sequences in higher organisms

| Sr. No | Organisms | Percent identity(%) | | | | | | | | | | |
|---|---|---|---|---|---|---|---|---|---|---|---|---|
| | **Higher organisms** | **Van R** | **Van S** | **Van H** | **Van A** | **Van X** | **Van Y** | **Van Z** | **Van B** | **Van C** | **Van D** | **Van M** |
| 1. | *Anophelis gambiae* | 93 | -- | -- | -- | -- | -- | -- | -- | -- | -- | -- |
| 2. | *Danio verio* | -- | -- | -- | -- | 91 | 90 | -- | 87 | -- | -- | -- |
| 3. | *Mus musculus* | -- | -- | -- | -- | 96 | -- | 91 | -- | -- | -- | -- |
| 4. | *Rattus norvegicus* | -- | -- | -- | -- | -- | 84 | 82 | -- | -- | -- | -- |
| 5. | *Taeniopygia guttata* | 87 | -- | 96 | -- | -- | -- | -- | -- | -- | -- | -- |
| 6. | *Gallus gallus* | -- | -- | -- | -- | 92 | 92 | -- | -- | -- | -- | -- |
| 7. | *Monodelphis domestica* | -- | -- | 87 | -- | -- | 93 | -- | -- | -- | -- | -- |

Note:VanR,VanS, VanH,VanA, VanX,VanY, VanZ are components of VanA gene

**FIGURE 1:** Flow chart for screening of Vancomycin resistance genes in various organisms

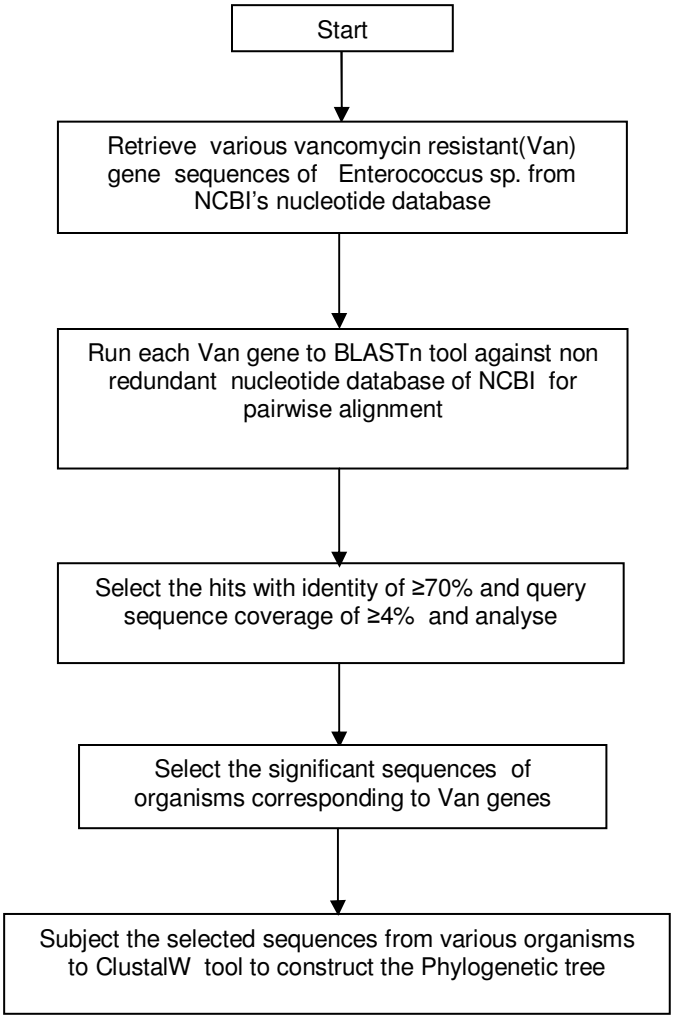

**FIGURE 2:** Distance based Phylogenetic tree (Neighbor- Joining) using percent identity

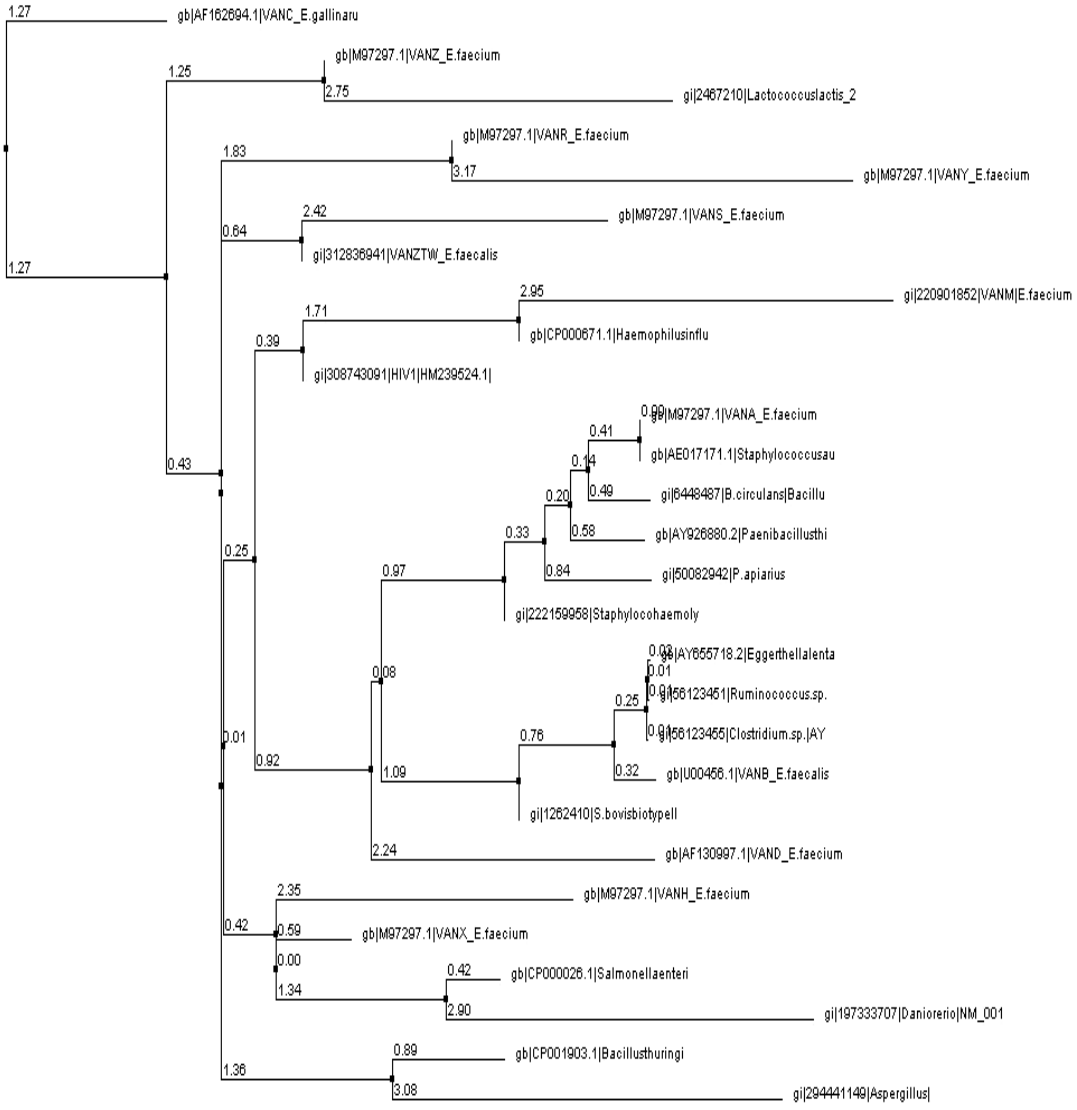

GRAPH 1: Presence of Vancomycin genes in Enterococcus and Streptococcus species

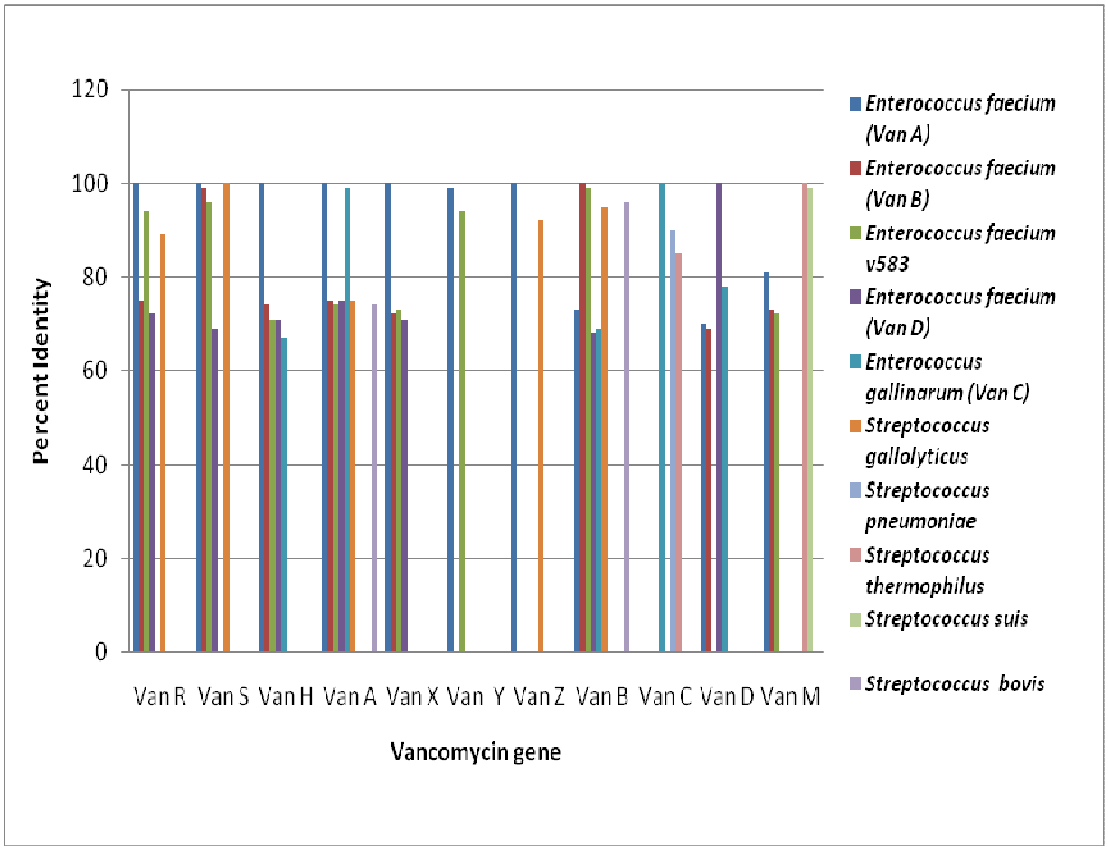

GRAPH 2: Presence of vancomycin genes in Staphylococcus and Lactococcus species

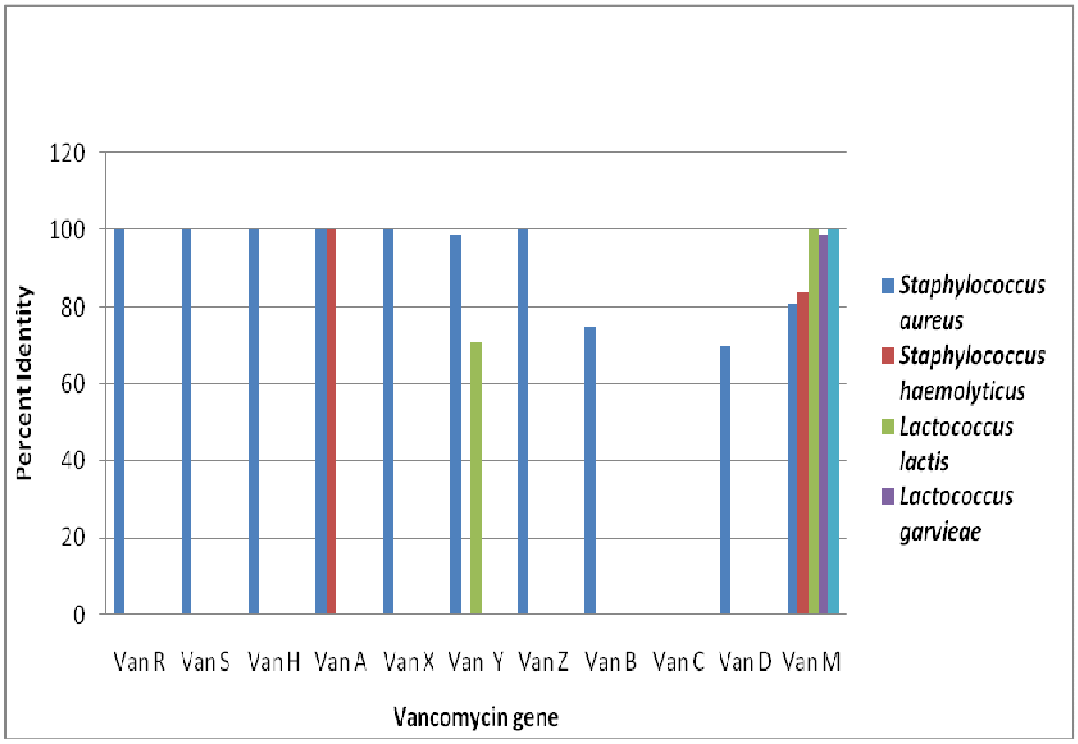


GRAPH 3: Presence of Vancomycin genes in Paenibacillus and Bacillus species

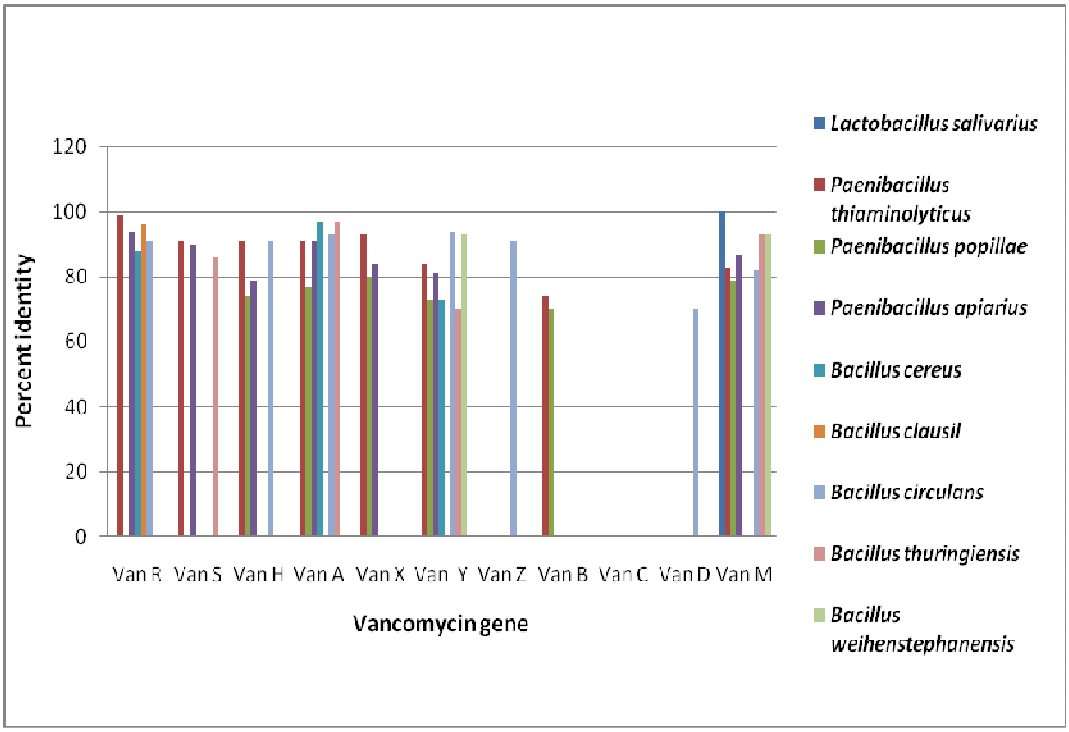

GRAPH 4: Presenceof vancomycin like genes in other organisms

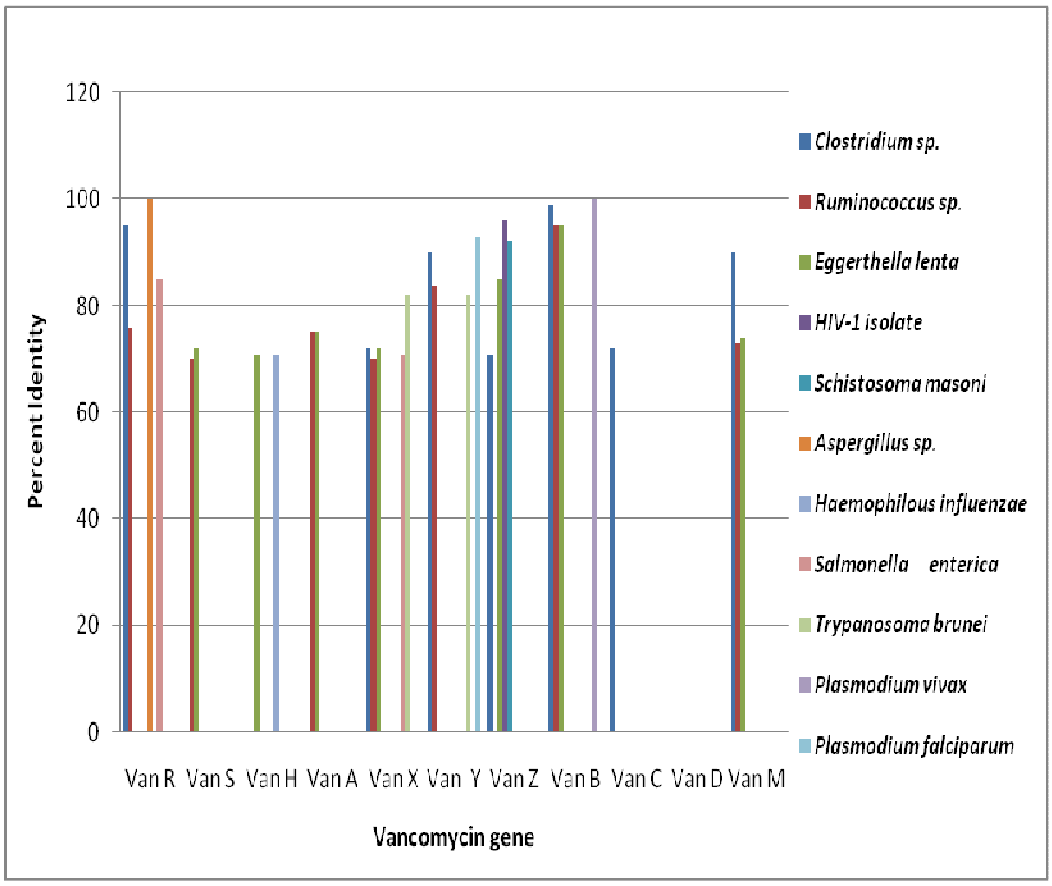

GRAPH 5: Presence of vancomycin like genes in higher organisms

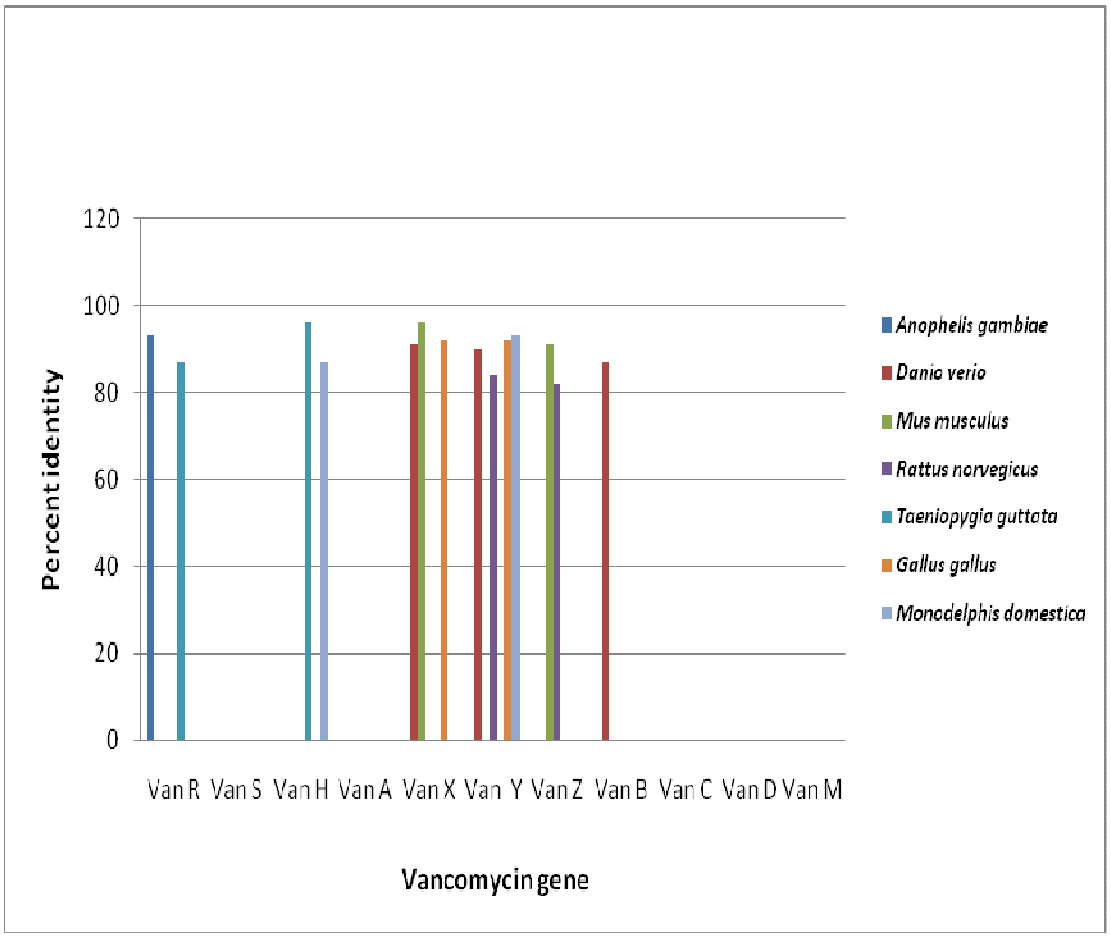

# A New Approach to Denoising EEG Signals - Merger of Translation Invariant Wavelet and ICA

**Janett Walters-Williams** *jwalters@utech.edu.jm*
*School of Computing & Information Technology*
*Faculty of Engineering & Computing*
*University of Technology, Jamaica*
*237 Old Hope Road,Kingston 6, Jamaica W.I.*

**Yan Li** *liyan@usq.edu.au*
*Department of Mathematics & Computing*
*Faculty of Sciences*
*University of Southern Queensland*
*Toowoomba, Australia*

**Abstract**

In this paper we present a new algorithm using a merger of Independent Component Analysis and Translation Invariant Wavelet Transform. The efficacy of this algorithm is evaluated by applying contaminated EEG signals. Its performance was compared to three fixed-point ICA algorithms (FastICA, EFICA and Pearson-ICA) using Mean Square Error (MSE), Peak Signal to Noise Ratio (PSNR), Signal to Distortion Ratio (SDR), and Amari Performance Index. Experiments reveal that our new technique is the most accurate separation method.

**Keywords:**Independent Component Analysis, Wavelet Transform, Unscented Kalman Filter, Electroencephalogram (EEG), Cycle Spinning

## 1. INTRODUCTION

The use of electroencephalogram (EEG) in the field of Medicine has had a great impact on the study of the human brain. The EEG itself represents the brain activity for a subject and gives us an objective mode of recording brain stimulation. It also has been suggested by several studies that EEGs can be used to detect several diseases such as Creutzfeldt-Jakob diseases (CJD), Alzheimer's, Dementia, Epilepsy, and Schizophrenia. The signals received, however, have several origins that lead to the complexity of their identification. This complexity is made of both the pure EEG signal and other non-cerebral signals called artifacts or noise. The artifacts have resulted in the contamination of the EEG signals; hence the removal of these noises has generated a large number of denoising techniques and methods, for example Fourier transform, time-frequency analysis, Wavelet Transform (WT), Neural Networks (NN), and Independent Component Analysis (ICA).

Independent Component Analysis (ICA) originated from the field of Blind Source Separation (BSS) [8]. In the BSS problem, a set of observations is given while the underlying signal information is hidden; the mixing weights of the individual signals are unknown. BSS is aimed at identifying the source signals and/or the mixing weights so as to separate these information sources into signal domain, feature domain or model domain [5]. ICA therefore calls for the separation of the EEG into its constituent independent components (ICs) and then eliminating the ICs that are believed to contribute to the noise. It is subjective, inconvenient and a time consuming process when dealing with large amount of EEG data.

Different types of ICA algorithms were proposed in the last 10 to 12 years. Most of them suppose that the sources are stationary and are based explicitly or implicitly on high order statistics computation. Therefore, Gaussian sources cannot be separated, as they don't have higher than 2

statistic moments. Other types of algorithms do not make the stationarity hypothesis, and use the non stationary structure of the signals (i.e. their time or frequency structure) to separate them. These methods use second order statistics (SOS) only, and they are called SOS algorithms. As EEG signals are highly non-stationary, these type of algorithms are the most widely used.

Like ICA, Wavelet Transform (WT) has been used to study EEG signals [3][20][32][35-36][41][44] successfully because of its good localization properties in time and frequency domain [13]. Here, the EEG signals pass through two complementary filters and emerge as two signals, approximation and details. This is called decomposition or analysis. The components can be assembled back into the original signal without loss of information. This process is called reconstruction or synthesis. The mathematical manipulation, which implies analysis and synthesis, is called discrete wavelet transform (DWT) and inverse discrete wavelet transform (IDWT). There have been many approaches to denoising using WT; those based on shrinkage are the most popular [32] where the EEG signals are decomposed into wavelets and noise removal done using thresholding and shrinkage.

Akin [1] in his research compared WT with fast Fourier transform and found that WT was better in detecting brain diseases. His research was confirmed by Hermann *et al* [16]. Unser *et al* [39] showed that wavelet is good at denoising EEG signals as well as other biomedical signals. WT has therefore emerged as one of the superior technique in analyzing non-stationary signals like EEG. Its capability in transforming a time domain signal into time and frequency localization helps to understand the behaviour of a signal better. WT however has limitations such as Gibbs phenomena [7].

Each of the above methods presents their own limitations. In our opinion a method that aims to fix these limitations should be a more effective denoising method. This is possible as each method is used to overcome the limitation of the other. We present in this paper a new method of extracting noise from EEG signals which aims to remove the limitations of ICA and WT while improving effectiveness – Cycle Spinning Wavelet Transform ICA (CTICA). The performance of CTICA is analyzed and compared with three known fixed-point ICA algorithms – FastICA, EFICA and Pearson-ICA, by using EEG signals contaminated with noise. Mean Square Error (MSE), Peak Signal to Noise Ratio (PSNR), Signal to Distortion Ratio (SDR), and Amari Performance Index are used as criteria for testing the quality of denoising.

## 2. SUPPORTING LITERATURE

### EEG Signals

The nervous system sends commands and communicates by trains of electric impulses. When the neurons of the human brain process information they do so by changing the flow of electrical current across their membranes. These changing current (potential) generate electric fields that can be recorded from the scalp. Studies are interested in these electrical potentials but they can only be received by direct measurement. This requires a patient to under-go surgery for electrodes to be placed inside the head. This is not acceptable because of the risk to the patient. Researchers therefore collect recordings from the scalp receiving the global descriptions of the brain activity. Because the same potential is recorded from more than one electrode, signals from the electrodes are supposed to be highly correlated. These are collected by the use of an electroencephalograph and called electroencephalogram (EEG) signals.

Understanding the brain is a huge part of Neuroscience, and the development of EEG was for the elucidation of such a phenomenon. The morphology of the EEG signals has been used by researches and in clinical practice to:

- Diagnose epilepsy and see what type of seizures is occurring.
- Produce the most useful and important test in confirming a diagnosis of epilepsy.
- Check for problems with loss of consciousness or dementia.
- Help find out a person's chance of recovery after a change in consciousness.
- Find out if a person who is in a coma is brain-dead.

- Study sleep disorders, such as narcolepsy.
- Watch brain activity while a person is receiving general anesthesia during brain surgery.
- Help find out if a person has a physical problem (in the brain, spinal cord, or nervous system) or a mental health problem.

The signals must therefore present a true and clear picture about brain activities. Being a physical system, recording electrical potentials, present EEG with problems; all neurons, including those outside the brain, communicate using electrical impulses. These non-cerebral impulses are produced from:

- Eye movements & blinking - Electrooculogram (EOG)
- Cardiac Movements - Cardiograph (ECG/ EKG)
- Muscle Movements - Electromyogram (EMG)
- Chewing & Sucking Movement – Glossokinetic
- The machinery used to record signals
- The power lines.

EEG recordings are therefore a combination of these signals called artifacts or noise and the pure EEG signal defined mathematically as:

$$E(t) = S(t) + N(t) \quad (1)$$

where *S* is pure EEG signal, *N* is the noise and *E* represents the recorded signal. The presence of these noises introduces spikes which can be confused with neurological rhythms. They also mimic EEG signals, overlaying these signals resulting in signal distortion (Figure 1). Correct analysis is therefore impossible, resulting in misdiagnosis in the case of some patients. Noise must be eliminated or attenuated.

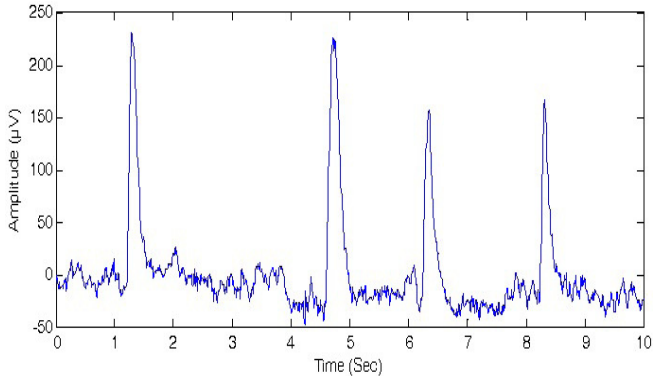


**FIGURE 1**: EEG contaminated with EOG producing spikes

The method of cancellation of the contaminated segments, although practiced, can lead to considerable information loss thus other methods such as Principal Components Analysis (PCA) [45], the use of a dipole model [18] and more recently ICA and WT have been utilized.

**Independent Component Analysis**

Independent Component Analysis (ICA) is an approach for the solution of the BSS problem [8]. It can be represented mathematically according to Hyvarinen, Karhunen & Oja [19] as:

$$X = As + n \quad (2)$$

where *X* is the observed signal, *n* is the noise, *A* is the mixing matrix and *s* the independent components (ICs) or sources. (It can be seen that mathematically it is similar to Eq. 1). The problem is to determine *A* and recover *s* knowing only the measured signal *X* (equivalent to *E(t)* in Eq. (1)). This leads to finding the linear transformation *W* of *X,* i.e. the inverse of the mixing matrix *A*, to determine the independent outputs as:

$$u = W X = W A s \qquad (3)$$

where *u* is the estimated ICs. For this solution to work the assumption is made that the components are statistically independent, while the mixture is not. This is plausible since biological areas are spatially distinct and generate a specific activation; they however correlate in their flow of information [18].

ICA algorithms are suitable for denoising EEG signals because

(i) the signals recorded are the combination of temporal ICs arising from spatially fixed sources and
(ii) the signals tend to be transient (localized in time), restricted to certain ranges of temporal and spatial frequencies (localized in scale) and prominent over certain scalp regions (localized in space) [28].

**Wavelet Transform**

Wavelet Transform (WT) is a form of time-frequency analysis been used successfully in denoising biomedical signals by decomposing signals in the time-scale space instead of time-frequency space. It is so because it uses a method called wavelet shrinkage proposed by Donoho & Johnstone [9]. Each decomposed signal is called a wavelet (Fig 2).

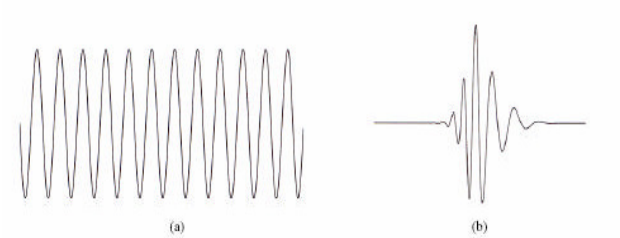


**FIGURE 2** : Demonstration of (a) a signal and (b) a wavelet

There are two basic types of WT. One type is designed to be easily reversible (invertible); that means the original signal can be easily recovered after it has been transformed. This kind of WT is used for image compression and cleaning (noise and blur reduction). Typically, the WT of the image is first computed, the wavelet representation is then modified appropriately, and then the WT is reversed (inverted) to obtain a new image.The second type is designed for signal analysis for study of EEG or other biomedical signals. In these cases, a modified form of the original signal is not needed and the WT need not be inverted.

WT decomposes a signal into a set of coefficients called the discrete wavelet transform (DWT) according to:

$$C_{j,k} = \sum_{t \in Z} E(t)\, g_{j,k}(t) \quad (4)$$

where $C_{j,k}$ is the wavelet coefficient and $g_{j,k}$ is the scaling function defined as:

$$2^{\frac{-j}{2}}\, g\,(2^{-j} t - k) \quad (5)$$

The wavelet and scaling functions depend on the chosen wavelet family, such as Haar, Daubechies and Coiflet. Compressed versions of the wavelet function match the high-frequency components, while stretched versions match the low-frequency components. By correlating the original signal with wavelet functions of different sizes, the details of the signal can be obtained at several scales or moments. These correlations with the different wavelet functions can be arranged in a hierarchical scheme called multi-resolution decomposition. The multi-resolution decomposition algorithm separates the signal into "details" at different moments and wavelet coefficients [35-36]. As the moments increase the amplitude of the discrete details become smaller, however the coefficients of the useful signals increase [44-45].

Considering Eq. (1) the wavelet transform of *E(t)* produces wavelet coefficients of the noiseless signal *S(t)* and the coefficients of the noise *N(t).* Researchers found that wavelet denoising is performed by taking the wavelet transform of the noise-corrupted *E(t)* and passing the detail coefficients, of the wavelet transform, through a threshold filter where the details, if small enough, might be omitted without substantially affecting the main signals. There are two main threshold filters – soft and hard. Research has shown that soft-thresholding has better mathematical characteristics [44-45] and provides smoother results [15]. Once discarded these coefficients are replaced with zeroes during reconstruction using an inverse wavelet transform to yield an estimate for the true signal, defined as:

$$\hat{S}(t) = D\left(E(t)\right]\right) = W^{-1}\left(\Lambda_{th}\left(W\left(E(t)\right)\right)\right) \quad (6)$$

where $\Lambda_{th}$ is the diagonal thresholding operator that zeroes out wavelet coefficients less than the threshold, *th.* It has been shown that this algorithm offers the advantages of smoothness and adaptation. However, as Coifman and Donoho [7] pointed out, this algorithm exhibits visual artifacts such Gibbs phenomena in the neighbourhoodof discontinuities.

**Unscented Kalman Filter**

Unscented Kalman Filter (UKF) is a Bayesian filter which uses minimum mean-squared error (MMSE) as the criterion to measure optimality [4][34]. For highly nonlinear systems, the linear estimate of the nonlinear model does not provide a good approximation of the model, and the Extended Kalman Filter (EKF) will not track signals around sharp turning points. Another problem with the EKF is that the estimated covariance matrix tends to underestimate the true covariance matrix and therefore risks becoming inconsistent in the statistical sense without the addition of "stabilising noise". UKF was found to address these flaws. It involves the Unscented Transformation (UT), a method used to calculate the first and second order statistics of the outputs of nonlinear systems with Gaussian. The nonlinear stochastic system used for the algorithm is:

$$\begin{aligned} x_{k+1} &= A\,x_k + B\,u_k + v_k \\ y_k &= H\,x_k + w_k \end{aligned} \quad (7)$$

where *A* and *H* are the known and constant matrices respectively, $x_k$ is the unobserved state of the system, $u_k$ is a known exogenous input, $y_k$ is the observed measurement signal, $v_k$ is the process noise and $w_k$ is the measurement noise.

UKF uses the intuition that it is easier to approximate a probability distribution function rather than to approximate an arbitrary nonlinear function or transformation. Following this intuition, a set of sample points, called sigma points, are generated around the mean, which are thenpropagated through the nonlinear map to get a more accurate estimation of the mean and covariance of the mapping results. In this way, it avoids the need to calculate the Jacobian, which for complex functions can be a difficult task in itself (i.e., requiring complicated derivatives if done analytically or being computationally costly if done numerically).

## 3. METHODOLOGY

**Reasons for Algorithm**

Although ICA is popular and for the most part does not result in much data loss; its performance depends on the size of the data set i.e. the number of signals. The larger the set, the higher the probability that the effective number of sources will overcome the number of channels (fixed over time), resulting in an over complete ICA. This algorithm might not be able to separate noise from the signals. Another problem with ICA algorithms has to do with the signals in frequency domain. Although noise has different distinguishing features, once they overlap the EEG signals ICA cannot filter them without discarding the true signals as well. This results in data loss.

WT utilizes the distinguishing features of the noise however. Once wavelet coefficients are created, noise can be identified. Decomposition is done at different levels (L); DWT produces different scale effects (Fig 3). Mallat [2] proved that as scales increase the WT of EEG and noise present different inclination. Noise concentrates on scale 21, decreasing significantly when the scale increases, while EEG concentrates on the 22-25 scales. Elimination of the smaller scales denoise the EEG signals. WT therefore removes any overlapping of noise and EEG signals that ICA cannot filter out.

Recently there has been research comparing the denoising techniques of both ICA and WT. It was found that

(i) if noise and signals are nearly the same or higher amplitude, wavelets had difficultly distinguishing them. ICA, on the other hand, looks at the underlying distributions thus distinguishing each [46] and
(ii) ICA gives high performance when datasets are large. It suffers however from the trade off between a small data set and high performance [20].

Research therefore shows that ICA and wavelets complement each other, removing the limitations of each [35]. Since then research has been done applying a combination of both with ICA as a per- or post- denoising tool. Inuso *et al.* [20] used them where ICA and wavelets are joint. They found that their method outperformed the pre- and post- ICA models.

With or without ICA, conventional wavelet coefficients of 2 signals maybe quite different in many properties as WT is not time invariant, consequently, if the noisy signal is shifted in time, denoised, and then shifted back, the result will, in general, be different from the estimate obtained from denoising without shifting. This result in serious problems such as pseudo-Gibbs phenomenaalternating undershoot and overshoot of a special target level near singularity points of signals [42].

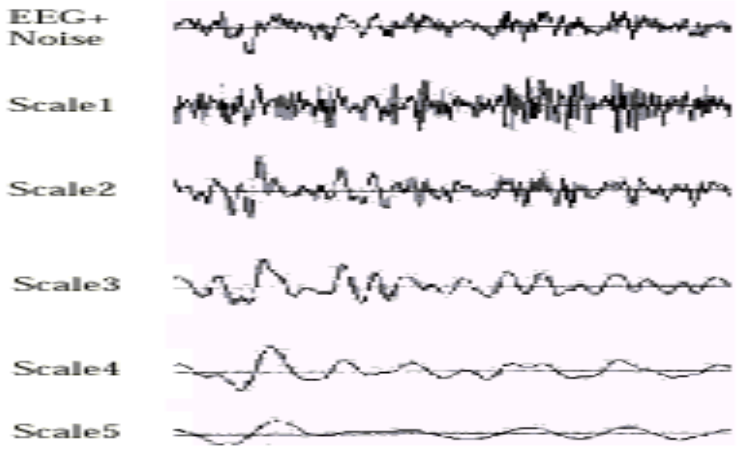


**FIGURE 3**: Noisy EEG and its Wavelet Transform at different scales

Cycle Spinning (CS) was proposed by Coifman & Donoho [7] as a simple yet efficient method that utilizes the periodic time-invariance of WT in fixing the noise found in wavelet coefficients and defined as:

$$\hat{s} = \frac{1}{k_1 k_2} \sum_{i=1,\, j=1}^{k_1 k_2} S_{-i,-j} \left( T^{-1} \left( \theta \left[ T \left( S_{i,j}(x) \right) \right] \right) \right) \quad (8)$$

where $(k_1,k_2)$ are maximum number of shifts, $T$ the shift variant transform, $S_{i,j}$ is the circulant shift, and $\theta$ the threshold operator. CS calls for the suppression of these noises by shifting the signals in time and computing the estimate. Using different shifts produce different estimates which are not completely independent; consequently averaging these estimates results in a reduction in the noise generated in each shift. This results in the denoising of all possible unique circularly shifted version of the signal and the creation of the Translation Invariant Wavelet Transform (TIWT) method.

Apart from the use of ICA improvements of WT have been investigated. The idea of Wiener filtering of individual wavelet coefficient arose from the fact that wavelet transforms tend to decorrelate data. An improved wavelet domain denoising technique was therefore proposed that utilizes the Wiener filtering of wavelet coefficients [13]. Research shows that this technique has superior performance over other denoising algorithms using thresholding or shrinkage of wavelet coefficients and has motivated the analysis of many denoising algorithms in terms of optimal filtering of noisy wavelet coefficients. In 2006 the combination of WT and the Kalman Filter (KF) was a novel idea. In the experiments, researchers found that the combination effectively correct overlapped spectra and reduce noise [38]. Mastriani *et al*. [29] created the KalmanShrink for the WT; simulations showed that the threshold had better performance than the most commonly used filters [29]. The use of KF and WT combination therefore improved denoising techniques. Research has also shown that the KF outperforms the Wiener Filter when applied to WT [31]. UKF is advancement on KF.

Each method aims at improving the other in that

(i) WT removes overlapping of noise signals that ICA cannot filter out.
(ii) ICA can distinguish between noise and signals that are nearly the same or higher amplitude which WT has difficultly with.
(iii) WT exhibits serious problems such as pseudo-Gibbs phenomena which CS eliminates and
(iv) Combination of filters and WT effectively correct overlapped spectra

This paper proposes a merger of all four methodologies.

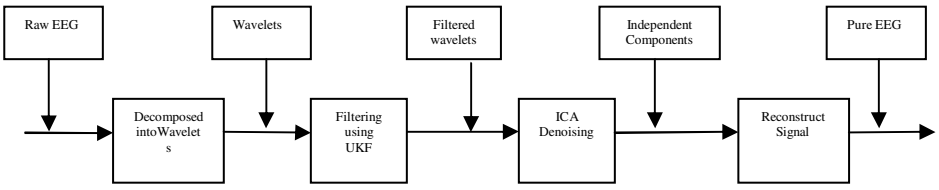


**FIGURE 4**: Proposed CTICA - Artifacts Removal System

**Design**

In this paper we are presenting another method to denoising EEG signals using WT and ICA along with smaller methods to improve their performance. Some of the ideas appear in earlier algorithms; however the main differences of CTICA are:

(i)the use of CS, and
(ii) the merger of WT, UKF and ICA into one ( this has never been done before).

A block diagram representation of the proposed work is shown in Figure 4. The algorithm can be divided into the following:

1. Signal Collection

This algorithm is designed to denoise both natural and artificially noised EEG signals. They should therefore be mathematically defined based on Eq. (1).

2. Apply CS to signal

The number of time shifts is determined; in so doing signals are forcibly shifted so that their features change positions removing the undesirable oscillations which result in pseudo-Gibbs phenomena. The circulant shift by h is defined as:

$$S_h\left(f(n)\right) = f\left((n+h) \bmod N\right) \quad (9)$$

where *f(n)* is the signal, *S* is time shift operator and *N* is the number of signals. The time-shift operator S is unitary and therefore invertible i.e. $(S_h)^{-1} = S_{-h}$

3. Decomposition of Signal

The signals are decomposed into 5 levels of DWT using the Symmlet family, separating noise and true signals. Symmlets are orthogonal and its regularity increases with the increase in the number of moments [11]. After experiments the number of vanishing moments chosen is 8 (Sym8).

4. Filter Coefficients

Perform UKF on the coefficients to filter out some noise reducing the shrinkage threshold.

5. Choose and Apply Threshold Value

Denoise using the soft-thresholding method discarding all coefficients below the threshold value using VisuShrink based on the universal threshold defined by Donoho & Johnstone [9] given as:

$$T = \sqrt{2\sigma^2 \log N} \quad (10)$$

where *N* is the number of samples and $\sigma^2$ is the noise power.

6. Apply ICA algorithm

Signals and noise may have nearly the same frequency characteristics and overlap in time thus producing noisy coefficients such as beta activity and muscle noise, that WT has not been able to distinguish and remove. ICA is able to look at the underlying distributions thus distinguish noise and remove them. Research has shown that ICA is a robust denoising method where its performance is not affected by the severity of the mixing signals [10]. We implemented a symmetrical fixed-point ICA algorithm based on the Hyvarinen model [19] where the gradient function is:

$$g(y) = \tanh(a, y) \quad (11)$$

A fixed-point algorithm has a cubic or at least a quadratic convergence, is not linear and no parameters have to be chosen for usage which makes it a better choice than other ICA models.

7. Reconstruction of Signals

EEG signals are reconstructed using inverse DWT.

8. Apply CS

Revert signals to their original time shift and average the results obtained to produce the denoised EEG signals.

The proposed algorithm can be expressed as Avg [Shift – Denoise -Unshift] i.e. using Eq. (9) it is defined as:

$$avg_{h \in H} \left( S_{-h} T S_h (f) \right) \quad (12)$$

where $H$ is the range of shifts, $T$ is the wavelet shrinkage denoising operator, $h$ the circular shift and the maximum of $H$is the length of the signal$N$ from Eq. (9).

**Evaluation**

There are different means to access the separation quality performed by ICA methods; however the performance measures used throughout this section will be:

(i) the Mean Square Error (MSE),
(ii) the Peak Signal to Noise Ratio (PSNR),
(iii) the Signal to Distortion Ratio (SDR), and
(iv) the Amari Performance Index

We employed fixed point benchmark ICAs with the linearity *g(u) = tanh* and the symmetric orthogonalization for comparison, namely:fixed-point - FastICA[19], EFICA[28] and Pearson-ICA [26]

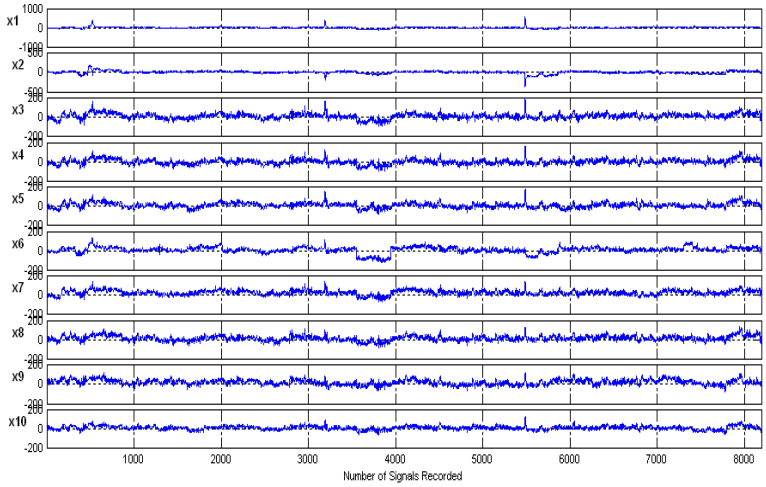


**FIGURE 5** : Sample EEG signals from a male subject

## 4. EXPERIMENTAL DATA

In order to do the study effectively data was collected for analysis from two sites.

(i) http://www.filewatcher.com/b/ftp/ftp.ieee.org/uploads/press/rangayyan.0.0.html [48]. Data was collected at a sampling rate of 100Hz but noise free. These signals were artificially contaminated.

(ii) http://sccn.ucsd.edu/~arno/fam2data/publicly_available_EEG_data.html [47]. All data are real comprised of EEG signals from both human and animals. Data were of different types.

(a) Data set acquired is a collection of 32-channel data from one male subject who performed a visual task. Fig. 5 shows 10 signals from this dataset.

(b) Human data based on five disabled and four healthy subjects. The disabled subjects (1-5) were all wheelchair-bound but had varying communication and limb muscle control abilities. The four healthy subjects (6-9) were all male PhD students, ages 30 who had no known neurological deficits. Signals were recorded at 2048 Hz sampling rate from 32 electrodes placed at the standard positions of the 10-20 international system.

(c) Data set is a collection of 32-channel data from 14 subjects (7 males, 7 females) who performed a go-nogo categorization task and a go-no recognition task on natural photographs presented very briefly (20 ms). Each subject responded to a total of 2500 trials. The data is CZ referenced and is sampled at 1000 Hz.

(d) Five data sets containing quasi-stationary, noise-free EEG signals both in normal and epileptic subjects. Each data set contains 100 single channel EEG segments of 23.6 sec duration.

These two sites produce real signals of different sizes as well as 1D and 2D signals. A total of 1,383 signals were tested.

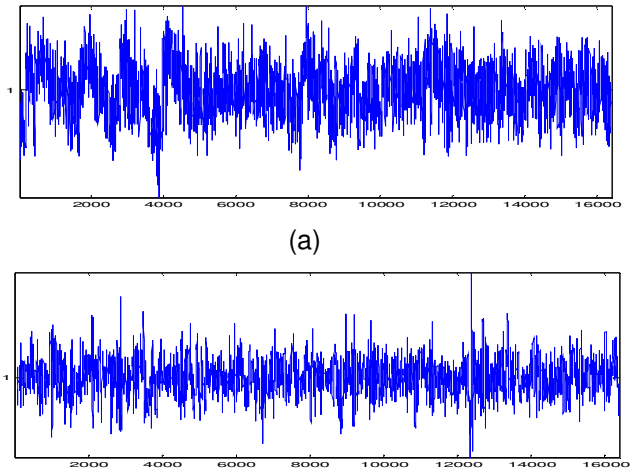


(a)

(b)

**FIGURE 6** : (a) EEG Signal with EOG (b) Denoised EEG Signal

## 5. RESULTS & DISCUSSION

We conducted experiments, using the above mentioned signals, in Matlab 7.8.0 (R2009) on a laptop with AMD Athlon 64x2 Dual-core Processor 1.80GHz. Noisy signals were generated by adding noise to the original noise-free signals and the length of all signals, *N*, were truncated to lengths of power of twos i.e. $2^x$.

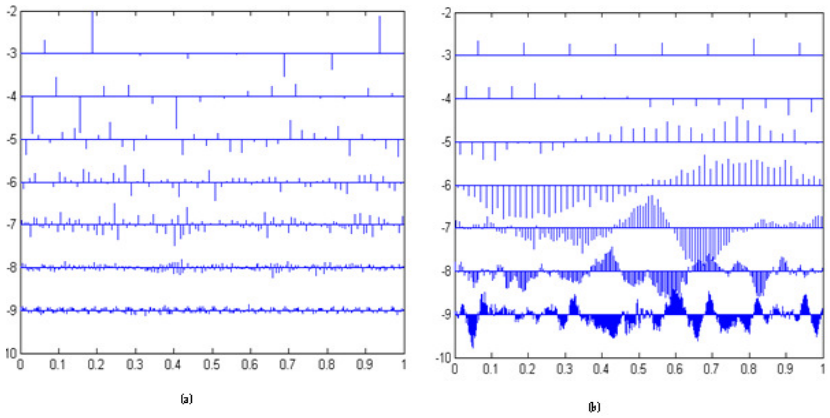

**FIGURE 7**: (a) Wave Coefficient before denoising
(b) Wave Coefficient after denoising

Figure 6 shows the results of the above algorithm on one EEG signal contaminated with EOG. Investigations on the wavelet coefficients (Figure 7) also show that there are major changes in the wavelets - some wavelets have been zeroed because of their identification to noise.

| CTICA | FASTICA | EFICA | PEARSON |
|---|---|---|---|
| 1411.00 | 1489.70 | 1412.40 | 1337.20 |
| 950.09 | 1014.80 | 951.75 | 890.67 |
| 714.51 | 769.91 | 715.31 | 662.73 |
| 693.71 | 749.04 | 694.70 | 642.40 |
| 757.94 | 815.16 | 758.81 | 704.47 |
| 858.63 | 920.96 | 859.34 | 799.85 |
| 849.22 | 923.80 | 849.61 | 778.53 |
| 788.22 | 850.93 | 788.77 | 728.96 |
| 875.44 | 941.76 | 876.23 | 813.07 |
| 369.86 | 410.65 | 370.30 | 332.04 |
| 297.61 | 333.63 | 298.10 | 264.57 |
| 526.54 | 574.16 | 527.08 | 482.01 |
| 636.14 | 696.30 | 636.44 | 579.28 |
| 1031.70 | 1116.70 | 1032.00 | 950.71 |
| 236.44 | 269.07 | 236.93 | 206.84 |
| 383.87 | 424.57 | 384.31 | 346.05 |
| 650.56 | 598.48 | 651.06 | 598.48 |
| 694.03 | 752.93 | 694.55 | 638.52 |
| 577.78 | 646.60 | 577.90 | 513.06 |
| 449.89 | 504.49 | 450.01 | 398.64 |

**TABLE 1**: MSE for 15 EEG signals with EOG noise

**Noise/Signal Measures**

The MSE measures the average of the square of the "error" which is the amount by which the estimator differs from the quantity to be estimated. Mathematically it is defined as:

$$MSE = \frac{1}{MN}\sum_{y=1}^{M}\sum_{x=1}^{N}[I(x,y) - I'(x,y)]^2 \quad (13)$$

The error is the amount by which the estimator differs from the quantity to be estimated. The difference occurs because of randomness or because the estimator doesn't account for information that could produce a more accurate estimate. . For a perfect fit, *I(x,y) = I'(x,y)* and MSE = 0; so, the MSE index ranges from 0 to infinity, with 0 corresponding to the ideal. The smaller the
MSE therefore the closer the estimator is to the actual data and the less the error on the signal;
CTICA was compared in both Table 1 and Table 2. Examination shows that on average our method had the second lowest MSE next to Pearson-ICA.

PSNR is the ratio between the maximum possible power of a signal and the power of corrupting noise that affects the fidelity of its representation. Mathematically it is defined as:

$$PSNR = 10 \times \log_{10}(\frac{MAX^2}{MSE}) \quad (14)$$

| CTICA | FASTICA | EFICA | PEARSON |
|---|---|---|---|
| 26351.00 | 26678.00 | 26352.00 | 26028.00 |
| 12824.00 | 13051.00 | 12823.00 | 12597.00 |
| 6449.30 | 6610.00 | 6447.80 | 6287.70 |
| 5493.40 | 5642.20 | 5492.60 | 5345.20 |
| 6221.40 | 6379.90 | 6220.60 | 6063.50 |
| 106.51 | 87.34 | 107.03 | 87.35 |
| 2481.90 | 2583.60 | 2482.60 | 2383.80 |
| 6457.50 | 6618.90 | 6456.80 | 6296.90 |
| 6451.60 | 6612.90 | 6450.70 | 6290.70 |
| 12811.00 | 13038.00 | 12810.00 | 12584.00 |
| 5508.10 | 5657.20 | 5507.50 | 5359.80 |
| 16004.00 | 16265.00 | 16008.00 | 15755.00 |
| 3839.70 | 3968.90 | 3842.10 | 3717.90 |
| 1999.40 | 20921.00 | 2000.20 | 1910.70 |
| 451.69 | 494.80 | 451.31 | 409.98 |
| 470.52 | 517.86 | 471.58 | 427.64 |
| 13454.00 | 13694.00 | 13458.00 | 13255.00 |
| 13089.00 | 13324.00 | 13092.00 | 12863.00 |
| 3850.60 | 3979.80 | 3853.00 | 3728.60 |

**TABLE 2**: MSE for 19 EEG signals with artificially added noise

Because many signals have a very wide dynamic range, PSNR is usually expressed in terms of the logarithmic decibel scale.In this research MAX takes the value of 255. Unlike MSE which represents the cumulative squared error between the denoised and mixed signal, PSNR represents a measure of the peak error i.e. when the two signals are identical the MSE will be equal to zero, resulting in an infinite PSNR.The higher the PSNR therefore, the better the quality of the reconstructed signal i.e. a higher PSNR indicates that the reconstruction is of a higher qualityand therefore the algorithm is considered good. Table 3 shows the PSNR for EOG contaminated signals and Table 4 shows those with artificially contaminated noise.

Examination of Table 3 and Table 4 show that Pearson-ICA is the algorithm that has the highest PSNR with CTICA been second. It can also be seen in Table 4 that CTICA and EFICA both have similar to MSE when signals have artificial noise added for 83%. The other 17% CTICA performed better. CTICA however in both cases presents more signal than noise in its denoised results than FastICA. CTICA is the second best in performance therefore because it outperformed FastICA and it never produces a PSNR lower than EFICA; in fact it sometimes performed better than EFICA. Algorithms therefore follow the same behavior as seen with the MSE investigations.

| CTICA | FASTICA | EFICA | PEARSON |
|---|---|---|---|
| 16.63 | 16.40 | 16.63 | 16.87 |
| 18.35 | 18.07 | 18.35 | 18.63 |
| 19.59 | 19.27 | 19.59 | 19.92 |
| 19.72 | 19.39 | 19.71 | 20.05 |
| 19.33 | 19.02 | 19.33 | 19.65 |
| 18.79 | 18.49 | 18.79 | 19.10 |
| 18.84 | 18.48 | 18.84 | 19.22 |
| 19.16 | 18.83 | 19.16 | 19.50 |
| 18.71 | 18.39 | 18.70 | 19.03 |
| 22.45 | 22.00 | 22.45 | 22.92 |
| 23.39 | 22.90 | 23.39 | 23.91 |
| 20.92 | 20.54 | 20.91 | 21.30 |
| 20.10 | 19.70 | 20.09 | 20.50 |
| 18.00 | 17.65 | 17.99 | 18.35 |
| 24.39 | 23.83 | 24.38 | 24.97 |
| 22.29 | 21.85 | 22.28 | 22.74 |
| 20.00 | 20.36 | 19.99 | 20.36 |
| 19.72 | 19.36 | 19.71 | 20.08 |
| 20.51 | 20.02 | 20.51 | 21.03 |
| 21.60 | 21.10 | 21.60 | 22.12 |

**TABLE 3** : PSNR for 20 EEG signals with EOG noise

**Separation Accuracy Measures**

How accurate the separation of an ICA algorithm in terms of the signals can be calculated by the total SDR which is defined as:

$$SDR(x_i, y_i) = \frac{\sum_{n=1}^{L} x_i(n)^2}{\sum_{n=1}^{L} (y_i(n) - x_i(n))^2} \quad i = 1, \ldots m \tag{15}$$

| CTICA | FASTICA | EFICA | PEARSON |
|---|---|---|---|
| 3.92 | 3.87 | 3.92 | 3.98 |
| 7.05 | 6.97 | 7.05 | 7.13 |
| 10.04 | 9.93 | 10.04 | 10.15 |
| 10.73 | 10.62 | 10.73 | 10.85 |
| 10.19 | 10.08 | 10.19 | 10.30 |
| 27.86 | 28.72 | 27.84 | 28.72 |
| 14.18 | 14.01 | 14.18 | 14.36 |
| 10.03 | 9.92 | 10.03 | 10.14 |
| 10.03 | 9.93 | 10.03 | 10.14 |
| 10.72 | 10.60 | 10.72 | 10.84 |
| 6.09 | 6.02 | 6.09 | 6.16 |
| 12.29 | 12.14 | 12.29 | 12.43 |
| 15.12 | 14.93 | 15.12 | 15.32 |
| 21.41 | 20.99 | 21.40 | 21.82 |
| 6.84 | 6.77 | 6.84 | 6.92 |
| 6.96 | 6.88 | 6.96 | 7.04 |
| 12.28 | 12.13 | 12.27 | 12.42 |
| 11.81 | 11.72 | 11.81 | 11.99 |

**TABLE 4** : PSNR for 18 EEG signals with artificially added noise

where $x_i(n)$ is the original source signal and $y_i(n)$ is the reconstructed signal. When the SDR is calculated if it is found to be below 8-10dB the algorithm is considered to have failed separation. Fig. 8 shows all four algorithms having SDR above 8dB; there is not much differentiation in the

graph for the algorithms however. Where there were difference in the SDR calculations CTICA had the most consistent. Table 5 showed that CTICA produced the largest SDR on average. This shows that on average CTICA had best separation of signal from noise than the other algorithms.

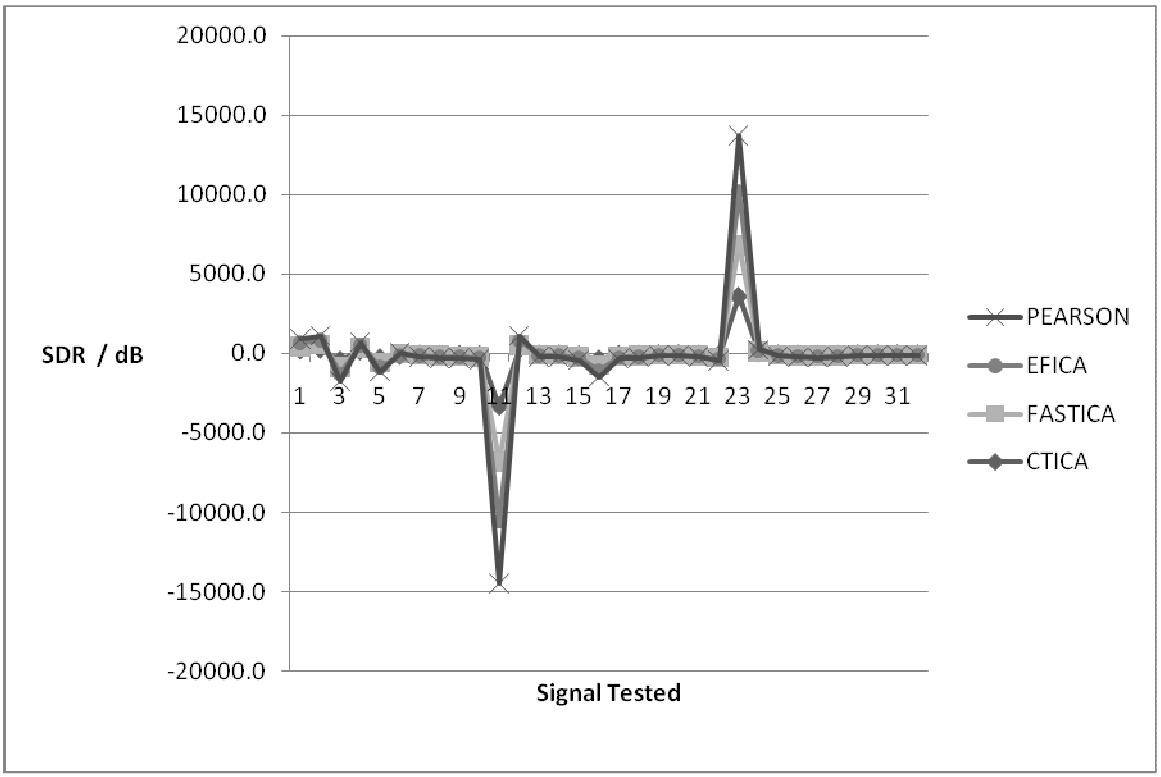


**FIGURE 8** : SDR for 32 signals with EOG

The most widely used measure for assessing the accuracy of the estimated mixing matrix is the Amari performance index defined as:

$$P_{err} = \frac{1}{2m}\sum_{i,j=1}^{m}\left(\frac{|p_{ij}|}{\max_k |p_{ik}|} + \frac{|p_{ij}|}{\max_k |p_{kj}|}\right) - 1 \qquad (16)$$

where $p_{ij} = (BA)_{ij}$. It assesses the quality of the de-mixing matrix *W* for separating observations generated by the mixing matrix *A***.** When the separation is perfect, the Amari index is equal to zero. In the worst case, i.e. when the estimated sources contain the same proportion of each original source signal, the Amari index is equal to *m*/2–1. However, the most common situation is between both. The lower the Amari index therefore, the more accurate the separation is. The Amari indexes obtained for the different algorithms and for different sample sizes are presented in Figure 9.

| CTICA | FASTICA | EFICA | PEARSON |
|---|---|---|---|
| 10089.00 | 9916.50 | 9977.60 | 10039.00 |
| 1900.10 | 1867.70 | 1884.20 | 1901.00 |
| 930.91 | 911.92 | 923.32 | 935.00 |
| 1141.00 | 1112.70 | 1127.00 | 1143.10 |
| 966.00 | 945.51 | 957.53 | 969.86 |
| 600.63 | 503.94 | 455.22 | 503.89 |
| -663.61 | -660.57 | -673.86 | -687.69 |
| 1266.60 | 1237.20 | 1252.60 | 1268.40 |
| 961.88 | 942.02 | 965.84 | 965.84 |
| 1371.90 | 1351.60 | 1363.60 | 1375.80 |
| 1074.20 | 1048.20 | 1062.40 | 1076.90 |
| 901.30 | 888.19 | 895.28 | 902.46 |
| 371.50 | 361.34 | 367.26 | 373.35 |
| 258.60 | 249.01 | 254.67 | 260.57 |
| -2441.10 | -6579.90 | -6889.70 | -7228.60 |
| 80.17 | 74.99 | 78.58 | 82.52 |
| 771.02 | 759.16 | 765.79 | 772.50 |
| 848.85 | 834.97 | 842.33 | 849.80 |
| 384.01 | 373.40 | 379.50 | 385.77 |
| 1095.42 | 849.36 | 841.53 | 836.29 |

**TABLE 5**: SDR for 20 with artificially added noise

Observations show that the Amari indexes for our method is lower for sample sizes greater than $2^7$ i.e. it clearly outperforms the other algorithms with sample size greater than 128. Figure 9 also shows that unlike the other algorithms, the Amari index for CTICA is inversely proportional to sample size.

## 6. CONCLUSION & FUTURE WORK

In recent years researchers have used both ICA algorithms and WT to denoise EEG signals. In this paper we propose a new method – Cycle Spinning Wavelet Transform ICA (CTICA). From the experiments we can conclude the following for CTICA

(i) It has outperformed FastICA and EFICA as far as MSE and PSNR were concerned.
(ii) It has the best SDR and
(iii) It has the best Amari index for signals greater than $2^7$ in size which decreases as sample size increases

Based on these results it can be concluded that CTICA is the most accurate separation method and is the second best at signal/noise measurement.

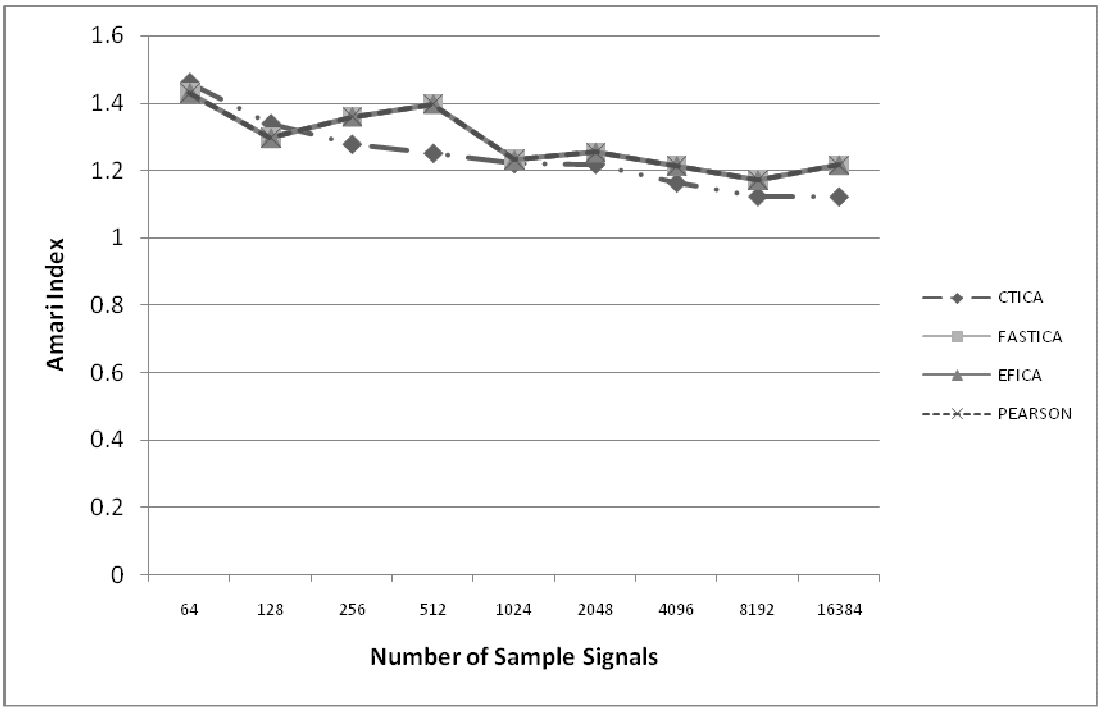


**FIGURE 9**: Amari Results for the four algorithms

## 7. REFERENCES

[1] M. Akin, "Comparison of Wavelet Transform and FFT Methods in the Analysis of EEG Signals", Journal of Medical Systems 26(3), 241-247, 2002.

[2] M. Alfaouri and K. Daqrouq, "ECGSignal Denoising By Wavelet Transform Thresholding", American Journal of Applied Sciences 5 (3), 276-281, 2008.

[3] M.I. Bhatti, A. Pervaiz and M.H. Baig, "EEG Signal Decomposition and Improved Spectral Analysis Using Wavelet Transform", In Proceedings of the 23rd Engineering in Medicine and Biology Society 2, 2001, 1862-1864.

[4] Z. Chen, "Bayesian Filtering: From Kalman Filters to Particle Filters, and Beyond", Adaptive Systems Lab., McMaster University., Hamilton, Ontario, Canada, 2003, Retrieved June 20, 2009, from: http://users.isr.ist.utl.pt/~jpg/tfc0607/chen_bayesian.pdf.

[5] J. Chien; H. Hsin-Lung and S. Furui, "A new mutual information measure for independent component analysis", In the Proceedings of the IEEE International Conference on Acoustics, Speech and Signal Processing, 2008 (ICASSP 2008), 2008, 1817 – 1820

[6] S. Choi, A. Cichocki, L. Zhang, and S. Amari, "Approximate Maximum Likelihood Source Separation Using the Natural Gradient",In the Proceedings of theIEICE Transaction Fundamental E84A(12), 2002.

[7] R.R. Coifman, and D.L. Donoho, "Translation Invariant Denoising",Lecture Notes in Statistics: Wavelets and Statistics, 125-150, 1995.

[8] P. Comon, "Independent Component Analysis, a new concept?", Signal Processing, Elsevier, 36(3), 287-314, 1994.

[9] D.L. Donoho and I. Johnstone, "Adapting to unknown smoothness via wavelet shrinkage", Journal of American Statistical Association, 90,1200—1224, 1995.

[10] U.E. Emuir, A. Akin, A. Ertuzun, B. Sankur and K. Harmanci, "Wavelet Denoising vs ICA Denoising for Functional Optical Imaging", In the Proceedings of the 1st International IEEE EMBS Conference on Neural Engineering, 2003, 384-387.

[11] B. Ferguson, D. Abbott, "Denoising Techniques for Terahertz Response of Biological Samples", Microelectronics Journal 32, 943-953, 2001.

[12] N. Gadhok, and W. Kinsner, "Robust ICA for Cognitive Informatics". International Journal of Cognitive Informatics and Natural Intelligence (IJCINI) 2(4),86-92, 2008.

[13] S. P. Ghael, A. M. Sayeed and R. G. Baraniuk, "Improved Wavelet Denoising via Empirical Wiener Filtering", In the Proceedings of theSPIEvol. 3169, 389-399, 1997.

[14] A. Graps, An Introduction to Wavelets. IEEE Journal of Computational Science and Engineering 2(2),1-17, 1995.

[15] Y.M. Hawwar, A.M. Reza, and R.D. Turney, Filtering(Denoising) in the Wavelet Transform Domain,, Unpublished, Department of Electrical Engineering And Computer Science, University of Wisconsin-Milwaukee, 2002.

[16] C.S. Herrmann, M. Grigutsch and N.A. Busch, (2005). EEG oscillations and wavelet analysis. Event-related potentials: A methods handbook,MIT Press, 229-259, 2005.

[17] G.G. Herrero, and K. Egiazarian, "Independent Component Analysis by a Resampling Strategy", Technical Report 2005, Retrieved September 18, 2009, fromhttp://www.cs.tut.fi/~gomezher/projects/bss/rica/rica.pdf

[18] S. Hoffman, and M. Falkenstien , "The Correction of Eye Blink Artefacts in the EEG: A Comparison of a Two Prominent Methods", PLoS One 3(8):e3004, 2008

[19] A. Hyvärinen and E. Oja, "A Fast Fixed-Point Algorithm for Independent Component Analysis", Neural Computation,9(7), 1483-1492, 1997

[20] A. Hyvarinen, J. Karhunen and E. Oja , Independent Component Analysis, eds. Wiley & Sons, 2001

[21] G. Inuso, F. La Foresta, N. Mammone, and F.C. Morabito, "Wavelet-ICA methodology for efficient artifact removal from Electroencephalographic recordings", In the Proceedings of the International Conference on Neural Networks,1524-1529, 2007.

[22] N. Jacob, and A. Martin, "Image Denoising in the Wavelet Domain Using Wiener Filtering", Unpublished course project, University of Wisconsin, Madison, Wisconsin, USA, 2004.

[23] S. Julier, and J.K. Uhlmann, "Unscented Filtering and Nonlinear Estimation",Proceedings of the. IEEE 92(3), 401-421, 2004.

[24] S. Julier, and J.K. Uhlmann, "A New Extension of the Kalman Filter to Nonlinear Systems" In the Proceedingd of AeroSense: 11th Int. Symp. Aerospace/Defense Sensing, Simulation and Controls,182-193, 1997.

[25] A. Kallapur, S. Anavatti, and M. Garratt, "Extended and Unscented Kalman Filters for Attitude Estimation of an Unmanned Aerial Vehicle,In the Proceedings of the 27th IASTED Int. Conf. Modelling, Identification, and Control (MIC 2008) , 2008

[26] J. Karvanen, J.,Eriksson, and K.V. Pearson, "System Based Method for Blind Separation", In the Proceedings of Second International Workshop on Independent Component Analysis and Blind Signal Separation, Helsinki 2000, 585—590, 2000.

[27] L. Kaur, S. Gupta, and R.C. Chauhan, "Image Denoising using Wavelet Thresholding", In the Proceedings of the 3rd Indian Conf. Computer Vision, Graphics & Image Processing (ICVGIP 2002), 22(14), 2002.

[28] Z. Koldovský and P. Tichavský, P., "Time-Domain Blind Audio Source Separation Using Advanced ICA Methods", In the Proceedings of the 8th Annual Conference of the International Speech Communication Association (Interspeech 2007), pp. 846-849, 2007.

[29] V. Krishnaveni, S. Jayaraman, A. Gunasekaran, and K. Ramadoss, Automatic Removal of Ocular Artifacts using JADE Algorithm and Neural Network, International Journal of Intelligent Systems and Technologies 1(4), 322-333, 2006.

[30] V. Krishnaveni, S. Jayaraman, S. Aravind, V. Hariharasudhan, and K. Ramadoss, "Automatic Identification and Removal of Ocular Artifacts from EEG using Wavelet Transform",Measurement Science Review 6(2, 4), 45-57, 2006.

[31] S. Makeig, J. Anthony, A. J. Bell, T. Jung, and T.J. Sejnowski,. "Independent Component Analysis of Electroencephalographic data", Advances in Neural Information Processing Systems 8, 1996.

[32] M. Mastriani, and A.E. Giraldez, "Kalman's Shrinkage for Wavelet-Based Despeckling of SAR Images", International Journal of Intelligent Systems and Technologies 1(3),190-196, 2006.

[33] N. Nikolaev, A. Gotchev, "ECG Signal Denoising using Wavelet Domain Wiener Filtering" In the Proceedings of the 10thEuropean Signal Processing Conference (EUSIPCO 2000), 2000

[34] S. Postalcioglu, K. Erkan, E.D. Bolat, "Comparison of Kalman Filter and Wavelet Filter for Denoising", In the Proceedings of the International Conference onNeural Networks and Brain 2005 Vol. 2, 951 – 954, 13-15 Oct. 2005

[35] V.V.K.D.V. Prasad, P. Siddaiah, and B. Prabhaksrs Rao, "A New Wavelet Based Method for Denoising of Biological Signals", International Journal of Computer Science and Network Security 8(1), 2008, 238-244, 2008.

[36] R. Romo-Vazquez, R., Ranta, V. Louis-Dorr, and D. Maquin, "Ocular Artifacts Removal in Scalp EEG: Combining ICA and Wavelet Denoising", In the Proceedings of Physics in Signal and Image Processing (PSISP 07), 2007

[37] R. Sameni, M.B. Shamsollahi, and C. Jutten, "Filtering Electrocardiogram Signals using the Extended Kalman Filter", In the Proceedings of the 27th IEEE Engineering in Medicine and Biology (EMBS) Annual Conference, 5639-5642, 2005.

[38] P. Senthil Kumar, R. Arumuganathan, K. Sivakumar, and C. Vimal, "A Wavelet based Statistical Method for De-noising of Ocular Artifacts in EEG Signals",IJCSNS International Journal of Computer Science and Network Security. 8(9), 87-92, 2008.

[39] P. Senthil Kumar, R. Arumuganathan, K. Sivakumar, and C. Vimal, "Removal of Ocular Artifacts in the EEG through Wavelet Transform without using an EOG Reference Channel", International Journal of Open Problems in Computer Science & Mathematics 1(3). 2008

[40] P. Shui, and Y. Zhao, Image Denoising Algorithm using Doubling Local Wiener Filtering with Block Adaptive Windows in Wavelet Domain, Signal Processing 87(7), 1721-1734, 2007.

[41] L. SuWen, L, WenQing, X. PinHua, Z. YuJui, "Application of Kalman Filtering and Wavelet Transform in DOAS", In the Proceedings of the 2006 IEEE International Conference on Information Acquisition, 748-753, 2006.

[42] M. Unser, and A. Aldroubi, "A Review of Wavelets in Biomedical Applications", In the Proceedings of the IEEE 84(4), 626-638, 1996.

# INSTRUCTIONS TO CONTRIBUTORS

The *International Journal of Biometric and Bioinformatics (IJBB)* brings together both of these aspects of biology and creates a platform for exploration and progress of these, relatively new disciplines by facilitating the exchange of information in the fields of computational molecular biology and post-genome bioinformatics and the role of statistics and mathematics in the biological sciences. Bioinformatics and Biometrics are expected to have a substantial impact on the scientific, engineering and economic development of the world. Together they are a comprehensive application of mathematics, statistics, science and computer science with an aim to understand living systems.

We invite specialists, researchers and scientists from the fields of biology, computer science, mathematics, statistics, physics and such related sciences to share their understanding and contributions towards scientific applications that set scientific or policy objectives, motivate method development and demonstrate the operation of new methods in the fields of Biometrics and Bioinformatics.

To build its International reputation, we are disseminating the publication information through Google Books, Google Scholar, Directory of Open Access Journals (DOAJ), Open J Gate, ScientificCommons, Docstoc and many more. Our International Editors are working on establishing ISI listing and a good impact factor for IJBB.

The initial efforts helped to shape the editorial policy and to sharpen the focus of the journal. Starting with volume 5, 2011, IJBB appears in more focused issues. Besides normal publications, IJBB intend to organized special issues on more focused topics. Each special issue will have a designated editor (editors) – either member of the editorial board or another recognized specialist in the respective field.

We are open to contributions, proposals for any topic as well as for editors and reviewers. We understand that it is through the effort of volunteers that CSC Journals continues to grow and flourish.

**LIST OF TOPICS**

The realm of International Journal of Biometrics and Bioinformatics (IJBB) extends, but not limited, to the following:

- Bio-grid
- Bioinformatic databases
- Biomedical image processing (registration)
- Biomedical modelling and computer simulation
- Computational intelligence
- Computational structural biology
- DNA assembly, clustering, and mapping
- Fuzzy logic
- Gene identification and annotation
- Hidden Markov models
- Molecular evolution and phylogeny
- Molecular sequence analysis
- Bio-ontology and data mining
- Biomedical image processing (fusion)
- Biomedical image processing (segmentation)
- Computational genomics
- Computational proteomics
- Data visualisation
- E-health
- Gene expression and microarrays
- Genetic algorithms
- High performance computing
- Molecular modelling and simulation
- Neural networks

**CALL FOR PAPERS**

**Volume:** 5 - **Issue:** 4 - July 2011

**i. Paper Submission:** July 31, 2011 **ii. Author Notification:** September 01, 2011

**iii. Issue Publication:** September / October 2011

## CONTACT INFORMATION

**Computer Science Journals Sdn BhD**
M-3-19, Plaza Damas Sri Hartamas
50480, Kuala Lumpur MALAYSIA

Phone: 006 03 6207 1607
006 03 2782 6991

Fax: 006 03 6207 1697

Email: cscpress@cscjournals.org

CSC PUBLISHERS © 2011
COMPUTER SCIENCE JOURNALS SDN BHD
M-3-19, PLAZA DAMAS
SRI HARTAMAS
50480, KUALA LUMPUR
MALAYSIA

PHONE: 006 03 6207 1607
006 03 2782 6991

FAX: 006 03 6207 1697
EMAIL: cscpress@cscjournals.org